EPITAXY OF BORON PHOSPHIDE ON AlN, 4H-SiC, 3C-SiC AND ZrB_2 SUBSTRATES

by

BALABALAJI PADAVALA

B.Tech., University of Mumbai, 2006

AN ABSTRACT OF A DISSERTATION

submitted in partial fulfillment of the requirements for the degree

DOCTOR OF PHILOSOPHY

Department of Chemical Engineering
College of Engineering

KANSAS STATE UNIVERSITY
Manhattan, Kansas

2016

Abstract

The semiconductor boron phosphide (BP) has many outstanding features making it attractive for developing various electronic devices, including neutron detectors. In order to improve the efficiency of these devices, BP must have high crystal quality along with the best possible electrical properties. This research is focused on growing high quality crystalline BP films on a variety of superior substrates like AlN, 4H-SiC, 3C-SiC and ZrB_2 by chemical vapor deposition. In particular, the influence of various parameters such as temperature, reactant flow rates, and substrate type and its crystalline orientation on the properties of BP films were studied in detail.

Twin-free BP films were produced by depositing on off-axis 4H-SiC(0001) substrate tilted 4° toward $[1\bar{1}00]$ and crystal symmetry matched zincblende 3C-SiC. BP crystalline quality improved at higher deposition temperature (1200°C) when deposited on AlN, 4H-SiC, whereas increased strain in 3C-SiC and increased boron segregation in ZrB_2 at higher temperatures limited the best deposition temperature to below 1200°C. In addition, higher flow ratios of PH_3 to B_2H_6 resulted in smoother films and improved quality of BP on all substrates. The FWHM of the Raman peak (6.1 cm^{-1}), XRD BP(111) peak FWHM (0.18°) and peak ratios of BP(111)/(200) = 5157 and BP(111)/(220) = 7226 measured on AlN/sapphire were the best values reported in the literature for BP epitaxial films. The undoped films on AlN/sapphire were *n*-type with a highest electron mobility of 37.8 $cm^2/V \cdot s$ and a lowest carrier concentration of 3.15×10^{18} cm^{-3}. Raman imaging had lower values of FWHM (4.8 cm^{-1}) and a standard deviation (0.56 cm^{-1}) for BP films on AlN/sapphire compared to 4H-SiC, 3C-SiC substrates. X-ray diffraction and Raman spectroscopy revealed residual tensile strain in BP on 4H-SiC, 3C-SiC, ZrB_2/4H-SiC, bulk AlN substrates while compressive strain was evident on AlN/sapphire and bulk ZrB_2 substrates.

Among the substrates studied, AlN/sapphire proved to be the best choice for BP epitaxy, even though it did not eliminate rotational twinning in BP. The substrates investigated in this work were found to be viable for BP epitaxy and show promising potential for further enhancement of BP properties.

EPITAXY OF BORON PHOSPHIDE ON AlN, 4H-SiC, 3C-SiC AND ZrB_2 SUBSTRATES

by

BALABALAJI PADAVALA

B.Tech., University of Mumbai, 2006

A DISSERTATION

submitted in partial fulfillment of the requirements for the degree

DOCTOR OF PHILOSOPHY

Department of Chemical Engineering
College of Engineering

KANSAS STATE UNIVERSITY
Manhattan, Kansas

2016

Approved by:

Major Professor
Dr. James H. Edgar

Copyright

Abstract

The semiconductor boron phosphide (BP) has many outstanding features making it attractive for developing various electronic devices, including neutron detectors. In order to improve the efficiency of these devices, BP must have high crystal quality along with the best possible electrical properties. This research is focused on growing high quality crystalline BP films on a variety of superior substrates like AlN, 4H-SiC, 3C-SiC and ZrB_2 by chemical vapor deposition. In particular, the influence of various parameters such as temperature, reactant flow rates, and substrate type and its crystalline orientation on the properties of BP films were studied in detail.

Twin-free BP films were produced by depositing on off-axis 4H-SiC(0001) substrate tilted 4° toward $[1\bar{1}00]$ and crystal symmetry matched zincblende 3C-SiC. BP crystalline quality improved at higher deposition temperature (1200°C) when deposited on AlN, 4H-SiC, whereas increased strain in 3C-SiC and increased boron segregation in ZrB_2 at higher temperatures limited the best deposition temperature to below 1200°C. In addition, higher flow ratios of PH_3 to B_2H_6 resulted in smoother films and improved quality of BP on all substrates. The FWHM of the Raman peak (6.1 cm^{-1}), XRD BP(111) peak FWHM (0.18°) and peak ratios of BP(111)/(200) = 5157 and BP(111)/(220) = 7226 measured on AlN/sapphire were the best values reported in the literature for BP epitaxial films. The undoped films on AlN/sapphire were *n*-type with a highest electron mobility of 37.8 $cm^2/V \cdot s$ and a lowest carrier concentration of 3.15×10^{18} cm^{-3}. Raman imaging had lower values of FWHM (4.8 cm^{-1}) and a standard deviation (0.56 cm^{-1}) for BP films on AlN/sapphire compared to 4H-SiC, 3C-SiC substrates. X-ray diffraction and Raman spectroscopy revealed residual tensile strain in BP on 4H-SiC, 3C-SiC, ZrB_2/4H-SiC, bulk AlN substrates while compressive strain was evident on AlN/sapphire and bulk ZrB_2 substrates.

Among the substrates studied, AlN/sapphire proved to be the best choice for BP epitaxy, even though it did not eliminate rotational twinning in BP. The substrates investigated in this work were found to be viable for BP epitaxy and show promising potential for further enhancement of BP properties.

Table of Contents

List of Figures

List of Tables

Acknowledgements

I would like to express my sincere thanks and deepest gratitude to my major professor, Dr. James H. Edgar, for giving me this opportunity to work in his group and provide invaluable guidance and encouragement throughout my studies. Without his patience and infinite support, I would have not been able to achieve my dream of pursuing Ph.D. I would also like to extend my thanks to all my committee members, Dr. Ryszard Jankowiak, Dr. John Schlup, Dr. Jennifer Anthony and Dr. Andrew Rys, for taking time to serve on my committee and for their valuable suggestions.

This study would not have been possible without help from so many people. A special thank you to Clint Frye for helping me in every possible way during my stay at K-State. Acknowledgements extend to our collaborators Dr. Rebecca Nikolic and group at LLNL, Dr. Balaji Raghothamachar and group at Stony Brook University, Dr. Peng Lu and Jason Schmitt at Nitride Solutions, Inc., Dr. Rositsa Yakimova and group at Linköping University and Dr. Hans Högberg and group at Linköping University and Dr. Hiroshi Amano at Nagoya University for helping with my research work and experimental results. Financial support from U.S. Department of Energy through grant nos. DE-SC000516, GEGF001846 and DE-AC02-98CH10886, and from National Science Foundation through grant no. EPSCoR IIA-1430493 is greatly appreciated.

Additional appreciation goes to all my current and former group members, colleagues and undergraduate students met during my stay at K-State for their various help, useful conversations and exchange of ideas. I like to thank David Threewit for his indispensable professional help and all the faculty and staff of the Chemical Engineering department whom I had pleasure to work with during my study at Kansas State University.

My heartfelt gratitude to my friends Lateef Uddin Syed and Subhash Appidi who helped me infinite times in my professional and personal life.

Finally, special thanks to my parents, my lovely wife Lilly Priya and son Krish and other family members for their support, encouragement and sacrifice through all my endeavors.

Dedication

To my dad, Sri.Venkata Krishnaiah Padavala.

Chapter 1 - Introduction

1.1 Dissertation Outline

This research was funded by the U.S. Department of Energy and is primarily focused on developing the semiconductor boron phosphide (BP) for neutron detector applications. It is interdisciplinary in nature and various stages such as crystal growth via chemical vapor deposition (CVD), characterization, electrical measurements, device fabrication and testing will involve learning new things and upgrading the knowledge associated with those specific processes. My non-collaborative work primarily involved the synthesis of BP films via CVD and characterization of the grown films using scanning electron microscopy (SEM), transmission electron microscopy (TEM), X-ray diffraction (XRD), Raman spectroscopy analysis and electrical measurements at Kansas State University. My collaborative work involved the detailed characterization of BP films using high-resolution X-ray diffraction, synchrotron white beam X-ray topography, Raman imaging and other techniques performed at other institutions.

This dissertation reports on the epitaxial growth of BP films on AlN, 4H-SiC, 3C-SiC and ZrB_2 substrates and their characterization, as individual chapters. Most of the data and results included in these chapters were already published in the form of peer-review papers in leading research journals, while some of the recent results will be submitted for publications in the coming days.

Chapter 1 discusses the properties of BP along with its potential applications in various devices. The motivation behind this research is discussed, in addition to the objectives and specific goals to be accomplished. The literature review of growth of epitaxial films, problems faced in the past studies are also discussed.

Chapter 2 discusses the details of CVD system employed to grow BP films. The improvements done to the CVD process during the entire work are discussed in this chapter. The characterization techniques employed to study the properties of deposited BP films are also given.

Chapter 3 has been published in the Crystal Growth & Design journal in 2016 with the title - *Epitaxy of Boron Phosphide on Aluminum Nitride(0001)/Sapphire Substrate*[1] and in the proceedings of the Materials Science and Technology conference in 2014 titled - *Heteroepitaxial Growth of Boron Phosphide on 3C-SiC/Si(100) and AlN/Sapphire(0001) Substrates*.[2] It discusses the growth of BP epitaxial films on AlN/sapphire substrate and characterization of the films. This is the first report of BP film growth on AlN substrates in the literature. In addition to the results published in this paper, BP growth on bulk AlN substrates and more detailed characterization of BP films on both bulk AlN and AlN/sapphire substrates were included in this chapter.

Chapter 4 was published in the Solid State Sciences journal in 2015 with the title - *Preparation, Properties, and Characterization of Boron Phosphide Films on 4H- and 6H-Silicon Carbide*[3] and in the proceedings of Materials Science and Technology conference in 2014 titled - *Crystal Growth and Characterization of Cubic Boron Phosphide on Silicon Carbide*.[4] It reports the growth of BP films on 4H-SiC and 6H-SiC substrates and their detailed characterization. The additional results obtained after the publication are also included in this chapter.

Chapter 5 has been recently published in the Journal of Crystal Growth in 2016 titled - *CVD Growth and Properties of Boron Phosphide on 3C-SiC*.[5] Part of the results and findings were published in the proceedings of Materials Science and Technology conference in 2014 titled - *Heteroepitaxial Growth of Boron Phosphide on 3C-SiC/Si(100) and AlN/Sapphire(0001) Substrates*.[2] This chapter comprises of successful growth and characterization of crystalline epitaxial BP films on 3C-SiC substrates for the first time in literature.

Chapter 6 discusses the growth of BP films on ZrB_2 substrates and evaluation of BP properties. This is the first of a kind study of BP epitaxy on ZrB_2 substrates. The structural analysis of BP films using TEM was summarized. The results included in this chapter will be soon submitted for a publication.

1.2 Boron Phosphide

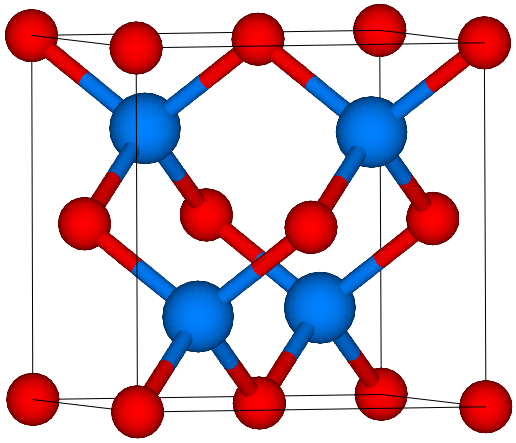

Figure 1.1 Zincblende structure of BP

Boron phosphide (BP), also referred as boron monophosphide, is III-V compound semiconductor material comprised of boron and phosphorus atoms arranged in a cubic zinc-blende crystal structure.[6] It is composed of light elements with small inner shells exhibiting strong covalent bonding with low ionicity.[7,8] BP has a wide indirect bandgap of 2.0 eV[9–11] and a compact crystal structure due to the small atomic radius of boron atoms. Consequently, its crystal structure is highly stable due to the increased overlap of atomic orbitals and higher ionization energy compared to other III-V compounds. Some of the physical properties of BP are listed in Table 1.1.

The structural properties of BP makes it a unique semiconductor compared to other III-V compounds. It has high melting point (>3000^{o}C) and high decomposition pressures (~10^5 atm at 2500^{o}C),[12] making it difficult to synthesize single crystals and study their properties. It is a refractory semiconductor that is mechanically strong with a Micro-Vickers hardness number of 4700 kg/mm^2, twice as large as that of sapphire (2250 kg/mm^2).[13] BP has a higher electron mobility than other III-V compound semiconductors and has both *n*-type and *p*-type conductivities.[14,15] BP has a high Debye temperature, high thermal conductivity, high thermal stability and chemical stability.[16] It can be easily doped to make it a useful refractory semiconductor material for applications in electronic devices operating under extreme conditions such as high temperature, radiation, and high energy environments. BP is not attacked by acids or boiling aqueous alkali water solutions except molten alkali metals.

Table 1.1 Physical properties of BP

Property	BP
Color	Pure BP - almost transparent *n*-type - orange-red, *p*-type - dark red
Lattice constant	0.45383 nm
Coefficient of thermal expansion	3.65×10^{-6} /°C (400 K)
Melting point	>3000°C
Density	2.90 g/cm^3
Heat capacity	0.8 J/(g·K) (300 K)
Thermal conductivity	4 W/(cm·K) (300 K)[17]
Debye temperature	985 K
Bulk modulus	155.7 GPa[18]
Microhardness	32 GPa
Refractive index	3.0 (0.63 μm)

1.3 Applications of BP

Boron phosphide has an indirect wide-bandgap (2.0 eV) with many outstanding properties, including high thermal neutron capture cross-section of the ^{10}B isotope, making it attractive for solid-state neutron detectors.[14] The focus of this research is to grow BP semiconductor material and to study and tune its properties for neutron detector applications.

BP is a refractory semiconductor with outstanding stability at high temperatures and high thermoelectric power. These properties make BP suitable for thermoelectric devices in extreme conditions such as high temperature, radiation, and high-energy environments[19,20] and for direct energy conversions.

BP heterojunction with other materials has many applications as electronic devices. Some of the applications include wide bandgap emitter transistors, as buffer layers on Si for GaN light emitting diodes and laser diodes[21] and as electrodes and optical window material in photoelectrochemical solar cells.

BP films are used as protective coatings for infrared transmitting substrate materials, Ge and Zn, from erosion encountered in high speed flight.[22] It is also used as wear plates, for example

in grinders and crushers due to its wear-resistant properties. Crystalline BP is used as a nuclear reactor shield in the operation of atomic piles and other reactors in the field of atomic energy.[23,24]

The crystalline cubic BP can be fabricated to achieve both dense (e.g. nearly theoretical density) and porous surfaces to fabricate a solid nose in the form of cone shape intended for a guided missile.[23] This crystalline BP is highly resistant against heating and thus withstands the attack by erosive gases to which a missile nose cone is subjected upon re-entry into the atmosphere.[23]

1.4 Background

Neutron detectors are widely used by the U.S. Department of Energy, Homeland Security and other agencies and departments for various applications including portal monitoring of vehicles at international borders, radiation monitoring, compliance monitoring at radioisotope enrichment facilities, emergency response to nuclear accidents, particle physics, neutron diffraction, astronomy, well logging for determining rock properties, and medical applications.

The demand for neutron detectors has increased in the past few years to strengthen the internal security and international borders to stop smuggling of nuclear weapons, nuclear proliferation and terrorism. Most conventional detectors use helium-3 gas for the neutron detection. The Helium-3 isotope forms when tritium isotope decays. It has a thermal neutron capture cross-section of 5330 barns. However, the ^{3}He isotope is increasingly rare and expensive due to its declining stockpiles and decreased production. Hence, there are strong economic and national security motivations to develop high efficiency neutron detectors with alternative neutron capturing materials. Therefore, the impact of creating a high efficiency solid state neutron detector is enormous.

Solid state neutron detectors will be more compact, more sensitive, and less expensive compared to conventional ^{3}He gas proportional detectors, which are huge in size. Such devices can have higher efficiencies than ^{3}He gas-filled detectors because of their high density (more atoms per volume). Since they are small and inexpensive detectors, they can be readily deployed and more widely used to strengthen international borders and internal security. Solid state detectors typically detect neutrons through the absorption of neutrons by absorber materials, which will have

high capture cross section area for thermal neutrons. Typical absorber materials include helium-3 (5333 barns), lithium-6 (940 barns), boron-10 (3840 barns) and uranium-235 (585 barns). Each of these absorber materials react with neutrons with emission of high energy ionized particles, the ionization track of which can be detected by number of means. However, the solid state detectors require isotopes in the solid form such as ^{6}Li, ^{10}B and ^{235}U. ^{10}B isotope is more favorable compared with ^{6}Li and ^{235}U, since it is the solid element with the next highest thermal neutron cross section after ^{3}He.

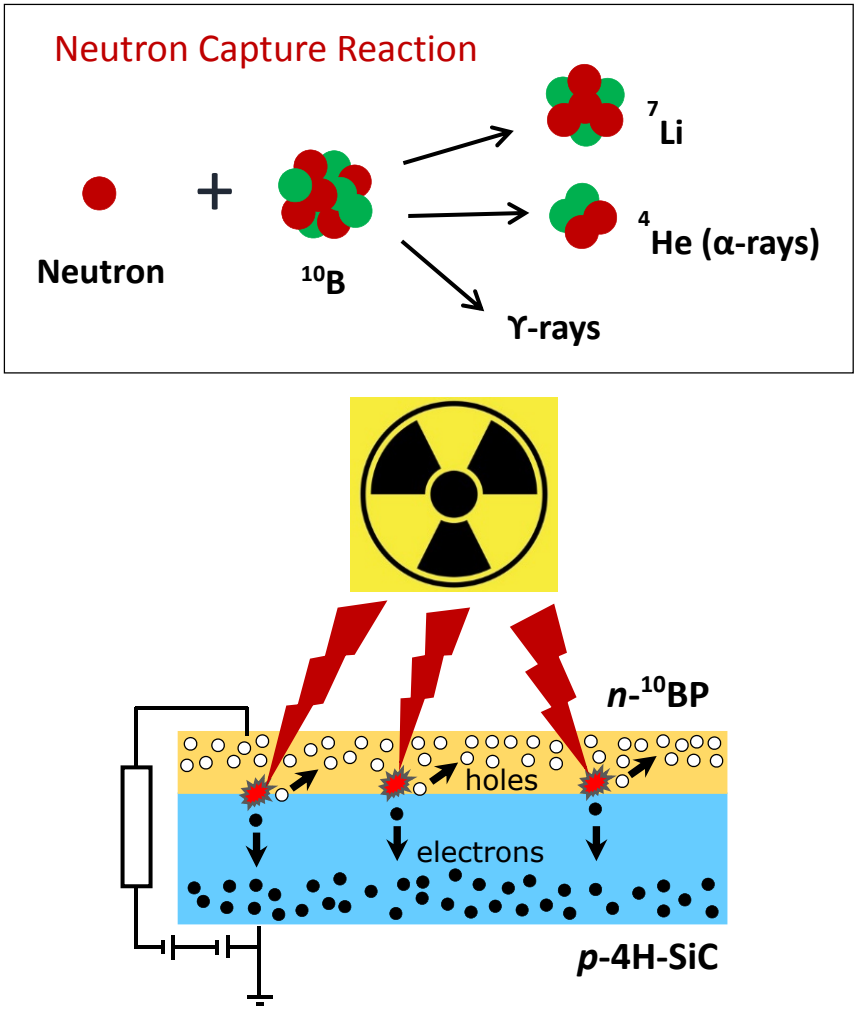

Figure 1.2 Depiction of neutron capture by ^{10}B isotope (top) and generation of charge carriers in the ^{10}BP semiconductor (bottom).

When a ^{10}B atom captures a thermal neutron (0.025 eV), it quickly undergoes two nuclear reactions producing highly energetic Li ions and alpha (^{4}He) particles as shown in the following equations.

$^{10}B + n \rightarrow {}^{7}Li\ (0.84\ MeV) + {}^{4}He\ (1.47\ MeV) + \gamma\ (0.48\ MeV)\ (94\%)$ …….. (1)

$^{10}B + n \rightarrow {}^{7}Li\ (1.02\ MeV) + {}^{4}He\ (1.78\ MeV)\ (6\%)$ …….. (2)

Each neutron captured in a ^{10}B-containing semiconductor creates a large number ($\sim 1.5\times10^{6}$) of electron-hole pairs when the ionizing radiation/particles pass through the semiconductor material. The generated electron-hole pairs serve as the signal for detecting the neutrons. In effect, a few high-energy particles are transduced to a much larger number of low energy charged particles. The signal generated from a single neutron can be relatively strong because of the many charge carriers produced. Thus, semiconductors can make quite sensitive neutron detectors.

1.5 Motivation

The ultimate goal of this research is to develop a ^{10}B-based semiconductor neutron detector that will be more sensitive, energy efficient, compact, robust and lower cost per unit than current devices. There are several boron-based compounds ranging in properties from metallic to insulators including boron phosphide (BP), icosahedral boron phosphide ($B_{12}P_2$), boron arsenide (BAs), icosahedral boron arsenide ($B_{12}As_2$), cubic boron nitride (cBN), hexagonal boron nitride (hBN) and boron carbide (B_4C) that have been investigated for potential neutron detector applications over the past years. Some of the properties of these compounds are listed in Table 1.2.

Table 1.2 Electrical properties of boron based compounds

Compound	Conductivity	Mobility ($cm^2/V\cdot s$)	Carrier density (cm^{-3})	Resistivity (Ω-cm)	Reference
BP	*n type* *p type*	0.5-500 1.77-350	6×10^{10}-1×10^{21} 5.4×10^{10}-1×10^{20}	1.1×10^{-4}-4×10^{4} 10^{-2}-7.8×10^{6}	Table 1.3 in this chapter
$B_{12}P_2$	*p type only*[25]	100	8.9×10^{11}	9.0×10^{4}	26
		700	1×10^{11}	7.3×10^{5}	27
BAs	*p type only*[28]	100-400	10^{18}-10^{19}	0.01	28
$B_{12}As_2$	*p only*	80	10^{17}	10^{4}-10^{5}	29
cBN	*n & p type*	500	5×10^{18}	1-1000	30

$B_{12}P_2$ has high hole mobilities but has only *p*-type conductivity. BAs is unstable at high temperatures limiting its applications as a neutron detector. $B_{12}As_2$ has many desirable properties, but only *p*-type conductivity; this limits its device capabilities. cBN is difficult to synthesize, and

is produced as only as small crystals at extremely high pressures and temperatures or as thin films with high defect densities. hBN is an insulator for which control of the electrical properties has not been demonstrated. Upon careful evaluation, BP stands alone for electronic devices, as it has many favorable properties among other boron compound semiconductors as mentioned below.

- BP can be readily doped with impurities to produce both *p*-type and *n*-type conductivities which improve the ease of device fabrication. BP is the most covalently bonded of all III-V semiconductors, which aids in its ability to be doped. Control of the conductivity type can be achieved with conventional doping, as is done with other III-V semiconductors.
- The electron and hole mobilities in BP are significantly higher than those reported for other boron compound semiconductors. Whereas the hole mobility in pure rhombohedral boron carbide crystals is less than 1 $cm^2/V \cdot s$, electron and hole mobilities as high as 357 $cm^2/V \cdot s$ and 500 $cm^2/V \cdot s$, respectively have been reported. These relatively high charge carrier mobilities improve the prospects of collecting all electron and holes created by the ions produced as discussed above.
- BP has an excellent ability to distinguish between gamma and neutron radiation. Since it is composed of elements of low atomic numbers, its interaction with gamma rays will be low.
- BP has a relatively wide indirect energy bandgap of 2.0 eV. Since the bandgap is indirect, its minority carrier lifetime will be longer than a direct bandgap semiconductor. Because the bandgap is wide, its devices will have low background leakage currents and hence low device noise even at elevated temperatures.
- BP has high temperature stability and a high thermal conductivity (4.0 $W/cm \cdot K$), which can easily dissipate the considerable heat generated in the device through nuclear reactions.
- BP is mechanically hard and chemically inert, which can impart its devices with tremendous durability.
- BP epitaxy and bulk crystal growth are relatively simple and straightforward.

Based on these properties and attributes, BP makes an ideal material for neutron capture, charge creation, and charge collection for a solid state neutron detector. Hence, the focus of this work is to develop BP as a semiconductor material that is suitable for neutron detector applications.

1.6 Growth Techniques

BP crystals have been synthesized by various methods including chemical vapor deposition (CVD),[11,31] chemical vapor transport (CVT),[32] flux growth,[33–35] and high-pressure growth at high temperature.[36–38] Among these, conventional melt techniques proved to be difficult because BP decomposes incongruently before reaching its melting point (>3000°C) and it has a high decomposition vapor pressure of 94,500 atm at 2500°C[12]. CVD and flux growth methods were the most common because of their ability to produce BP at relatively low temperatures (<1400°C).

In this work, CVD was employed because of its ability to produce high quality single crystalline BP epitaxial films over large areas of substrates enabling better neutron capture and efficient detection. Control of the electrical properties of BP by doping with known impurities is also relatively straightforward with CVD. In addition, gas sources for boron and phosphorus are available in extremely high purities. BP epitaxy is commonly carried out through thermal decomposition of hydrides such as phosphine (PH_3) and diborane (B_2H_6) mixtures in a hydrogen atmosphere (equation 3) or through the thermal reduction of halides such as phosphorus trichloride (PCl_3) and boron tribromide (BBr_3) mixtures with hydrogen gas (equation 4) as per the following reactions.

$$B_2H_6 + 2\,PH_3 \rightarrow 2\,BP + 6H_2 \quad \ldots\ldots\ldots\ldots\ldots\ldots\ldots\ldots (3)$$

$$BBr_3 + PCl_3 + 3H_2 \rightarrow BP + 3HBr + 3HCl \quad \ldots\ldots\ldots (4)$$

Both reactions rely on passing the precursor gases over hot substrates placed on the susceptor, which is externally heated by a RF generator. The entire assembly is placed inside a quartz tube that is sometimes cooled with a water jacket. However, the only difference is that the carrier gases in the thermal reduction reaction are bubbled through two constant temperature bubblers containing liquid BBr_3 and PCl_3.

1.7 Literature Review

In order to grow BP films via CVD, either BP bulk single crystals or foreign substrates with large surface area are needed as substrates. So far, bulk crystals of BP are produced in small

sizes, and hence they are not readily available. Hence, BP films have to be deposited on foreign substrates. In the heteroepitaxy of BP, the quality of the films is influenced by choosing the most suitable single crystal substrate, along with optimum growth conditions. The choice of the substrate in turn influences the morphology, crystal orientation, defect densities, impurities, and residual strain of the epitaxial layers.

Table 1.3 Electrical properties of BP films grown via CVD

Substrate Used	Mobility ($cm^2/V \cdot s$)	Carrier density (cm^{-3})	Resistivity (Ω-cm)	Type	Reference
Si	80–150	10^{18}–10^{21}	-	*n*	39
Si	27	2.6×10^{19}	-	*n*	40
Si	80	8×10^{17}	-	*n*	41
Si	140	4×10^{18}	-	*n*	42
Si	5.6	4×10^{19}	-	*n*	43
Si	0.5–37.3	2×10^{17}–6×10^{18}	0.08–27.0	*n*	44
Si	145	1×10^{17}	0.41	*n*	45
Si	107–120	2.5×10^{16}–3.7×10^{17}	0.15–2.5	*n*	46
Sapphire	37.7	4.8×10^{18}	3.7×10^{-2}	*n*	47
Si and Silica glass	8.6	1.3×10^{16}	53.5	*n*	48
Si	357	1.5×10^{20}	1.1×10^{-4}	*n*	49
SOI and Sapphire	31.9	2.66×10^{19}	7.35×10^{-3}	*n*	50
Hexagonal SiC	-	2×10^{17}–1×10^{19}	1–0.2	*p*	11
Si	80–150	10^{19}–10^{20}	-	*p*	39
Si	350	5×10^{19}	-	*p*	42
SOI and Sapphire	38	1.94×10^{17}	0.838	*p*	50
Si	20–37	1.6×10^{16}–3.1×10^{16}	10–12.5	*p*	46

When selecting a substrate for BP epitaxy, several factors must be evaluated such as the film-substrate lattice constant mismatch, coefficient of thermal expansion matching, chemical stability, quality, availability, and price. The matching of crystal symmetries and the stacking sequence of close-packed planes are also important. Ideally the substrate should have a lattice mismatch that is equal to the lateral strain of the epitaxial layer i.e., growth with an elastic relaxation of the strain without formation of defects. Additional variables in selecting any substrate

would be its misorientation (tilt direction and magnitude) from the main crystal plane, substrate orientation and its major plane and polarity.

The heteroepitaxial growth of BP films has been studied for more than 45 years on many single crystal substrates including silicon,[15,51–55] sapphire,[47,50] SiC,[3,11,56,57] and GaN/sapphire.[58] Some of the published data on the electrical properties of BP films grown on different types of substrates via CVD technique are summarized in Table 1.3. It is obvious from Table 1.3 that Si and sapphire have been the most common substrates in the past studies because they are relatively inexpensive and readily available. Si substrates are available with *n* and *p* conductivities or high resistivity and in many crystal orientations, so BP can be deposited on Si(100), Si(111) and Si(110) in domain matching epitaxy.[40,59] Si is sometimes chosen because it can be removed by selective etching to create a free-standing BP wafer.[31,52]

The electrical properties of BP reported in the literature vary significantly among different researchers and experiments due to the difficulty in growing high quality BP films and adequately analyzing them. The reported electron mobility ranges between 0.5 $cm^2/V{\cdot}s$ to 500 $cm^2/V{\cdot}s$ and hole mobility ranges from 1.77 $cm^2/V{\cdot}s$ to 350 $cm^2/V{\cdot}s$. With few exceptions, most previous studies produced BP with poor electrical properties due to high background carrier concentrations, unintentional impurities, and structural defects introduced in the films during epitaxy.

The primary reasons for generation of these impurities and defects are poor chemical stability of the substrate, large mismatches of the lattice constants and thermal expansion coefficients between the substrate and BP, and growth conditions employed during epitaxy. For example, silicon is not chemically stable and forms rough, intermixed interfaces with BP when the latter is deposited at temperatures above 950ºC.[51] Furthermore, high Si concentrations (~10^{19} cm^{-3} or more) incorporate into BP films due to Si diffusion and autodoping from the Si substrate, thereby altering the electrical properties of BP.[14,52–55] The thermal instability of silicon limits the maximum temperature to less than 1050°C for its use as a substrate; at higher temperatures, Si incorporation makes it difficult to control the BP's electrical properties.

The large mismatch in lattice constants and thermal expansion coefficients between BP and substrates such as Si and sapphire result in a high density of dislocations and other defects. BP deposited on Si(100), Si(111) and Si(110) substrates all exhibit high densities of planar defects

and /or rotational twins defects.[11,15,40,49,56,60–62] The strain caused by lattice and CTE mismatch makes the surface morphology of the BP film rough and also causes the BP wafer to bow after the silicon is removed.[31,63] Furthermore, the high density of dislocations incorporating into the films further degrade the charge transport properties of BP. BP films deposited on Si frequently crack[51] due to tensile stresses generated in the films.

BP films grown directly on sapphire above 1000°C peel-off from the surface[47] due to poor adhesion; this was witnessed by the present author as well. Higher deposition temperatures improve the overall quality of BP,[11] but some substrates are unstable at elevated temperatures. GaN/sapphire is a case in point: even though the lattice constant mismatch between BP and GaN is very small, GaN begins to decompose at 850°C.[58]

For a BP neutron detector to be efficient and effective at detecting thermal neutrons, BP should have high crystalline quality along with optimum electrical properties. Both of these could be achieved by minimizing planar defects, rotational twins, and impurities in BP during the crystal growth. For this purpose, alternate substrates that are superior to silicon or sapphire are essential.

1.8 Hypothesis

BP epitaxy was extensively studied more than 20 years ago, before new alternate substrates that are superior to Si and sapphire became commercially available. New materials with outstanding features such as AlN, 4H-SiC, 6H-SiC, 3C-SiC, and ZrB_2 are now available in the form of single crystal wafers that may significantly improve the properties of BP. These materials offer better matches of lattice constants and coefficients of thermal expansion with BP, in addition to higher chemical and thermal stability compared to Si and sapphire. The important properties and features of various substrate materials considered for BP epitaxy are given in Table 1.4 and are discussed more in subsequent chapters.

To date, there has been no prior reports of BP epitaxy on AlN and ZrB_2 substrates and very little information of BP films on 4H-SiC, 6H-SiC and 3C-SiC substrates. The present research investigates these new materials as substrates for growing BP epitaxial films with high quality.

Table 1.4 General properties of various substrates considered for BP epitaxy

Material	Structure	Lattice mismatch with BP (%)	CTE@300K [$\times 10^{-6}$/K]	Chemical stability	Thermal stability	Impurity concerns
BP	Zincblende	–	2.94	Good	High	–
Si	Diamond	High (16.4)	2.57	Medium	Poor	Very High
Sapphire	Trigonal	High (32.6)	5.15	High	High	High
GaN	Wurtzite	Very low (0.63)	3.95	Poor	Poor	None
4H-SiC	Wurtzite	Low (4.5)	2.91	High	High	Low
6H-SiC	Wurtzite	Low (4.2)	2.91			Low
3C-SiC	Zincblende	Low (4.1)	2.22			Low
AlN	Wurtzite	Low (3.2)	2.56			None
ZrB_2	Wurtzite	Low (1.26)	3.21	High	High	Low

1.9 Objectives & Goals

A better understanding of the structural properties, charge transport and electrical properties of BP will definitely enable the researchers to make better electronic devices, in which one of the key potential applications is making a neutron detector. The ultimate goal of this project is to demonstrate that the BP semiconductor has the properties necessary to produce a high efficiency (approaching 100%) thermal neutron detector. This objective will be realized by dividing the project into the following individual goals.

1) Demonstrate the growth of high quality epitaxial films of BP on various AlN, 4H-SiC, 3C-SiC and ZrB_2 substrates with improved structural properties.
2) Investigate a full range of process parameters such as temperature, growth rate, reactant flow rates and ratios of PH_3 and B_2H_6 to control the overall properties of the BP.
3) Study the influence of process parameters on the morphology, grain size, crystalline orientation, residual strain and electrical properties of BP films.
4) Characterize in detail BP films grown on various types of AlN, 4H-SiC, 3C-SiC and ZrB_2 substrates having different planes, on-axis and off-axis orientations and polarity.
5) Investigate the use of crystal symmetry matched 3C-SiC and intentionally misoriented 4H-SiC(0001) substrates to eliminate rotational twinning in BP.

After completing the above tasks, emphasis will be on 1) CVD growth of high structural quality thick BP films with low defect densities and low residual impurity concentrations. 2) Achieving optimum electrical properties of BP films for neutron detection. 3) Fabrication of BP p-n junction diodes and testing their electrical performance such as threshold voltage, reverse-bias leakage current, minority carrier lifetime etc. 4) Thermal neutron detection performance such as sensitivity, efficiency, lifetime of BP diodes will be tested to evaluate the longtime potential of these devices at nuclear engineering facility at K-State.

Chapter 2 - CVD System and Experimental Techniques

2.1 Hydride Vapor Phase Epitaxy System

The hydride vapor phase epitaxy (HVPE) system used for depositing BP films in this research consists mainly of a chemical vapor deposition (CVD) reactor, gas-handling system, and toxic gas monitoring system, in addition to other ancillary equipment. A schematic of the HVPE system is shown in Figure 2.1. The CVD reactor consists of a horizontal cold wall quartz tube fitted with a water-cooled jacket. The gas mixture was fed to the entry side of the reactor and was distributed evenly over the heated substrates using a tube made of quartz. Typically, each deposition produces large amounts of fine particles in the form of boron phosphide, boron and phosphorus. To avoid contamination of fresh samples inside the reactor and cleaning of the reactor walls after each run, depositions were performed inside a dump tube made of quartz. After the deposition, the dump tubes were transferred inside a fumehood, soaked in water overnight and finally cleaned prior to use for new deposition. The substrates were heated on a susceptor using an induction heater. The system is evacuated and purged with N_2 using a dry vacuum pump and turbomolecular pump. A constant pressure inside the reactor is maintained by using a butterfly valve and controller. The particle filters installed at the reactor outlet remove solid particles up to 5 μm in size from the exiting gas stream process before it enters the vacuum pump. A pump by-pass line can be used when a true atmospheric pressure deposition is required. The gas stream exiting from particle filters is mixed with N_2 in the rough pump gas and fed to the activated carbon cylinders. The unreacted phosphine and diborane in the diluted stream is adsorbed on the activated carbon before the gas stream is pumped out of the system through fumehood vent.

The reactant gases used for the BP deposition are phosphine (PH_3) and diborane (B_2H_6), both of which are extremely toxic gases. A highly sensitive toxic gas detector (Honeywell CM4 Toxic Gas Monitor) was used to ensure safe handling of these gases. The detector has four sampling probes installed at strategic locations and a chemcassette to monitor and detect any accidental leakage of PH_3 and B_2H_6 gases out of the CVD system. The probe samples gas around its tip and feeds it to the chemcassette. The chemcassette reacts with both phosphorus and boron hydrides, such as PH_3, B_2H_6 etc., and sends alarm if the concentrations are above the set limits at each location. The detection limit of the toxic gas monitor is 0.1 ppb. The reactor is purged with

N_2 gas for multiple time to remove trace PH_3 and B_2H_6 and is only opened after the confirmation with the toxic gas monitor that no trace amounts were present in the system.

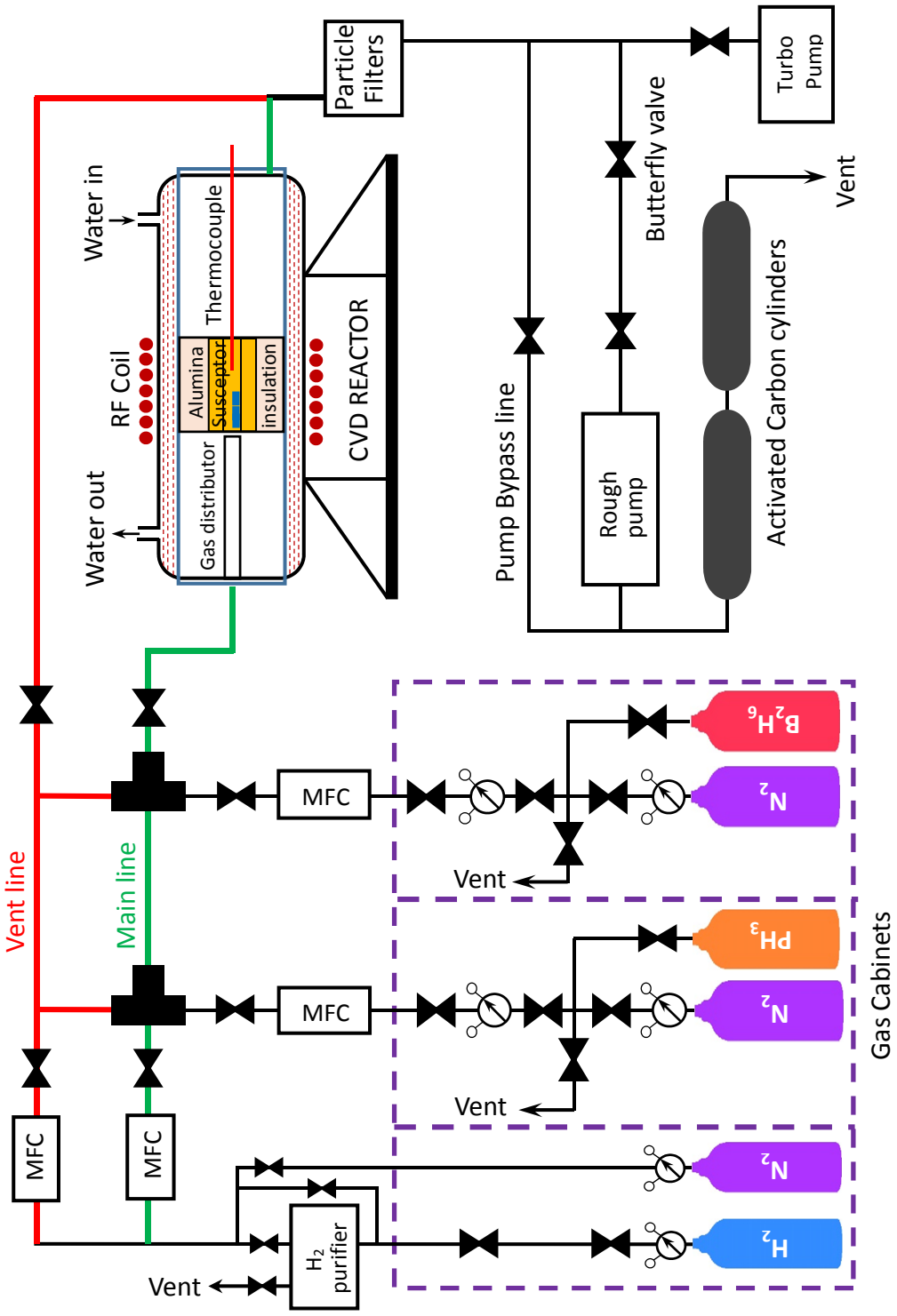

Figure 2.1 Schematic of Hydride Vapor Phase Epitaxy System

The gas handling system consists of cabinets for cylinders storage, a manifold, gas lines, pneumatic valves and mass flow controllers. The gas cabinets contain process gas cylinders including phosphine, diborane, hydrogen and inert gases such as nitrogen or argon. Phosphine and diborane lines have cross purge assemblies in order to remove air from the respective lines before they are introduced into the main line and vent line. Nitrogen is used as cross purge gas for both PH_3 and B_2H_6 cylinders. In addition, hydrogen (carrier gas) and nitrogen (inert gas) cylinders are connected to main line and vent line. All the gas lines from gas cabinets are connected to a manifold where the flow rates and sequence of process gases are controlled and directed to either the main line or vent line. Various pneumatic valves and mass flow controllers control and direct the individual gas streams into the reactor and vent lines. Ultra-high purity phosphine and diborane (1% in H_2) reactant gases are fed to a 3-way pneumatic valve system, which switches the gas flow to either the reactor line or vent lines. H_2 carrier gas is fed through a palladium membrane purifier system to the reactor and vent lines where it mixes with reactant gases and the flows to the reactor.

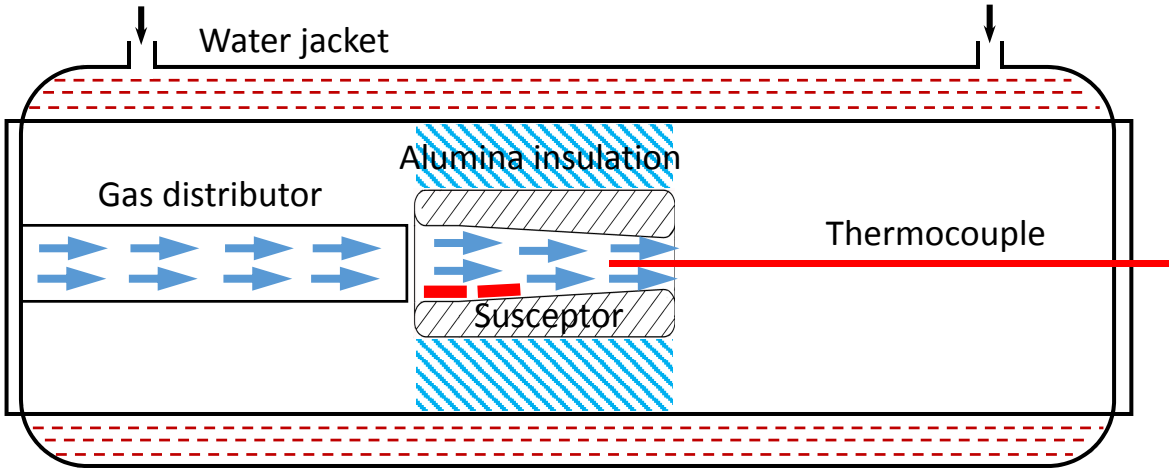

Figure 2.2 Schematic depicting the components inside the reactor quartz tube

A detailed schematic of the reactor's quartz tube and its components is shown in Figure 2.2. The susceptor is made of graphite (ISO-63 grade), which is coated with tantalum carbide (TaC) to prevent carbon contamination in BP films during epitaxy. The susceptor was optimally designed in the form of a hollow rectangular tube with tapered walls toward the downstream to ensure even gas distribution and to increase the velocity of gas stream over the heated substrates. The susceptor is insulated with a premium grade alumina machined as circular rings. Prior to the deposition, the quartz gas distributor, susceptor and alumina insulation are precisely aligned with each other to ensure a smooth and uniform gas flow. The temperature of the substrates was

measured using a platinum, type R thermocouple enclosed in a protective alumina sheath. The thermocouple was placed in the hollow space of the susceptor at the downstream side. The temperature of substrates was accurately calibrated by melting a Si piece on the susceptor with a similar setup and conditions used for BP deposition. The thermocouple readout temperature was noted when a Si piece melts, and the difference between actual melting temperature of Si piece and thermocouple readout was adjusted accordingly for regular BP depositions. Photographs of various components of the system are shown in Figure 2.3.

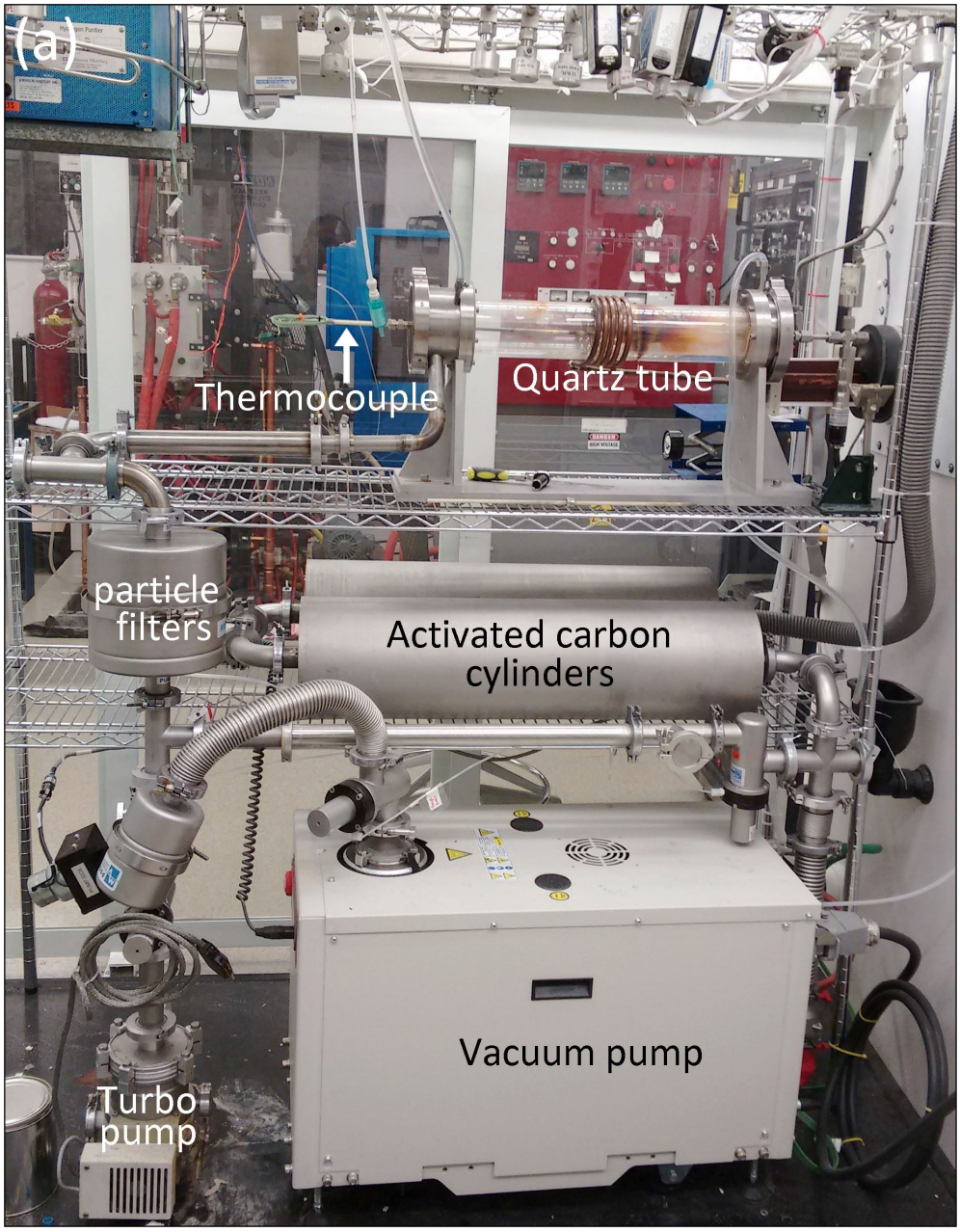

Figure 2.3 (a) CVD system components (b) quartz tube during deposition (c) control panel and (d) gas cabinets

2.2 Susceptor Design & Modifications

Various materials were investigated as susceptors for heating the substrates during BP epitaxy. These included a graphite (ISO-63 grade) susceptor coated with tantalum carbide, a graphite susceptor coated with pyrolytic-boron nitride, zirconium, and a composite of titanium diboride and boron nitride. The advantages and disadvantages of these materials as susceptors are discussed in the following sections.

2.2.1 Tantalum Carbide-Coated Graphite Susceptor

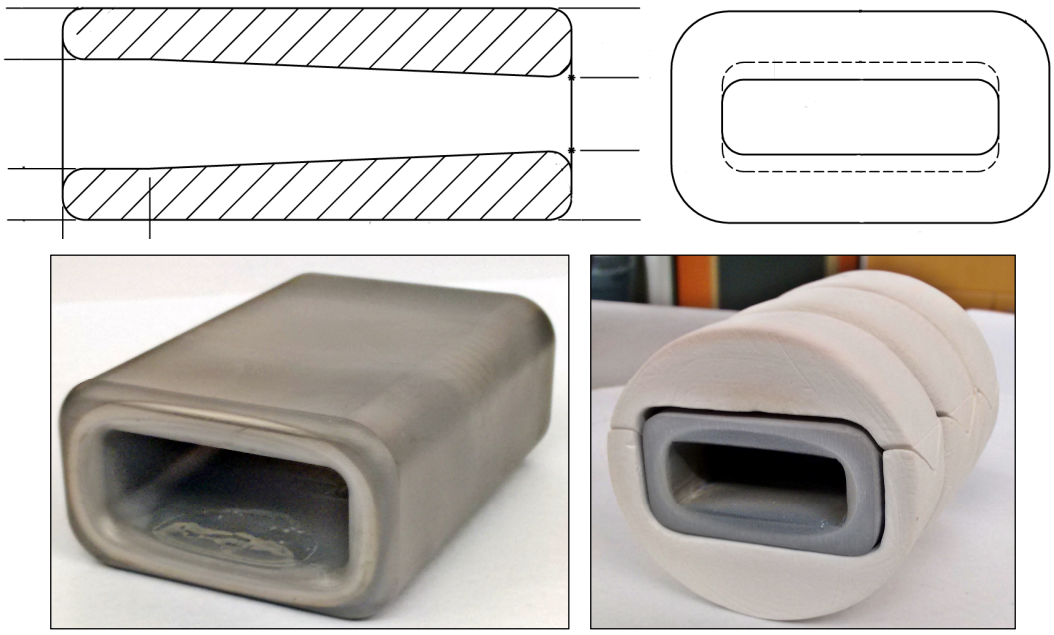

Figure 2.4 TaC-coated graphite susceptor drawing (above) and susceptor with and without alumina insulation (below)

Graphite has high thermal stability and electrical conductivity facilitating its use as refractory material in high temperature material processing applications. For these reasons, halogen purified graphite (ISO-63 grade) coated with tantalum carbide (TaC) was used as a susceptor in this work. Graphite is not stable in hydrogen as it forms CH_4. Hence, the TaC coating is done on graphite as it is stable in H_2 and prevent graphite from reacting with H_2. Hard porous alumina (ZAL-45AA grade) was used as insulation for this susceptor. The susceptor was coated with TaC to minimize contamination of the BP films with carbon impurities from the graphite. In addition, all edges and corners of the graphite were curved prior to TaC coating to avoid sharp

edges and corners as they are highly susceptible to wear & tear after repeated usage and consequently increasing the chance of exposure of underlying graphite. Rounding off edges and corners improved the lifetime of the susceptor considerably compared to earlier susceptors with sharp edges and corners.

The inner walls of susceptor (top and bottom) were tapered to increase the velocity and uniformly distribute the gas stream over the substrates. The opening on the downstream side of susceptor was wide enough to accommodate the thermocouple without touching the susceptor. Temperatures up to 1700^{o}C were easily achieved with this susceptor design. The TaC coating was stable up to 1650^{o}C and was intact for a long period even after several depositions. So far, the TaC-coated graphite and current susceptor design proved to be efficient for achieving uniform gas distribution and high substrate temperatures (1650^{o}C) without any unwanted reactions. In conclusion, the TaC-coated graphite was better than other materials for the susceptors. Other materials tested are discussed in the following sections. All the BP depositions and experimental results obtained on all substrates that are included in this chapter were performed using this TaC-coated graphite susceptor.

2.2.2 Zirconium Susceptor

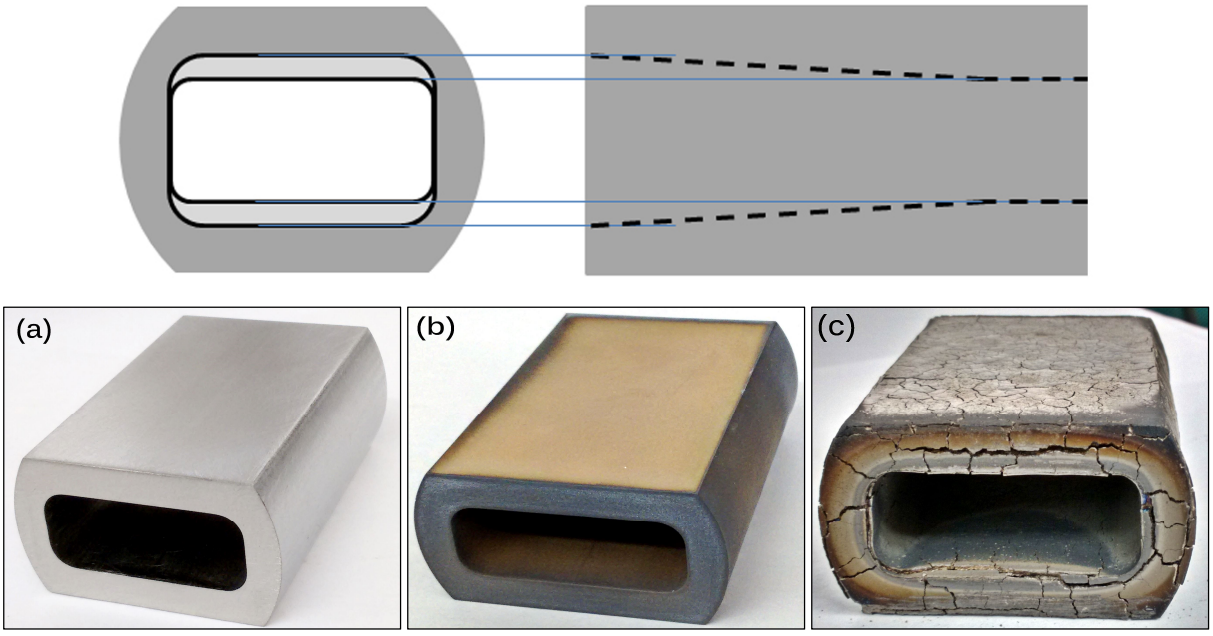

Figure 2.5 Top: Zr susceptor drawing. Bottom: (a) Zr susceptor as received (b) ZrN layer formed on Zr (c) Zr susceptor after BP deposition

Zirconium (Zr) is a refractory material with a melting point of 1855^{o}C that makes it fit to use as a susceptor in this work. When Zr is reacted with N_2 at 1500^{o}C, it forms zirconium nitride (ZrN) which has a much higher melting point of about 2980^{o}C. Here, the initial idea was to form a ZrN layer a few microns thick on the Zr susceptor and then take advantage of the high melting temperature and chemical stability of ZrN. The susceptor was machined from a Zr rod to the shape as shown in Figure 2.5 and zirconia (ZrO_2) as used as insulation material. The bottom and top sides on the inside were tapered, but not on the sides.

Ultimately, when the reactor was backfilled with H_2 during the first pre-purge cycle, the ZrN layer reacted with H_2 at room temperature and the entire ZrN layer turned to black powder and came off from the surface. Then, a pure Zr metal susceptor, without ZrN formation on the surface was tested. The Zr was initially stable up to about 700^{o}C during heating in H_2, but at about 800^{o}C, Zr metal has undergone allotropic transformation, involving phase change of its crystal structure. This phase change occurred at about 800^{o}C, and was noticeable from constant temperature in the thermocouple readout, even though the power output of the induction heater was increased. The temperature of the susceptor increased only when phase change was completed. The extreme expansion and shrinkage during the phase change resulted in cracks present all over the susceptor (Figure 2.5c). When temperature was increased further to typical deposition temperatures (above 1000^{o}C), the intensity of cracking increased. During the entire susceptor heating process, small black particles came off from Zr surface and deposited on the substrates. When the same susceptor was heated for the third time, rapid thermal expansion of Zr susceptor resulted in cracks in the inner quartz dump tube. In summary, based on these experiments, Zr is not a suitable susceptor for the BP epitaxy, especially when H_2 is present in the system.

2.2.3 Pyrolytic Boron Nitride-Coated Graphite Susceptor

The exploration of other materials as susceptors was taken up after SIMS analysis detected high impurity concentrations in $B_{12}P_2$ films grown using TaC-coated graphite susceptor with exactly same CVD setup and materials. A significant concentration of carbon impurities in the $B_{12}P_2$ films were detected in the SIMS analysis. Hence, TaC coating was replaced with pyrolytic boron nitride (pBN) coating on the graphite susceptor, with an aim to significantly reduce carbon contamination. However, pBN coating using the CVD technique on the graphite susceptor peeled

off due to the complex design of susceptor, especially tapered walls inside. Then, as a last attempt, a BN coating on the inner walls of susceptor was applied by dipping in boron nitride (BN) paint and cured the coating at 80ºC for an hour.

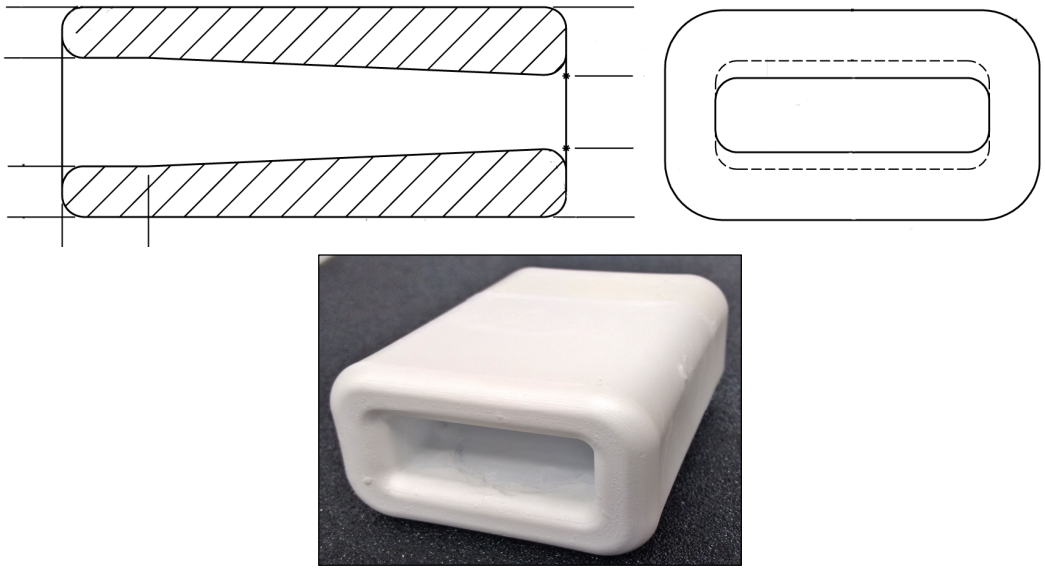

Figure 2.6. Susceptor drawing of pBN-coated graphite susceptor (above) and susceptor after dipping in BN paint before heating

However, the BN films quickly came off while heating the susceptor beyond 500ºC irrespective of the thickness of the BN layer. After several failed attempts, we concluded that dip coating of pBN on graphite is not a practical possibility. Pyrolytic BN on a simpler, wedge shaped graphite susceptor may be suitable, and could be tested in the future.

2.2.4 Titanium diboride + Boron nitride composite Susceptor

A final attempt was made to try a composite material consisting of boron nitride and titanium diboride (TiB_2) as substrate to reduce carbon impurities when TaC-coated graphite susceptor was used. This composite material with grade AC6043 was procured from Momentive. The material was machined as per the shape shown in Figure 2.7, and alumina was used as an insulation material during heating. The desired temperature was achieved, and no abnormalities such as cracks in the susceptor were observed either during heating the susceptor or post BP deposition. SIMS analysis of BP films deposited using this susceptor is yet to be performed to assess the impurities in the films and rate the performance of this composite material as a susceptor.

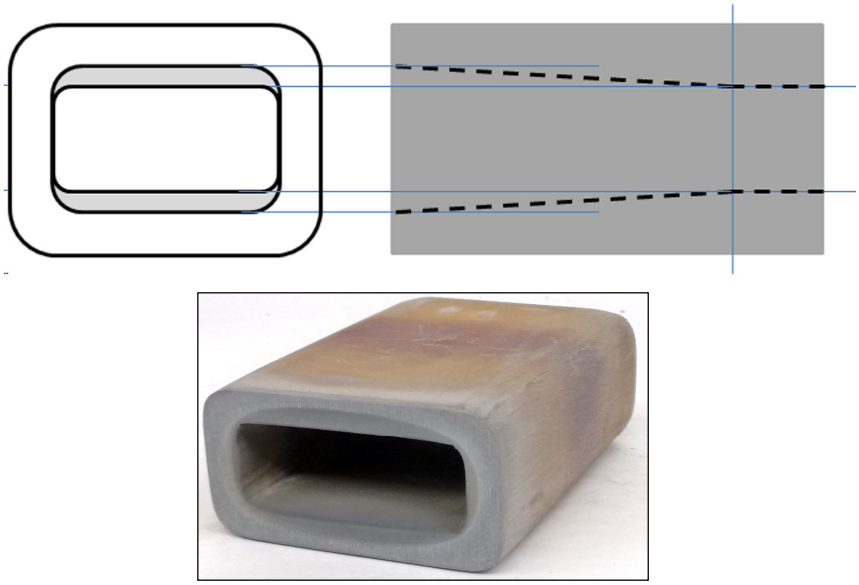

Figure 2.7 TiB_2+BN susceptor drawing (above) and susceptor after BP deposition (below)

In addition to the design of susceptors and susceptor materials, a few other minor improvements were done to the CVD system during the initial depositions. The insulation was changed from fiber alumina to a machined hard porous alumina that holds the susceptor inside. The insulation and susceptor can be moved in and out of the dump quartz tube easily. Consequently, the susceptor as well as substrates were positioned at the same height and angle with respect to the gas distributor (i.e., gas stream) for every deposition. This modification in the insulation design significantly improved the process reproducibility and reliability between depositions, which was not possible when alumina fiber insulation was used.

2.3 Process Conditions

In addition to the selection of a good substrate material, the films must be deposited at optimum process conditions in order to obtain epitaxial films with high crystal quality. The full range of process parameters that needs to be evaluated include temperature, pressure, reactant flow rates of PH_3 and B_2H_6 and their ratios (PH_3/ B_2H_6) and superficial gas velocity (residence time).

2.3.1 Temperature

The temperature of the substrates plays an important role in controlling: the nucleation mechanism and growth rate; crystalline orientation and grain size of crystallites; defect densities

and residual impurities in films; surface roughness; and the stability of the reactants, substrates and epitaxial layers. For example, in the case of off-axis substrates employed in this work, the surface of wafer breaks into monoatomic steps with terraces and edges when the wafer is cut slightly misoriented from a low-index plane in a specific direction. Nucleation occurs on the terraces when substrate temperature is sufficiently low or the flow rate of the reactants is high enough to prohibit fast surface migration of the reactant species.[64] At this condition, film may grow on the terraces. However, when the substrate temperature is high enough or the flux is sufficiently low, then the adatoms are more mobile, in comparison with their encounter probability, and incorporate directly on the step edges. Thus, a controlled nucleation takes place and the growth of the epitaxial film occurs by the advancement of steps along the terraces.

The most common growth temperature for BP in the literature was in the range of 850°C to 1050°C. The crystal quality of BP films improved with higher temperatures,[11,15] but the maximum temperature is constrained by the stability of the reactants, crystalline BP and underlying substrate. BP decomposes to icosahedral boron phosphide ($B_{12}P_2$) at phosphorus vapor pressure less than 1 torr at 1100°C with an exponential dependence on phosphorus overpressure. At 1200°C, 1250°C and 1300°C the decomposition pressure of phosphorus over BP increases to 6.3, 12.6 and 24.2 torr respectively.[65] At higher deposition temperatures, a phosphorus pressure equal to that of the decomposition pressure must be maintained to ensure a 1:1 ratio of elements in BP and prevent decomposition to $B_{12}P_2$. This requires flowing high amounts of phosphine gas at higher temperatures above 1100°C. For this reason, pure phosphine (99.9999%) was used in this work primarily to increase phosphine partial pressure in the gas stream and have more flexibility to play with process parameters. Additionally, the stability of the substrate has to be considered while increasing the growth temperature. For example, Si melts at 1414°C and when the substrate temperatures reach beyond 1400°C, 3C-SiC/Si substrate may decompose or deform when etched in H_2 prior to BP deposition.

In this work, most depositions were performed at three temperatures 1000°C, 1100°C and 1200°C and the reactant flow rates were adjusted accordingly to prevent BP decomposition and ensure 1:1 ratio of B to P in the thin film.

2.3.2 Pressure

The overall operating pressure has several indirect but significant effects on the film growth and quality. A higher total pressure increases the partial pressure of phosphorus and helps to prevent BP decomposition to $B_{12}P_2$ at temperatures beyond 1100°C. However, the higher pressure also increases the collisions between phosphorus and boron precursors, increasing the likelihood of gas phase homogeneous nucleation. In addition, as higher pressures lower the superficial gas velocities, the deposition rate may be limited by reactant diffusion through the gas boundary layer above the film. Hence, the operating pressure must be reduced to allow kinetic control of the deposition rate while simultaneously maintaining enough phosphorus overpressure to prevent BP decomposition. Most prior experiments in the literature were performed at near atmospheric pressure; under these conditions, the reaction is kinetically controlled[15] at temperatures up to at least 1000°C.

In this work, the majority of the depositions were performed at 700 torr. Although few depositions were done at 300 torr, the experiments were not successful in producing crystalline BP films.

2.3.3 Reactant flow rates and ratios:

The reactant flow rates, in addition to temperature, plays an important role in controlling the growth rate and in maintaining the stoichiometric composition and stability of the BP. BP is susceptible to deviations from stoichiometry, with B and P antisites i.e., a B atom on a P lattice site and vice-versa. Hence, an excess of phosphorus precursors was always used in BP epitaxy (similar to a high V/III ratios for GaAs and GaN and other III-V compound semiconductors), so the boron precursor flow rate invariably controls the reaction/deposition rate. However, the magnitude of excess phosphorus precursors can affect the structural and electrical properties of BP. Films deposited with high P or B reactants may alter the point defect concentrations by changing the lattice site of residual impurities. The excess phosphorus is specified by the V/III (PH_3/B_2H_6) ratio of the gas phase reactants. Shohno *et al*[15] found that BP deposited on Si(100) between 950°C-1100°C produced polycrystalline or amorphous deposits at V/III ratios below about 14, while ratios from 14 to 30 resulted in *p*-type BP layers, and ratios above 30 created *n*-

type BP. This suggests that phosphorus atoms occupy the boron sites at high ratios becoming donors and boron atoms occupy phosphorus sites at lower ratios becoming acceptors.

In this work, the gas flow rates were varied between 4000-6000 sccm of H_2, 20-100 sccm of PH_3 and 30-80 sccm of B_2H_6 (1% in H_2). The minimum PH_3 flow rates to prevent BP decompositions at 1000°C, 1100°C, and 1200°C were determined to be 30, 40 and 80 sccm, respectively. In addition, the PH_3 flow rate was kept at least several times (>75) higher than the B_2H_6 flow rate in order to grow single crystalline films. This was accomplished by maintaining the minimum flow rate of PH_3 at the respective temperature and varying the B_2H_6 (1% in H_2) flow rate between 20-80 sccm. For example, at 1200°C, PH_3 flow was maintained at 80 sccm and B_2H_6 (1% in H_2) flow rate was varied between 40-80 sccm.

2.4 Characterization Techniques

A detailed characterization of the BP films is essential to understanding the growth process and evaluating the structural and electrical properties of BP. The major characterization techniques described below helped identify the crystalline orientation, surface morphology and roughness, epitaxial relationship between BP and substrate, chemical composition, strain and defects present in BP films.

2.4.1 Differential Interference Contrast (DIC) Microscopy

This technique, also known as Nomarski Interference Contrast (NIC) microscopy, is a beam-shearing interference system in which the reference beam is sheared by a minuscule amount producing both high and low spatial frequencies present in the specimen. These systems are usually coupled with a polarizer where the polarized light interacts strongly with the sample and generates contrast with the background, enabling the observation of peaks and valleys present in the specimen (see Figure 2.8).

Nomarski microscopy was employed in this research to evaluate the surface features and smoothness of produced BP films. The DIC microscope was Nikon Eclipse LV100 coupled with a polarizing filter.

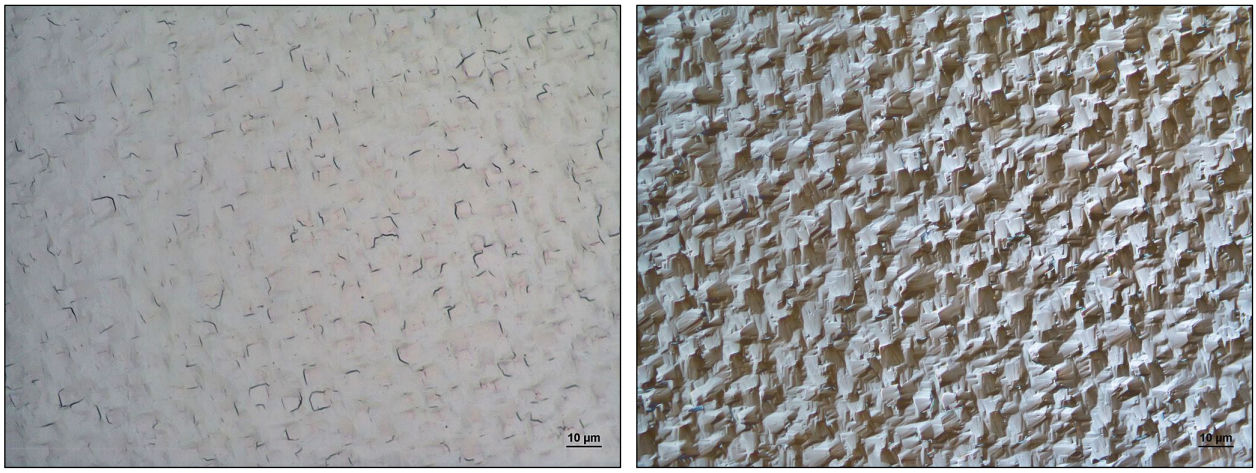

Figure 2.8 DIC micrographs taken on BP film on 3C-SiC(100)/Si (left) with and (right) without a polarizing filter. Peaks and valleys were evident using a polarizer.

2.4.2 Scanning Electron Microscopy (SEM)

A scanning electron microscope produces images by collecting electrons emitted from the sample scanned with a focused beam of electrons. The incident electrons interact with atoms in the sample, producing backscattered and secondary electrons that contain information about the sample's surface topography and composition. SEM was employed in this work to investigate the crystalline orientation, surface morphology, roughness and grain size of BP films. The BP films were characterized by two microscopes: an FEI Nova NanoSEM 230 and an FEI Versa 3D DualBeam microscope. The electron beam energy, spot size and type of detector were varied accordingly to image the surfaces of BP films on different substrates. In general, the beam energy was between 10-30 KV, spot sizes were between 2 to 4 nm with mostly ETD, TLD, vCD and ICE detectors. Based on the grain sizes of the crystallites on the film, the films were imaged at several magnifications of about 1000× to 50,000×.

2.4.3 Energy-dispersive X-ray Spectroscopy (EDS)

The chemical composition and elemental analysis of BP films was assessed by energy-dispersive X-ray spectroscopy. The four main components of EDS setup are the excitation source, X-ray detector, the pulse processor and the analyzer. The excitation source was scanning electron microscope and transmission electron microscope and silicon drift detector. Aztec analysis software was used for the analysis.

2.4.4 Transmission Electron Microscopy (TEM)

The TEM technique analyzes a beam of electrons after it is transmitted through an ultra-thin sample (generally less than 100 nm thick). An image is formed from the interaction of the electrons transmitted through the sample; the image is magnified and detected by a CCD camera.

In this work, the specific types of defects and lattice arrangement of atoms at the substrate-film interface were investigated using TEM. The microscope was a FEI Tecnai operated at a maximum magnification of about 115,000x using PELCO 300 Lacey C/Cu mesh grids.

2.4.5 Atomic Force Microscopy (AFM)

The surface roughness was quantitatively measured by atomic force microscopy (AFM), which can resolve features at a nanometer scale. The AFM instrument was an Asylum Research (Asylum Research, Santa Barbara, CA 93117) MFP-3D instrument operated in AC mode using WaveMetrics Igor Pro 5.0.5.7 software (WaveMetrics, Inc., Portland, OR 97223). Olympus AC240TS-R3 cantilever probes (silicon with aluminum reflex coating and tetrahedral tip geometry with a radius of ~9 ± 2 nm) were used. Flattening was done to remove the background of the topography scans. Line-by-line background subtraction was the only post processing performed on the images.

2.4.6 High Resolution X-Ray Diffraction (HRXRD)

The crystalline orientation of BP with respect to its substrate and overall quality of films deposited at different temperatures and reactant flow rate ratios was determined by X-ray diffraction (XRD). Two types of XRD instruments were employed for the characterization: 1) a Rigaku Miniflex II x-ray diffractometer equipped with $CuK\alpha_1$ (1.54A) source and 2) a high resolution x-ray diffraction (HRXRD) using Bede D1 diffractometer with $CuK\alpha_1$ (1.54A) source and beam conditioning using Max-Flux optics and Ge (111) channel-cut monochromator. The Rigaku diffractometer performed $\theta/2\theta$ scans to evaluate peak widths of preferred BP orientation and relative peak intensities of preferred BP orientation with other BP orientations. HRXRD double axis rocking curves (ω scan and ω-2θ scan) were performed to assess the rocking curve widths and mismatch between BP layer and underlying substrate.

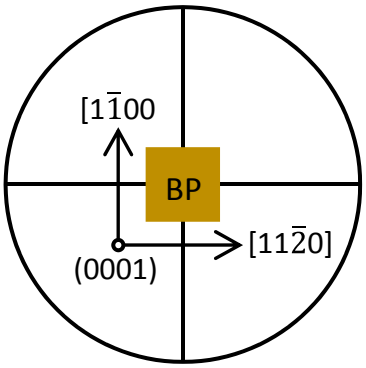

Figure 2.9 Sample alignment in the HRXRD sample holder

For HRXRD measurements of BP films on off-axis hexagonal substrates, the samples were mounted as shown in Figure 2.9. When the rocking curve was measured, the omega of the (0002)AlN peak, for example, would be around ±1° off from the expected peak position due to the substrate off-cut magnitude and direction. Thus, the sample is effectively mounted for the scattering vector to be perpendicular to the substrate surface. Compared to the symmetrical reflection FWHM, the FWHM measurement would be slightly different by a factor of $\sqrt{\frac{\sin(\theta_B+\phi)}{\sin(\theta_B-\phi)}}$

Where ϕ is the off-axis angle. For an offcut of ~1°, the measured FWHM is approximately 0.93-0.95 times FWHM in a symmetrical geometry.

Lattice strain in the BP films was calculated by comparing the measured mismatch with theoretical one, using the formula,

$$\tau = \frac{m^*_{measured} - m^*_{theoretical}}{m^*_{theoretical}} \times 100\%$$

Where $m^*_{measured}$ is the lattice mismatch measured from HRXRD and $m^*_{theoretical}$ is the lattice mismatch calculated based on theoretical d-spacing values of BP. The formulae for both terms are

$$m^*_{measured} = \frac{d'_{BP} - d_{Substrate}}{d_{Substrate}} \times 100\%$$

$$m^*_{theoretical} = \frac{d_{BP} - d_{Substrate}}{d_{Substrate}} \times 100\%$$

Where d'_{BP} is the measured d-spacing from HRXRD using the formula given below and d_{BP} and $d_{Substrate}$ are the theoretical d-spacing values obtained from the lattice parameters of BP and respective substrate.

$$d'_{BP} = \frac{n\lambda}{2sin\theta_B}$$

Where n is a positive integer, λ is the wavelength of incident light, and θ_B is the Bragg angle measured based on the angular distance between BP and substrate peaks obtained from HRXRD ω-2θ rocking curves.

The lattice parameters of BP and various substrates used for calculations are BP (a = 4.5383 Å), 4H-SiC (a = 3.073 Å, c = 10.053 Å), 6H-SiC (a = 3.073 Å, c = 15.11 Å), 3C-SiC (a = 4.3596 Å) and AlN (a = 3.112 Å, c = 4.982 Å).

2.4.7 Synchrotron White Beam X-Ray Topography (SWBXT)

X-ray topography (XRT) is a nondestructive characterization technique for imaging, by means of X-ray diffraction, the micrometer-sized to centimeter-sized defect microstructure of crystals. In this technique, an X-ray beam illuminates the crystal sample, and images of the diffracted beams are recorded. These images are generally formed from X-ray wave fields interfering with one another inside the crystal. The image from a perfect crystal is usually completely homogeneous. Changes in the image contrast are seen if there are imperfections in the crystal, which cause deviations from perfect long-range atomic order. In most cases, the defects themselves are not visible in the image, but rather the lattice deformations surrounding the defects are seen.

The epitaxial relationship, rotational twin defects, and lattice-induced strain in the BP films was determined by the XRT technique. XRT was carried out at beamline X19C at the National Synchrotron Light Source, Brookhaven National Laboratory. Transmission topographs were recorded using white beam radiation aligned parallel to the [0001] direction of hexagonal substrates such as 4H- and 6H-SiC, AlN(0001)/sapphire substrates and parallel to the [100] and [111] directions of the 3C-SiC(100)/Si and 3C-SiC(111)/Si substrates.

2.4.8 Raman Spectroscopy

Raman spectroscopy is based on the interaction of light with the chemical bonds of a sample. Due to vibrations in the chemical bonds, the interaction with photons causes specific energy shifts in the back scattered light that appear in a Raman spectrum. Raman spectroscopy was employed to assess the chemical composition, residual strain, defects, and qualitative and quantitative information of the BP films. Confocal Raman microscopy is a high-resolution imaging technique where chemical properties of samples can be analyzed with diffraction-limited spatial resolution ($\lambda/2$ of the excitation wavelength, down to 200 nm) without labeling or other sample preparation techniques. Raman images provide information regarding the chemical compounds and their spatial distribution within the sample.

Both traditional Raman spectroscopy and confocal Raman mapping techniques were employed to assess the crystal quality and residual strain in the BP films. The traditional Raman instrument consisted of a 0.55 m spectrometer (iHR550, Horiba-Jobin Yvon) coupled to an upright microscope (BX41, Olympus) and a light source of 633 nm HeNe laser. 3D confocal Raman mapping was performed using an Alpha300 AR+ confocal Raman imaging system (WITec Instruments Corp.) equipped with a UHTS300 spectrometer, DV970 EMCCD camera and 532 nm frequency-doubled Nd:YAG laser as an excitation light source. 3D Raman images were acquired and analyzed using WITecControl and WITecProject Plus softwares, respectively.

2.4.9 Hall Effect Measurements

The Hall effect is a voltage difference (the Hall voltage) produced across an electrical conductor, transverse to both the electric current in the conductor and a magnetic field perpendicular to the current. This simple technique accurately determines the carrier density, electrical resistivity, and the mobility of carriers in semiconductors.

In this research, the electrical properties of BP were measured by the Van der Pauw method between room temperature and 700K using the LakeShore Hall measurement system model no. 7704A. Ohmic contacts were made by evaporating the Al metal on the four corners of the BP film and annealing the contacts in N_2 at 400^{o}C for 1 hr. For measuring the electrical properties of some BP samples at room temperature, indium was the Ohmic contact metal.

Chapter 3 - Growth of BP on AlN Substrates

3.1 Aluminum Nitride

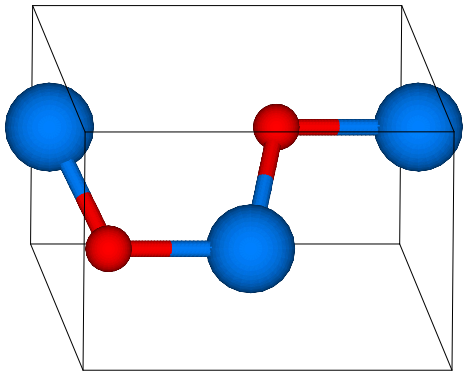

Figure 3.1 Wurtzitic unit cell of Aluminum nitride

AlN is a direct wide bandgap (6.0 eV) semiconductor and exists as a stable wurtzite structure at ambient conditions. AlN is a promising substrate material due to its lower lattice mismatch (3.2%) with BP compared to 4H-SiC (4.2%), Si (16.4%), and sapphire (32.6%) substrates. It has high thermal conductivity of 3.3 W/cm·K and excellent electrical insulation properties. In addition, the excellent chemical stability of AlN enables BP epitaxy at elevated temperatures (>1100°C), potentially improving the crystal quality. BP and AlN are composed of group III and V elements and therefore, are isoelectronic with each other. Consequently, unintentional doping in BP films by the substrate can be significantly minimized by using AlN substrate. Furthermore, the electrical properties of BP can be accurately measured when it is deposited on this substrate, as AlN is an electrical insulator and its interference with electrical measurements would be minimal. Based on these reasons, AlN substrate has the potential to improve the structural and electrical properties of BP. To date, there are no reports of BP epitaxy on either bulk AlN or AlN templates in the literature. Therefore, bulk AlN and AlN templates on sapphire substrates were explored for BP epitaxy in this work.

3.2 Experimental Methods and Conditions

BP films were deposited on three types of AlN substrates: 1) AlN templates on on-axis sapphire(0001), 2) AlN templates on off-axis sapphire(0001): tilted 0.2° toward $[1\bar{1}00]$; 1° toward

[11$\bar{2}$0]; and 2° toward [11$\bar{2}$0] and 3) bulk AlN. The AlN/sapphire substrates were a commercial product. The AlN templates on sapphire substrates have a thickness of about 2 μm. All depositions were made in the horizontal cold-wall CVD reactor, described in Chapter 2.1. Ultra-high purity phosphine (99.9999%) and diborane (1% in H_2) gases were the phosphorus and boron sources. The carrier gas was ultra-high purity hydrogen (99.99999%) purified through a palladium membrane. Most of the substrates used for growing BP films were diced into 5 cm × 5 cm or 10 cm × 10 cm square pieces from a 2-inch AlN/sapphire(0001) wafer.

The substrates were initially cleaned with Q-tips cotton swabs dipped in acetone to remove dust particles and debris on the surface. Further, they were sonicated sequentially in isopropyl alcohol, acetone, and methanol for 5 min each. Trace amount of solvent on the surface was dried using filtered compressed air. The TaC-coated graphite susceptor and alumina insulation were cleaned to remove the dust particles from the previous run. The susceptor is placed inside the alumina rings which is further placed inside a quartz dump tube. The cleaned substrates were then placed inside the susceptor (in the front end) and the entire dump tube is placed inside the water jacket of the CVD reactor.

The system is then evacuated using a dry vacuum pump by slowly opening the butterfly valve using a controller. When good vacuum is achieved, ~50 mTorr, the system is backfilled with H_2 and then evacuated using butterfly valve. After completing about 3 fill-purge cycles, hydrogen is flowed at the desired flow rate and the operating pressure is set to 100 torr. While flowing H_2, the substrates were heated to 1200°C to remove the native oxide layer and clean the surface prior to BP deposition. Then the operating pressure was increased to 700 torr, and temperature of the substrates was brought down to the deposition temperature. Soon after the pressure and temperature are stabilized, reactant gases were then introduced into the carrier gas stream to deposit the BP films. First, PH_3 (99.9999%) was flowed over the substrates for about 1 min and then the BP reaction time starts by introducing B_2H_6 (1% in H_2) in the gas stream. The growth temperature was varied between 1000-1200°C and gas flow rates were varied between 4000-6000 sccm of H_2, 20-100 sccm of PH_3 and 30-80 sccm of B_2H_6 (1% in H_2). All depositions were performed at a constant operating pressure of 700 torr. Films were grown for a period of 30 min to 3 hrs.

3.3 Results and Discussion

3.3.1 Growth and Morphology of BP Films

BP Growth on AlN/sapphire Substrates

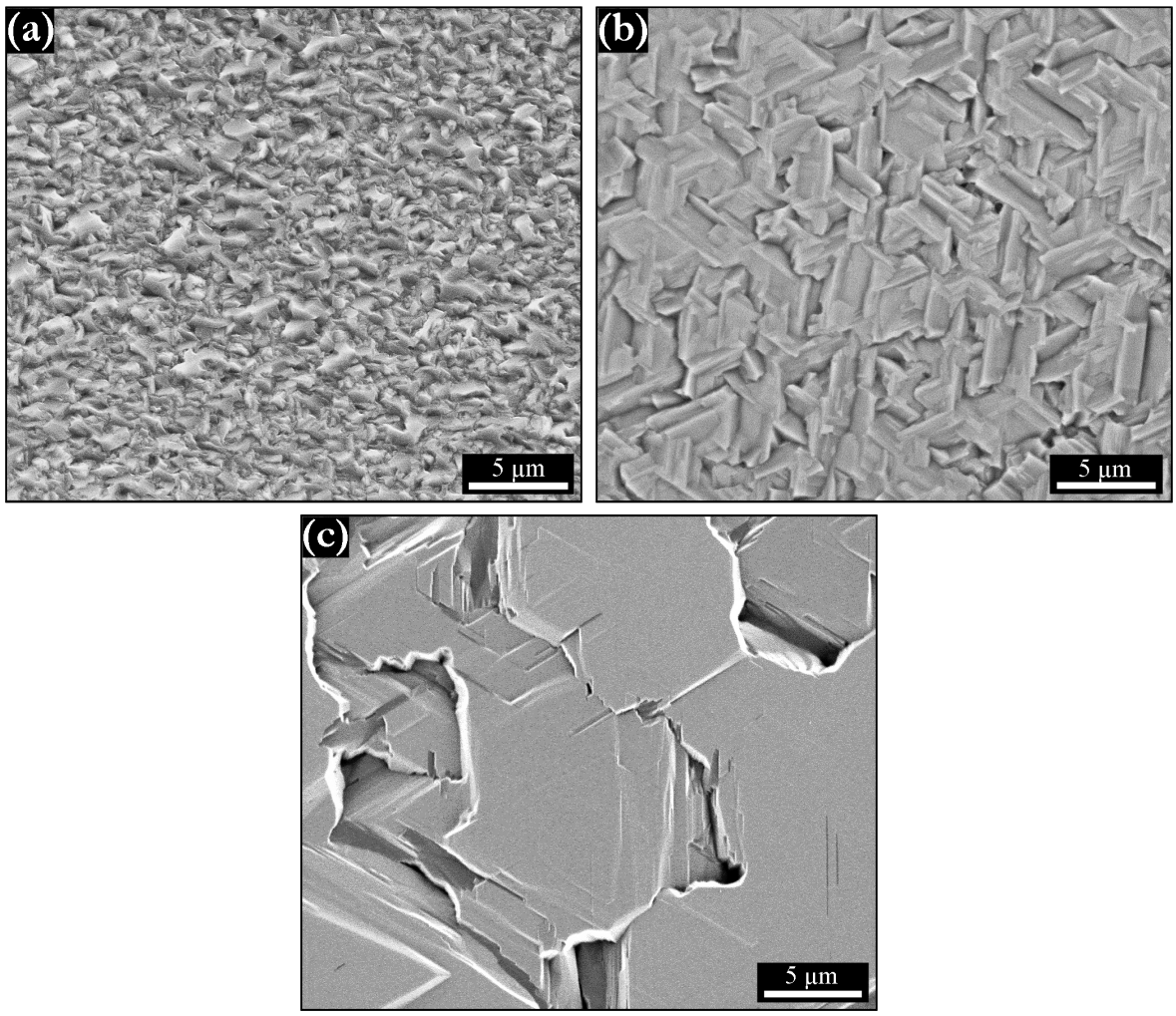

Figure 3.2 BP films grown on on-axis AlN/sapphire depicting increase in grain size and crystalline orientation of BP(111) crystallites at increased temperatures (a) 1000°C, (b) 1100°C, and (c) 1200°C. Magnification at 10000×.

The grain size and crystalline orientation of BP grown on various types of AlN(0001)/sapphire substrates were initially evaluated by SEM. For all types of substrates, the grain size and film texture were strongly dependent on temperature and reactants' flow rate ratio but mostly independent of tilt angle and tilt direction of the sapphire substrate. SEM indicated that crystalline orientation improved with temperatures between 1000°C and 1200°C. The morphology

of BP films grown at 1000°C, 1100°C and 1200°C on on-axis AlN/sapphire are shown in Figure 3.2. Films grown at 1000°C or less were composed of a polycrystalline mixture of fine triangular- and irregular-shaped grains with some degree of common alignment. At temperatures above 1000°C, larger grains were formed with enhanced degree of faceting. At the highest deposition temperature studied (1200°C), grains were preferentially deposited as large triangles with base parallel to the substrate surface, indicating highly textured films with epitaxial relationship between the BP(111) and *c*-plane of the AlN/sapphire substrate. The grain size measured at 1200°C (~15 μm) was approximately 6 times the size measured at 1000°C (~2.5 μm).

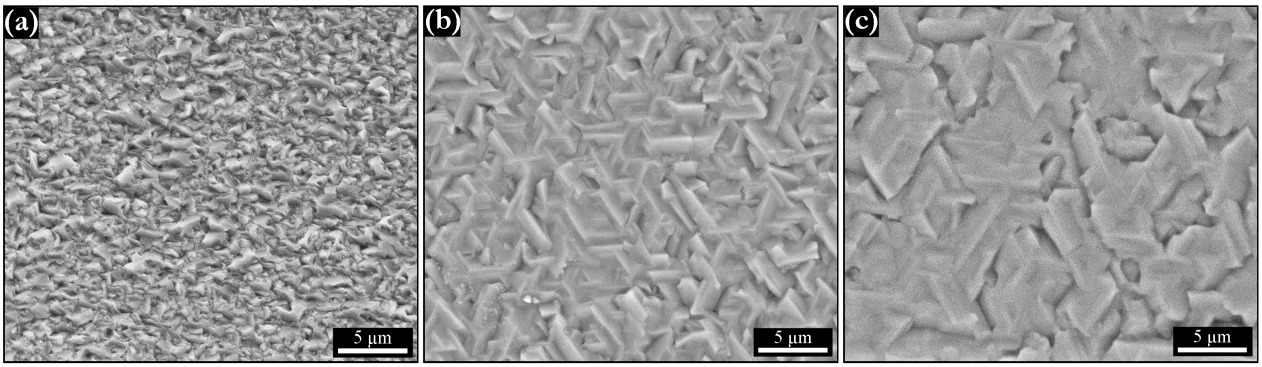

Figure 3.3 BP films grown on AlN/sapphire tilted 1° toward $[11\bar{2}0]$ at temperatures (a) 1000°C, (b) 1100°C, and (c) 1200°C and a PH_3/B_2H_6 flow rate ratio of 150.

A similar increase in grain size and better crystalline orientation with temperature was observed on off-axis AlN(0001)/sapphire substrates that were misoriented in different tilt angles and directions. Figure 3.3 shows the SEM micrographs of BP films grown on AlN/sapphire tilted 1° toward $[11\bar{2}0]$. However, there were minor differences in grain size and surface smoothness when BP films on the substrates were compared.

The deposition temperature is constrained by stability of the reactants, crystalline BP and underlying substrate. BP decomposes to $B_{12}P_2$ at 1100°C and phosphorus pressure less than 1 torr with an exponential dependence on phosphorus overpressure. This requires flowing high amounts of phosphine gas at temperatures above 1100°C. In addition to the temperature, reactant flow rates were also shown to be important process variables for improving the crystalline quality of films. The influence of reactant flow rates on surface morphology, and roughness was studied by varying the PH_3 flow rate and B_2H_6 flow rates separately at a fixed temperature. The minimum PH_3 flow rates to prevent BP decomposition at 1000°C, 1100°C, and 1200°C were determined to be 30, 40

and 80 sccm, respectively. Flow rates below these values resulted in amorphous or polycrystalline films with scattered island growth on the surface. In addition, PH_3 flow rate must be kept at least 75 times higher than the B_2H_6 flow rate in order to grow single crystalline films. This was accomplished by maintaining the minimum flow rate of PH_3 at the respective temperature and varying then B_2H_6 (1% in H_2) flow rate over a range of 20-80 sccm. For example, at 1200°C, PH_3 was maintained at 80 sccm and B_2H_6 (1% in H_2) flow rate was varied between 40-80 sccm in order to obtain single crystalline films that were uniform and continuous over the entire surface.

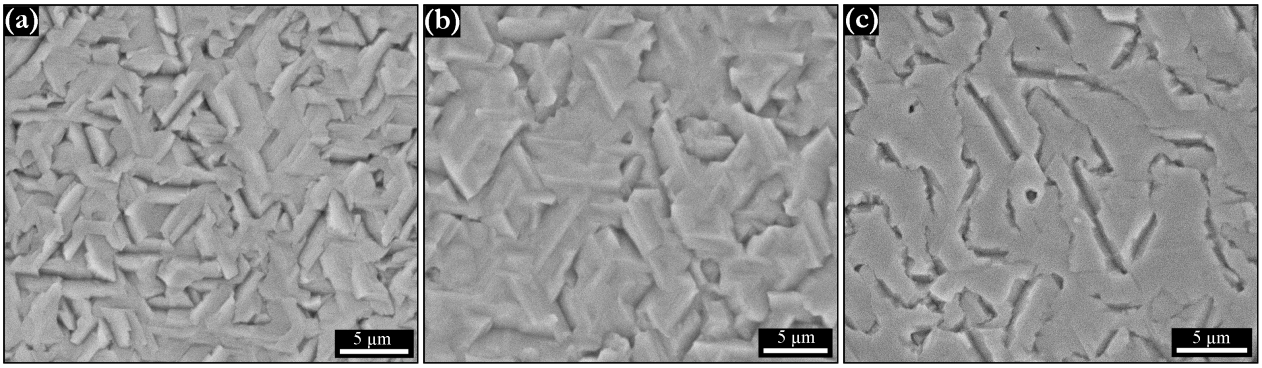

Figure 3.4 Micrographs showing morphology of BP films deposited on AlN/sapphire tilted 1° toward $[11\bar{2}0]$ at 1200°C and PH_3/B_2H_6 flow rate ratios of (a) 100, (b) 150, and (c) 200.

As excess phosphine was used to prevent decomposition of BP to $B_{12}P_2$, deposition rate was limited by the diborane flow rate. Initially, depositions were made at 1150°C with gas flow rates of 3500 sccm H_2, 80 sccm PH_3 and 80 sccm B_2H_6 (1% in H_2). These films had rough surfaces with a large number of spheres (or ballas) on the surface resulted due to high supersaturation and rapid deposition of reactants on the surface similar to shown in Figure 4.6. When PH_3 and B_2H_6 (1% in H_2) flow rates were reduced below 30 sccm and 20-30 sccm respectively to control the deposition rate, thin, non-uniform and polycrystalline BP films were achieved. Reactant flow rates were subsequently tuned to control the growth rate and to obtain smooth, single crystalline films. Optimum flow rates at temperatures of 1000°C and 1150°C were determined to be 4000 sccm H_2, 30-40 sccm PH_3 and 30-40 sccm B_2H_6 (1% in H_2). Temperatures above 1150°C required the phosphine flow rate to be increased in order to maintain phosphorus vapor pressure because phosphorus decomposition pressure increases exponentially with temperature. Flow rates optimized at 1200°C were 4000 sccm H_2, 40-80 sccm PH_3 and 40-80 sccm B_2H_6 (1% in H_2).

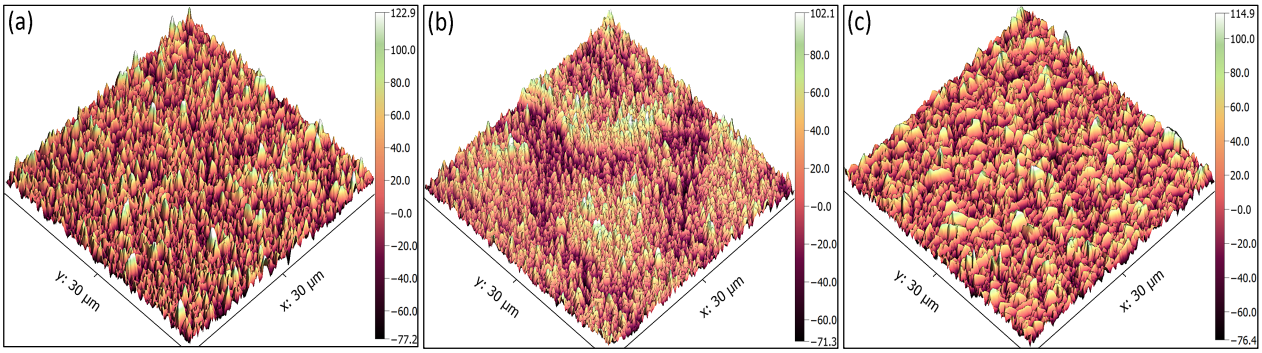

Figure 3.5 AFM images recorded on BP grown on on-axis AlN/sapphire at 1000°C and reactant flow ratios of (a) 100, (b) 150 and (c) 200. Units in nm.

The BP films were highly textured with triangular facets at 1200°C and a PH_3/B_2H_6 flow rate ratio of 100, but were rough due to high deposition rate of BP. When the flow ratio was increased to 150 and 200, by decreasing B_2H_6 flow rate, the surface roughness of films decreased as shown in Figure 3.4. Similarly, the films became smooth when the PH_3/B_2H_6 ratio was increased from 100 to 200 when deposited at 1000°C and 1100°C. The roughness of BP films grown at 1000°C and different flow ratios measured using AFM confirmed this trend (see Figure 3.5). The RMS roughness values at the reactant flow ratios 100, 150 and 200 were measured to be 33.3 nm, 30 nm and 28.7 nm, respectively. However, increasing the PH_3/B_2H_6 flow rate ratio did not change the texture and crystalline orientation of the films. It is worth noting that all BP films grown on AlN/sapphire substrates at all reaction conditions studied were intact and did not peel-off from the substrate, unlike BP on bare sapphire substrates.

BP Growth on Bulk AlN Substrates

BP films were grown on a limited number of bulk AlN(0001) substrates at 1000°C and 1200°C as shown in Figure 3.6. The BP film grown at lower temperature (1000°C) produced a mixture of crystalline and amorphous grains, although some common alignment of small crystallites was observed. However, grain size and crystalline orientation significantly improved at higher temperature (1200°C), consistent with the trend observed on AlN templates.

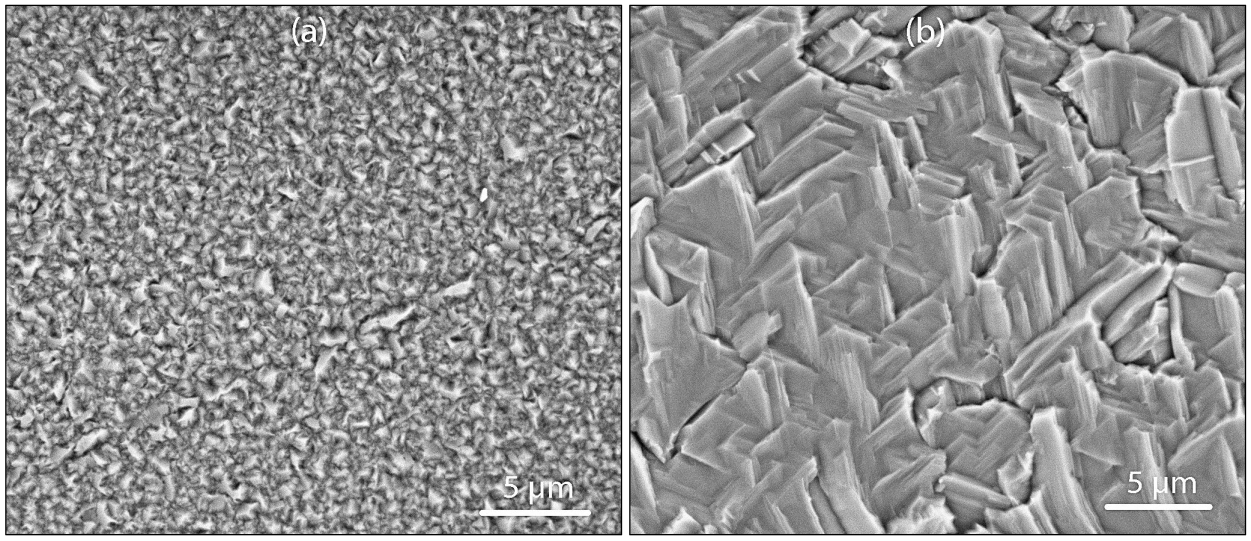

Figure 3.6 Effect of temperature on grain size and crystalline orientation of BP(111) facets on bulk AlN(0001) substrate at (a) 1000°C and (b) 1200°C

In summary, varying the PH_3 flow rate at a constant temperature influenced the crystallinity and continuity of the film on the substrate surface, whereas varying the B_2H_6 flow rate (PH_3/B_2H_6 ratio) influenced roughness and growth rate. Temperature significantly affected grain size and orientation of the preferential BP(111) crystallites, whereas reactant flow rates affected surface roughness and uniformity of the films.

3.3.2 Crystalline Orientation of BP

Representative XRD patterns extracted from θ/2θ scans for films deposited at 1000°C, 1100°C and 1200°C on on-axis AlN/sapphire substrate are shown in Figure 3.7. Diffraction peaks from the substrate occur at 36.04°, 76.44°, and 41.68° in the figure, representing the AlN(0002), AlN(0004), and sapphire(0006) planes, respectively. Intense peaks at 34.30° and 72.03° at all temperatures show the preferential BP(111) and BP(222) orientations, respectively. Additional peaks at 39.67°, 57.4°, and 68.54°, corresponding to BP(200), BP(220), and BP(311) orientations, respectively, along with few minor unknown peaks below 34° were also visible for films deposited at 1000°C, indicating that these films had some degree of polycrystallinity. However, the intensities of these additional peaks were significantly smaller than the preferred BP(111) orientation. At 1100°C and 1200°C, BP(111) orientation was predominant and additional BP orientations were negligible, thereby validating SEM results that the films were single crystalline.

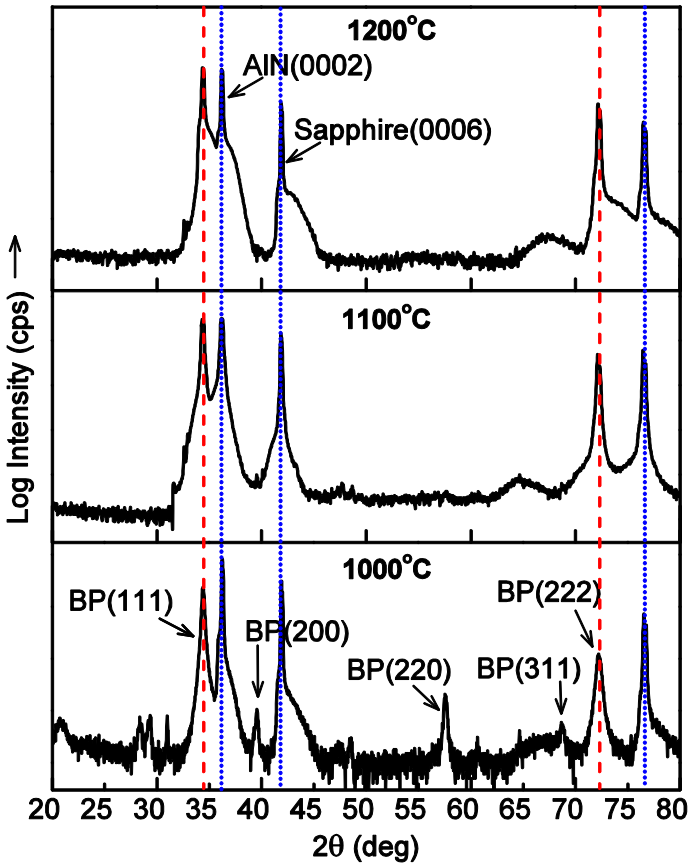

Figure 3.7 θ/2θ XRD pattern showing the effect of temperature on crystalline orientation of BP. Dash lines and dotted lines indicate peaks from preferred BP(111) and AlN(0001)/sapphire substrate, respectively.

The full width at half maximum (FWHM) values of preferred BP(111) peak and relative peak intensity ratios of BP(111) and other BP orientations extracted from XRD θ/2θ scans on films deposited on AlN/sapphire tilted 1° toward [11$\bar{2}$0] direction are shown in Figure 3.8. Peak widths of BP(111) decreased as growth temperature increases from 1000 to 1200°C at a constant reactant flow rate ratio (Figure 3.8a). This decrease in FWHM is perhaps due to the increase in crystallite size with temperature since FWHM values are inversely proportional to crystallite size. Overall results showed that the FWHM decreased with temperature and PH_3/B_2H_6 ratio; the lowest value of 0.18° occurred at 1200°C and $PH_3/B_2H_6 = 200$.

The peak intensity ratios of BP(111)/BP(200) and BP(111)/BP(220) increased with temperature and PH_3/B_2H_6 flow rate ratio due to the improved texture and increased BP(111) peak intensity, as shown in Figure 3.8b and c. At low temperatures, adatoms on the surface will be less

mobile and hence deposit as individual fine grains during the initial growth phase. These fine individual grains with large numbers of grain boundaries act as multiple nucleation sites and enable the BP crystallites to grow in other crystallographic planes, such as (200), (220), and (311). Hence, polycrystalline films were obtained at low temperature (1000°C) in this study. In contrast, high temperatures (above 1000°C) enable more movement of the adatoms, resulting in the expansion and coalescence of small individual grains to form large grains with preferential BP(111) orientation. Similarly, when the diborane flow rate was reduced, surface smoothness improved due to decreased deposition rate. Hence, highest θ/2θ peak ratios of BP(111)/BP(200) = 5157 and BP(111)/BP(220) = 7226 occurred at a high temperature (1200°C) and high PH_3/B_2H_6 ratio of 200.

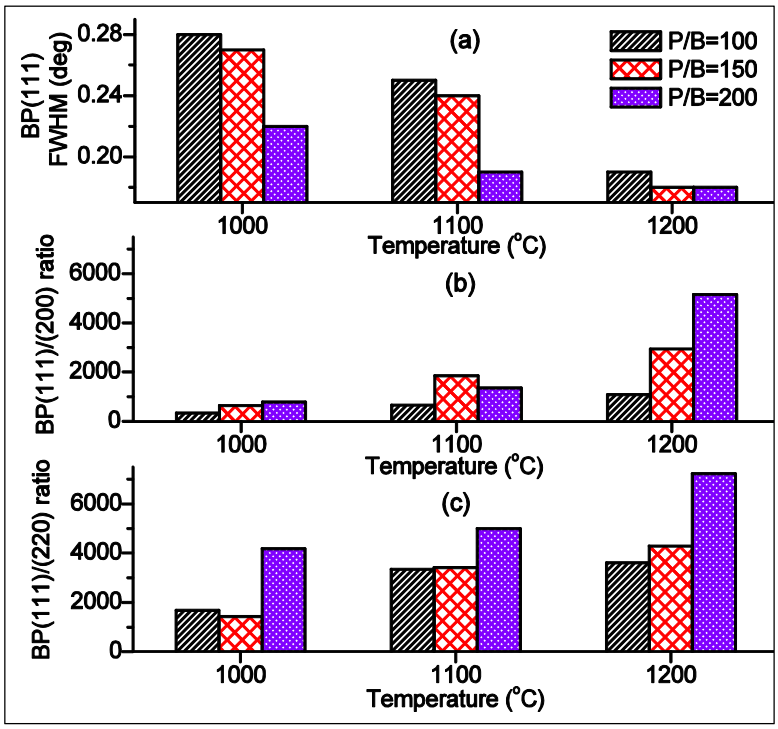

Figure 3.8 (a) FWHM values of BP(111) peak and relative peak intensities of (b) BP(111)/BP(200), and (c) BP(111)/BP(220) extracted from XRD θ/2θ scans.

To corroborate the above findings, HRXRD ω-scan and ω-2θ scan rocking curves were measured for BP films grown on both on-axis and off-axis AlN/sapphire substrates. The FWHM values of BP(111) ω and ω-2θ rocking curves, as shown in Figure 3.9, consistently decreased with increase in growth temperature and PH_3/B_2H_6 ratio, indicating best crystal quality obtained at 1200°C and flow ratio of 200.

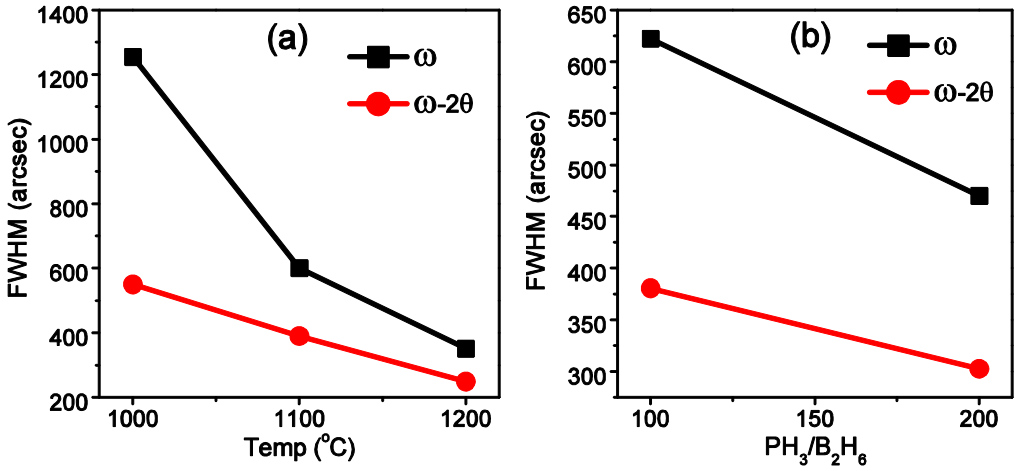

Figure 3.9 BP(111) ω and ω-2θ rocking curves FWHM measured on (a) AlN/sapphire tilted 1° toward [11$\bar{2}$0] at various temperatures and (b) on-axis substrate at various flow ratios.

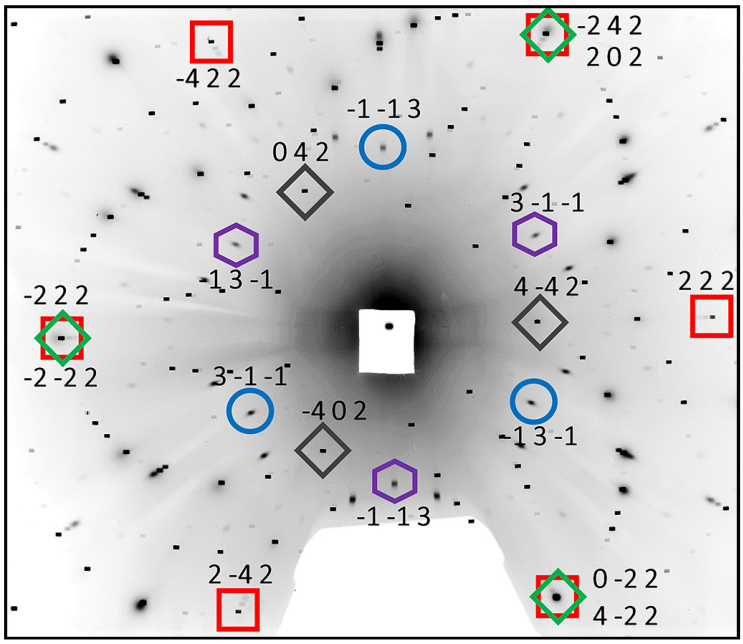

Figure 3.10 X-ray transmission topograph of BP grown on on-axis AlN(0001)/sapphire substrate. Diffraction spots shown by circles, hexagons, diamonds, and squares indicate BP(111), BP(111) twin, sapphire(0001), and AlN(0001) planes, respectively.

BP films were analyzed by synchrotron white beam X-ray topography to assess the epitaxial relationship between the film and substrate and rotational twinning in BP. Figure 3.10 shows the X-Ray topograph recorded on BP film (~3 μm) grown on *on-axis* AlN(0001)/sapphire substrate. The diffraction spots of BP(111), AlN(0001), and sapphire(0001) confirm the epitaxial

relationship between BP and the substrate. The epitaxial relationship between BP and AlN was $(111)_{BP}\langle 11\bar{2}\rangle_{BP} \parallel (0001)_{AlN}\langle 1\bar{1}00\rangle_{AlN}$. The spots indicated by hexagons confirm the presence of BP(111) rotational twins, which are defects formed due to the symmetry mismatch between BP(111) with 3-fold symmetry and underlying AlN(0001) substrate with 6-fold symmetry.

3.3.3 Strain Evaluation of BP Films

Residual strain in the BP films grown on on-axis and off-axis AlN/sapphire substrates was assessed by measuring the BP(111) ω-2θ rocking curves using HRXRD. The theoretical lattice mismatch was calculated from the d-spacing values that were obtained from the lattice parameters of BP and AlN. The measured mismatch was calculated from the Bragg angle obtained based on the angular distance between BP(111) and AlN(0002) planes measured from ω-2θ rocking curves. Finally, the residual lattice strain was calculated based on the measured and theoretical lattice mismatch values calculated before. More details of these calculations are given in chapter 2.4.6. Based on the out-of-plane lattice strain values given in Table 3.1, it can be concluded that BP films grown on AlN/sapphire substrates were mostly relaxed, although some amount of residual compressive strain may still be present. As expected, the out-of-plane strain increased with temperature from 1000°C to 1200°C, as the substrate and film strain more at higher temperatures.

Table 3.1 Out-of-plane strain in BP films deposited at various reaction conditions

Substrate	Temp (°C)	PH_3/B_2H_6	Theoretical mismatch (%)	Measured mismatch (%)	Out-of-plane strain (%)
AlN/sapphire, tilted 1° toward $[11\bar{2}0]$	1000	200	5.22	5.01	-4.04
	1100			5.18	-0.88
	1200			5.30	1.53
AlN/sapphire, on-axis	1200	100		5.25	0.52
		200		5.18	-0.75

Raman spectroscopy and confocal Raman imaging were employed to examine the residual strain and overall quality of the BP films. A typical Raman spectra measured from BP film grown on AlN/sapphire gives two characteristic optical phonon modes, TO mode at ~ 802 cm^{-1} and LO mode at ~833 cm^{-1}. The measured values were in good agreement with the values reported in the literature.[3,52,66,67] Usually the intensity of LO mode is stronger than the TO mode, hence, the data were collected for the LO mode only. Raman spectra were taken at 10,000 points over an area of

10 µm x 10 µm on BP film grown at 1200ºC on AlN/sapphire substrate tilted 2º toward [11$\bar{2}$0]. Two types of scans, XY scan and XZ scan, were performed to assess the film quality of BP film across the horizontal and vertical directions. A horizontal scan involves the raster scan across the film surface whereas a vertical scan involves raster scan in to the depth of the film. All obtained data points were mapped as a 3D plot based on the LO phonon's peak width and shift from its center position.

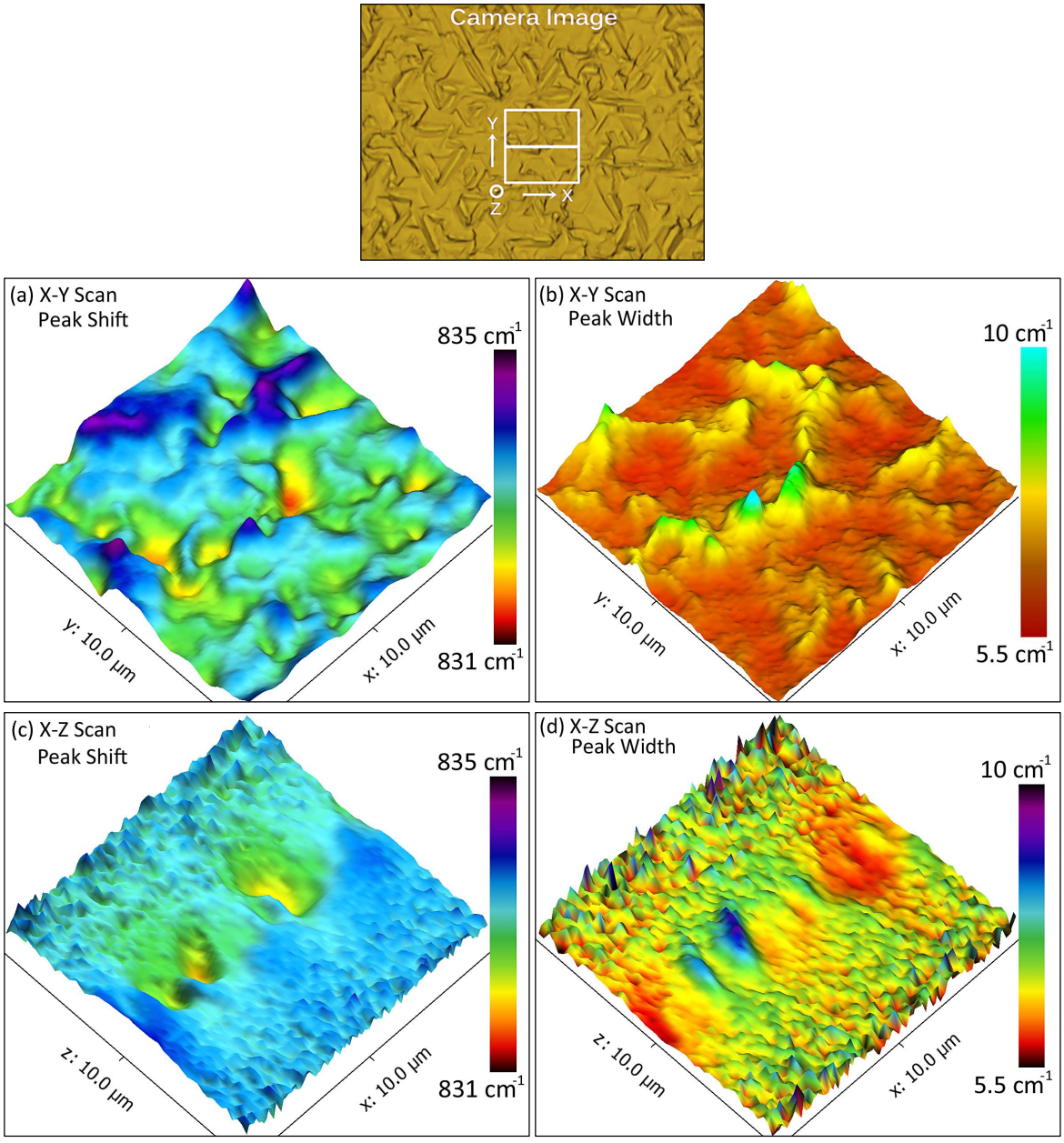

Figure 3.11 Raman images of BP(LO) mode's peak shift and FWHM obtained from (a, b) X-Y scan and (c, d) X-Z scan on BP film grown on AlN/sapphire tilted 2º toward [11$\bar{2}$0].

Figure 3.11 shows the Raman images of BP(LO) mode's peak shift and FWHM for both XY and XZ scans. The camera image placed above the Raman images show the BP film and scanned area for the Raman analysis. The peak shift from its center position in both XY and XZ scans were mostly uniform across the scanned area with average values of 833.1 and 833.2 cm^{-1}, respectively. The standard deviation of peak shift for both scans were 0.44 and 0.29 cm^{-1}, respectively. When the scanned area (shown as white box in camera image) and corresponding Raman images (Figure 3.11a and c) were compared, a slight shift in peak position to the lower side was observed at places where a small pit was present on the BP film surface (in camera image). This slight peak shift from average peak position indicated strain in the BP film.

Strain in the film causes structural disorder and can change equilibrium positions of atoms in the crystal lattice, consequently shifting phonon frequencies from the film depending on the local deformation in the lattice. The formation of pits on the surface during epitaxy could not be avoided because of the inherent property of the BP system. Since BP has to be deposited at high pressure and high reactant flow rates to avoid BP decomposition, all BP films grown in this research had some inherent surface roughness comprising of peak and valleys on the surface. A closer look at the FWHM Raman maps of both scans (Figure 3.11b and d) and the corresponding location of the pit indicated increase in peak width. The peak width across the entire scanned area, except at the pit region, was mostly uniform. The average peak widths of the film were about 6.4 and 6.8 cm^{-1} and standard deviations were 0.56 and 0.56 cm^{-1} for XY and XZ scans, respectively. Overall, the average values of peak shift and peak widths for both scans across the film were consistent, suggesting that the films were uniform and have good crystal quality.

Table 3.2 Comparison of statistical data obtained from Raman imaging of BP films on various substrates. All units are in cm^{-1}.

Substrate→		**AlN/sapphire XY Scan**	**AlN/sapphire XZ Scan**	**4H-SiC**	**3C-SiC(100)/Si**
Peak Shift	min-max	831.5 - 834.7	831.9 - 833.9	824.6 - 829.2	824.5 - 830.4
	Average	833.1	833.2	826.6	828.7
	Std. dev	0.44	0.29	0.72	0.50
Peak FWHM	min-max	5.6 - 10.1	4.8 - 10.0	6.6 - 13.3	5.2 - 20.5
	Average	6.4	6.8	8.9	6.9
	Std. dev	0.56	0.56	0.98	1.65

Raman imaging analysis of BP films grown on AlN/sapphire(0001), 4H-SiC(0001) and 3C-SiC(100)/Si substrates was performed to compare the residual strain and crystalline quality of BP between these substrates. A summary of the Raman imaging statistical data of BP deposited on these substrates was given in Table 3.2, while a detailed discussion on individual substrates is given in the respective chapters. Based on the standard deviation, minimum and maximum values and consistency, AlN/sapphire is proved to be the better substrate compared to 4H-SiC and 3C-SiC(100)/Si substrates.

Table 3.3 FWHM of Raman peaks for BP grown on AlN/sapphire tilted 1° off-axis [$11\bar{2}0$]

Temp (°C)	FWHM (cm^{-1})		
	PH_3/B_2H_6 = 100	PH_3/B_2H_6 = 150	PH_3/B_2H_6 = 200
1000	11.2	10.8	10.1
1100	7.9	8.4	7.3
1200	7.3	7.0	6.8

The following results and discussion are related to the Raman spectroscopy analysis of individual BP films grown on AlN/sapphire at different deposition conditions. The FWHM values of BP films grown on each substrate type at three deposition temperatures and reactant flow ratios were measured. The peak widths of BP on AlN/sapphire tilted 1° off-axis [$11\bar{2}0$] given in Table 3.3, decreased when the PH_3/B_2H_6 flow ratio was increased from 100 to 200. This trend is consistent for majority of the BP films on different types of AlN/sapphire substrate. The magnitude of decrease in FWHM values was more pronounced with increased temperature as compared to the increased flow ratio. A similar trend in reduced peak widths with temperature and reactant flow ratios was also observed for BP films grown on 4H-SiC(0001) under identical conditions, which will be discussed in Chapter 4. But, the FWHM values were consistently narrower for AlN/sapphire compared to 4H-SiC(0001) substrate when compared at identical temperatures and reactant flow rates. In general, the Raman peaks shifted slightly to higher wavenumbers with increased temperature, possibly due to increased residual strain generated by cooling the BP films over a wider temperature range.

The Raman spectra of BP films grown on various AlN/sapphire substrates at 1000°C, 1100°C, and 1200°C for 30 min are shown in Figure 3.12. The FWHM values consistently decreased with increase in deposition temperature for all substrates. The peak width of 6.1 cm^{-1}

measured at 1200°C on AlN/sapphire substrate 0.2° toward [1$\bar{1}$00] was the lowest value ever reported in the literature for BP epitaxial films.[3]

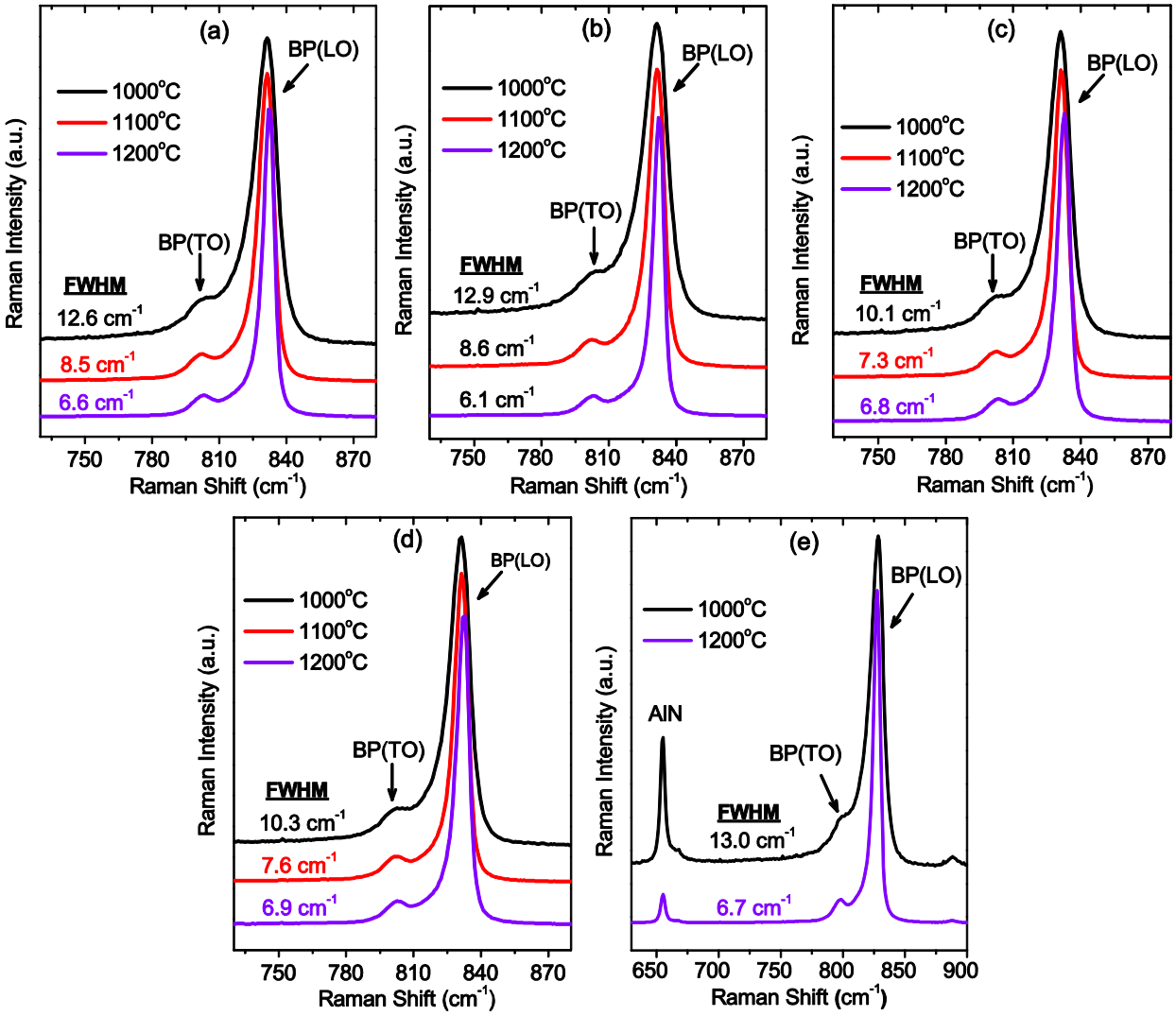

Figure 3.12 Raman spectra showing optical modes and FWHM values of BP(LO) for films deposited on AlN/sapphire (a) on-axis and tilted (b) 0.2° toward [1$\bar{1}$00] (c) 1° toward [11$\bar{2}$0] (d) 2° toward [11$\bar{2}$0] and (e) bulk AlN substrates.

A detailed Raman analysis of various BP films was performed by comparing the data on different substrates grown at different deposition conditions all measured at the same time and with same equipment setup. The Raman peak positions were calibrated using standard Si substrate at frequent intervals and peak position were corrected as necessary to minimize variability between the measurements. It was found that the average TO mode and LO mode peak positions were notably different for BP grown on bulk AlN and AlN templates on AlN/sapphire. The average

peak positions of TO and LO modes on bulk AlN measured were ~798 cm^{-1} and ~827.5 cm^{-1}, and on AlN/sapphire were ~802 cm^{-1} and ~832.6 cm^{-1}, respectively. These peak positions were compared with that of BP whiskers grown on 4H-SiC(0001) at 1200°C via VLS mechanism using Cr metal catalyst. BP whiskers are expected to be strain-free since they freely grow outward off the substrate relaxing the strain unlike an epitaxial film, which is constrained by the substrate.

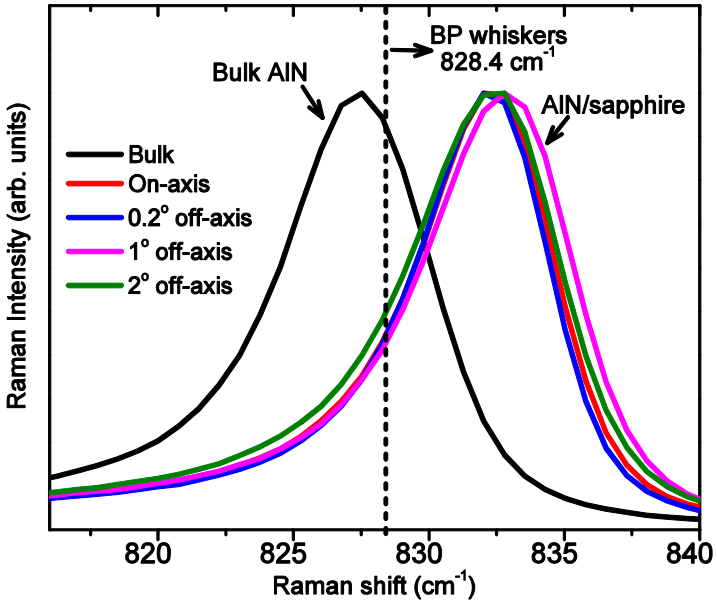

Figure 3.13 Comparison of peak positions of BP(LO) mode between grown on bulk AlN and AlN/sapphire substrates.

As shown in Figure 3.13, the peak positions on AlN templates were consistently on the higher side of the BP whiskers, whereas on bulk AlN substrates they were on the lower side. As we know, higher shift in Raman peak positions indicate compressive strain and lower shift indicate tensile strain in the BP films. The observed trend is in agreement with the coefficient of thermal expansion (CTE) of BP, AlN and sapphire that were reported in the literature.[68,69] At room temperature, AlN has lower or similar thermal expansion coefficient to that of BP, whereas sapphire has much higher compared to BP. Consequently, when BP films were cooled to room temperature after the deposition, tensile strain was introduced in BP film on bulk AlN leading to lower shift whereas compressive strain dominated on AlN templates /sapphire resulting in higher shift. In the latter case, thermal expansion of sapphire dominates to that of AlN, as sapphire has much higher CTE compared to AlN layer. For the same reason, peak positions of BP were

remarkably different between 3C-SiC and 4H-SiC, bulk AlN, AlN/sapphire, bulk ZrB_2, and ZrB_2/4H-SiC substrates.

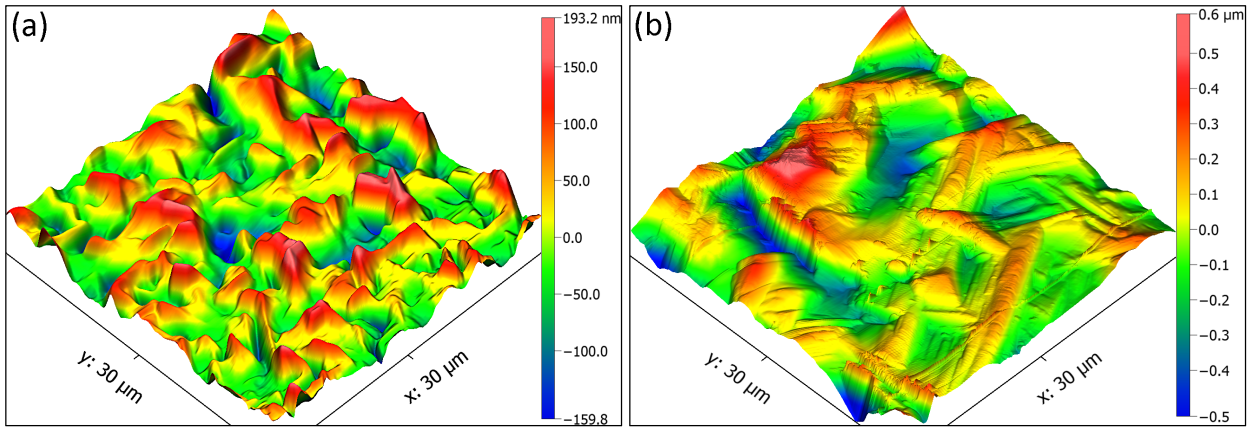

Figure 3.14 AFM images of BP films on AlN/sapphire with a thickness of (a) 2 µm and (b) 12 µm

Two films with thicknesses 2 µm and 12 µm were deposited the best conditions determined so far, 1200°C and a PH_3/B_2H_6 flow ratio of 200, to study the effect of film thickness on properties of BP. As shown in Figure 3.14 and Table 3.4, a significant increase in RMS roughness was observed from 60 nm to 292 nm when thickness was increased from 2 µm to 12 µm. Raman spectra on both films showed slight differences in the peak positions and peak widths, but they were not significantly different. The peak shift has changed from 833.5 cm^{-1} to 832.0 cm^{-1} when thickness was increased. This small difference could be due to either increase in tensile strain or fluctuations in the measurement. The XRD θ/2θ scans on both films showed minor differences in BP(111) peak width and notable decrease in relative peak intensity ratios when thickness was increased. The Hall measurements of both films is discussed below.

Table 3.4 Comparison of XRD, Raman peak widths for BP films deposited at 1200°C and PH_3/B_2H_6 ratio of 200

Film thickness (µm)	Time (min)	RMS roughness (nm)	Raman FWHM (cm^{-1})	Raman peak position (cm^{-1})	XRD FWHM (deg)	XRD BP(111)/ BP(200)	XRD BP(111)/ BP(220)
2	30	60	6.6	833.5	0.27	5849	6970
12	180	292	6.2	832.0	0.28	4647	6337

3.3.4 Electrical Properties of Undoped BP Films

Preliminary Hall effect measurements were performed on undoped BP films grown at 1200ºC on AlN/sapphire tilted 1º off-axis [11$\bar{2}$0] direction. BP films measured at room temperature had *n*-type conductivity with a carrier concentration in the range of 10^{18} cm^{-3} (Table 3.5). The electron mobility slightly increased as PH_3/B_2H_6 ratio was increased from 100 to 150 (No. 1 to 3). For comparison, BP films were deposited on polished AlN layers, sample no.4 (~2 μm thick) and sample no. 5 (~12 μm thick) under identical conditions to evaluate the influence of surface roughness of the starting substrate and film thickness on mobility. Mobility increased significantly on both polished substrates compared to unpolished ones, perhaps due to the deposition of BP on a smoother AlN layer. Mobility for the thicker film decreased slightly from 35.3 $cm^2/V{\cdot}s$ to 27.5 $cm^2/V{\cdot}s$, but was still higher than the mobility of films grown on unpolished AlN substrates (No. 1 to 3). As the 12 μm thick film was crack-free and had reasonably high mobility, film thickness could be further increased to test BP performance in neutron detector applications.

Table 3.5 Electrical properties of BP films grown at 1200ºC measured at room temperature

Sample	PH_3/B_2H_6	Growth Time (min)	Conductivity type	Carrier density n (cm^{-3})	Carrier mobility μ ($cm^2/V{\cdot}s$)
No. 1	100	30	n	8.76×10^{18}	14.2
No. 2	150	30	n	6.04×10^{18}	15.4
No. 3	200	30	n	5.25×10^{18}	18.0
No. 4	200	30	n	4.50×10^{18}	35.3
No. 5	200	180	n	3.39×10^{18}	27.5

The temperature dependence of electron concentration and mobility are shown in Figure 3.15a and b. The intrinsic electron concentration increased exponentially with increasing temperature. The solid lines represent the least-squares fit to the experimental data per the relation, $n(T) \propto exp(-E_D/kT)$, where $n(T)$ is electron concentration as function of temperature. The unintentional donor activation energy (E_D) calculated from the slope of $ln(n)$ $vs.$ (1/T) plot was in the range of 0.02 to 0.03eV. Hall mobility of electrons increased with temperature initially, reaching the maximum value at approximately 450 K, and then decreased slowly with further increase in temperature. The highest mobility was consistently above the room temperature values for all samples. The mobility trend in the entire temperature range was difficult to interpret

because neither empirical laws $\mu \sim T^{-3/2}$ nor $\mu \sim (T^{3/2}/N_I)$ satisfactorily explain the observed phenomenon. These preliminary mobility measurements indicate that more than one scattering mechanism was taking place. An extensive analysis of additional BP films needs to be performed to confirm this phenomenon.

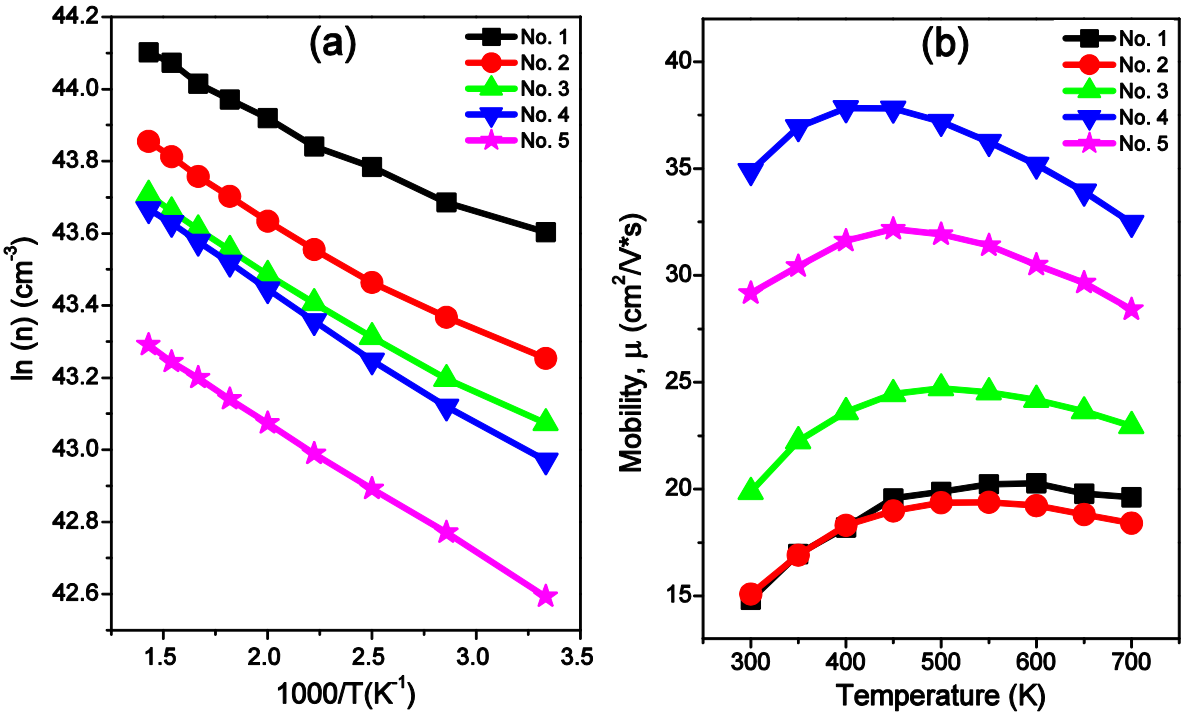

Figure 3.15 Temperature dependence of (a) carrier concentration and (b) Hall mobility of BP films deposited at 1200°C on AlN/sapphire tilted 1° toward $[11\bar{2}0]$.

3.4 Conclusions

Epitaxial growth of BP films on various AlN substrates were successfully demonstrated for the first time in literature. The deposition temperature was the most important parameter that influenced the growth rate, crystal quality and residual strain in the films. The crystalline orientation, texture and grain size of BP crystallites improved consistently with temperature. Polycrystalline films were obtained at and below the deposition temperature of 1000°C, while the films grown at 1200°C were single crystalline on all types of AlN substrate, except change in grain size and surface smoothness. In addition to the temperature, reactant flow rates were also important process variables that influenced the surface smoothness and deposition rate of BP films. A minimum amount of PH_3 flow rate should be maintained at respective temperature to prevent the

BP decomposition and formation of scattered polycrystalline BP islands on the surface. Variation in the B_2H_6 flow rate at fixed PH_3 flow rate influenced the surface roughness and deposition rate, but no significant difference in crystalline orientation was observed.

XRD θ/2θ scans showed narrower BP(111) peak widths and increased relative intensity ratios of BP(111)/(200) and BP(111)/BP(220) at increased temperatures and PH_3/B_2H_6 flow rate ratios. The FWHM values of BP(111) ω and ω-2θ rocking curves obtained on both on-axis and off-axis AlN/sapphire substrates by HRXRD consistently showed better crystal quality at a growth temperature of 1200ºC and PH_3/B_2H_6 flow ratio of 200. In addition, Raman spectroscopy of BP films confirmed the improved crystalline quality at increased growth temperatures and PH_3/B_2H_6 flow ratios, validating the SEM and XRD findings. It is also worth noting that the FWHM values of BP Raman peak (6.1 cm^{-1}) and ω rocking curve (352 arcsec) obtained on AlN/sapphire substrate are lower than the values in the literature for BP epitaxial films.

Rotational twinning in the BP films on on-axis AlN/sapphire substrates, due to mismatch of crystal symmetry between 3-fold BP(111) and 6-fold AlN(0001) planes, was confirmed by synchrotron white beam X-ray topography. The comparison of BP's Raman positions indicated the existence of tensile strain in the films when deposited on bulk AlN substrate whereas compressive strain was evident on AlN templates on sapphire substrates. HRXRD and Raman spectroscopy results revealed that the deposited BP films were mostly relaxed although small residual strain could be still present. Confocal Raman imaging showed uniform peak shift and FWHM values across the scanned area, except at the pits on the surface. Raman imaging revealed that BP films had better crystalline quality when grown on AlN/sapphire compared to 4H-SiC and 3C-SiC(100)/Si substrates. The preliminary Hall Effect measurements of BP films on AlN/sapphire substrates showed the films were *n*-type with a highest electron mobility of 37.8 $cm^2/V{\cdot}s$ and a lowest carrier concentration of $3.15x10^{18}$ cm^{-3}. The films adhered well to the AlN substrates and were crack-free. The reported results so far in this work confirmed that AlN is a superior substrate for epitaxial BP films with promising potential for further enhancement of BP properties.

Chapter 4 - Growth of BP on 4H-SiC Substrates

4.1 Hexagonal Silicon Carbide (4H-SiC and 6H-SiC)

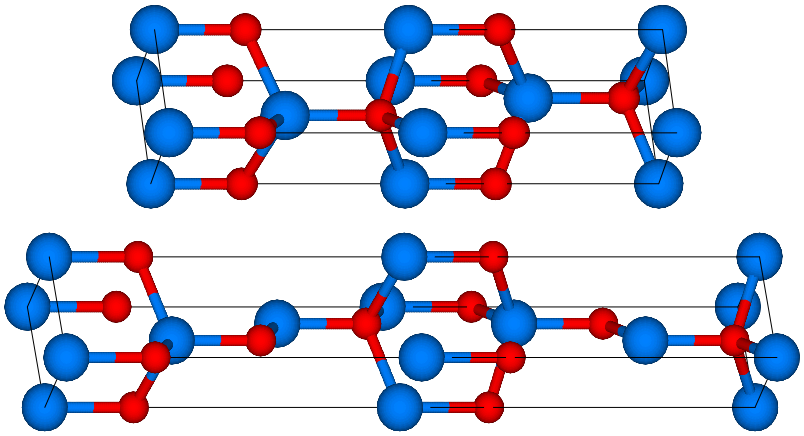

Figure 4.1 Hexagonal unit cell of 4H-SiC (top) and 6H-SiC (bottom)

Silicon carbide is a synthetically produced crystalline compound of Si and C having a chemical formula of SiC. It exists in many different polytypes that vary in the stacking order of the close-pack planes along the *c*-axis causing variations in crystal symmetry such as hexagonal, rhombic, and cubic. However, only three of all those SiC polytypes are commercially available, including cubic SiC (3C-SiC) and hexagonal 4H-SiC and 6H-SiC. SiC has many interesting properties such as excellent thermal stability, chemical inertness, high hardness and high thermal conductivity.

Three polytypes of SiC, namely 4H-SiC, 6H-SiC and 3C-SiC substrates were explored for BP epitaxy in this work due to the following reasons. SiC establishes a smaller lattice constant mismatch (4.1 to 4.5%) with BP compared to Si (16.4%), and sapphire (32.6%) substrates. Also, it has a nearly identical thermal expansion coefficient to that of BP from 300 K to 1200 K, as shown in Figure 4.2.[69] Due to the smaller lattice mismatch and identical thermal expansion, SiC has the potential to lower defect densities in BP films and better control of its crystal orientation. In addition, thermal strain in BP films can be minimized and growth of thick BP films devoid of cracks can be achieved on these substrates. Past studies of BP on Si substrates confirmed the diffusion and incorporation of Si impurities from the Si substrate into the BP films when deposited at elevated temperatures (discussed in Chapter 1.4). The excellent thermal stability and chemical

inertness of SiC can facilitate BP deposition at much higher temperatures above 1000°C and potentially minimize autodoping of BP films from the substrate.

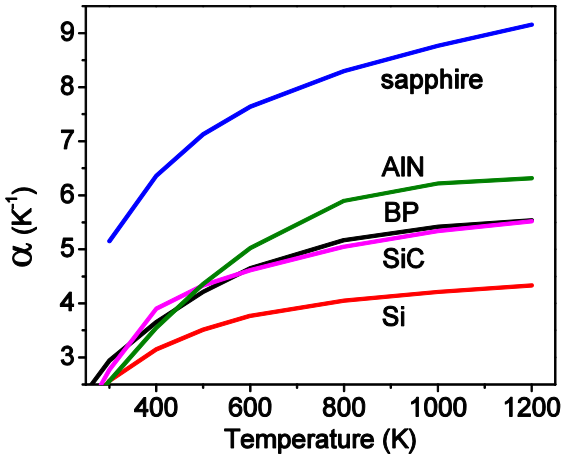

Figure 4.2 Coefficients of thermal expansion of BP, Si, sapphire, SiC and AlN

There were very few reports of BP on SiC substrates mentioned in the literature. Chu *et. al*[11] (1971) reported the growth of BP films using two types of reactions: thermal decomposition of PH_3-B_2H_6 mixtures in H_2 and thermal reduction of BBr_3 and PCl_3 mixtures with H_2. BP deposition using hydride reaction was carried out at 900°C and using halide reaction was done at 850 to 1150°C. Although epitaxial relationship was reported, the BP films deposited on SiC substrate had two equivalent {111} orientations related by two-fold rotation, confirming rotational twinning.

Udagawa *et. al*[56] reported the growth of BP epitaxial films on 6H-SiC(0001) substrates in 2005. The epitaxial relationship between BP and 6H-SiC was (0001), <11$\bar{2}$0>-SiC // (111), [110]-BP. They also confirmed the rotational BP(111) twins and random configuration of atomic planes at the BP-SiC interface.

The most recent work on BP films on SiC substrates was reported by Li[70] in 2013. The optimum growth temperature to grow best quality BP films was determined as 950°C on a C-face epi-ready 4H-SiC wafer with 4° offcut. The optimum gas flow rates were 2500 sccm of H_2, 100 sccm of PH_3 (5% in H_2) and 20 sccm of B_2H_6 (1% in H_2). He determined that the lattice-mismatch strain relief process brings about twins, stacking faults, accompanied dislocation loops, and misfit dislocations at the interface. Rotational twins were observed in BP films grown on C-face 4H-SiC tilted 4° toward [11$\bar{2}$0] direction.

Although hexagonal substrates such as 4H-SiC, 6H-SiC, AlN and ZrB_2 have many advantages, past studies of BP on 4H-SiC(0001) confirmed the existence of stacking faults and rotational twins defects about the BP(111) plane.[11,57,71] Rotational twin defects are the most common type of defect among III-V compound semiconductors and have been a concern when deposited heteroepitaxially. These defects form when the substrate material has a higher symmetry than the epilayer crystal. For example, BP prefers the (111) orientation when deposited on a (0001) plane of a hexagonal substrates. BP(111) has a three-fold rotational symmetry whereas the (0001) plane of the hexagonal substrates has a six-fold rotational symmetry. This difference in crystal symmetry allows two orientations of BP(111), that are related by a rotation of 180°, to be deposited on the (0001) plane leading to rotational twinning (see Figure 4.3). Rotational twin defects could significantly affect the electrical properties of BP, such as lifetime of minority carriers and carrier mobility.

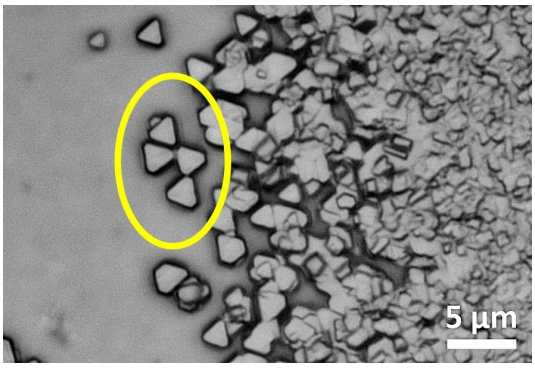

Figure 4.3 Rotational BP(111) twins on an on-axis 4H-SiC(0001) substrate

Zhang *et al*[72] reported that use of off-axis 4H-SiC(0001) substrates tilted 8° toward the $[1\bar{1}00]$ direction eliminated rotational twinning in icosahedral boron arsenide ($B_{12}As_2$) epitaxial films. A similar approach was employed in this work by using off-axis 4H-SiC substrates to eliminate/minimize rotational twinning in BP. Typically, when a 4H-SiC(0001) wafer is cut at an angle (θ) from a low-index plane in a specific direction, its surface breaks up into monoatomic steps with precise oriented steps and terraces, as shown in Figure 4.4. The off-cut angle and direction control the size of exposed crystal planes that were formed after the steps were etched in hydrogen. The sequence of formation of steps, in turn, influence the orientation of incoming adatoms and thus formation of rotational twins. In addition to the elimination of rotational twinning, off-axis substrates enable better control of the nucleation mechanism and can potentially improve the overall crystal quality of the films.

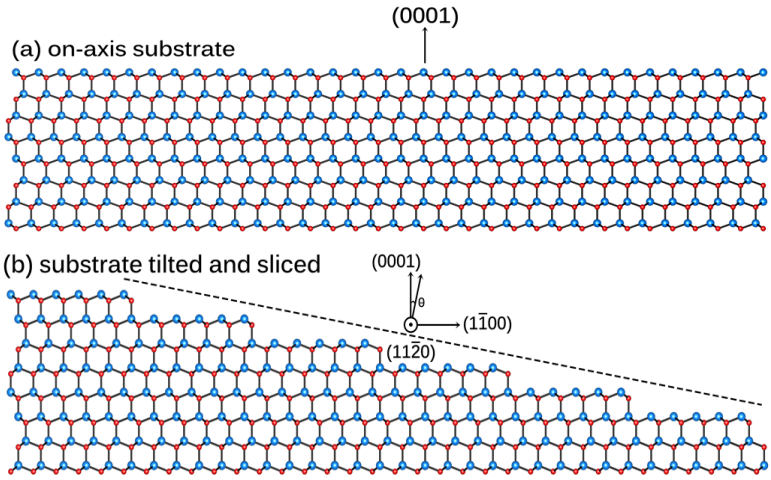

Figure 4.4 Formation of steps and terraces on the surface of 4H-SiC when sliced at an angle (θ) toward [1$\bar{1}$00] direction.

Although SiC substrate has many advantages, its full potential as a substrate for growing BP films was not thoroughly established. Except very few reports in the literature, BP epitaxy on SiC substrates and its overall properties with respect to various growth conditions were not fully established. In this work, BP epitaxy on a variety of 4H-SiC(0001) and 6H-SiC(0001) substrates with both on-axis and off-axis orientations was studied in detail. The effect of process variables such as temperature, reactant flow rates, and substrate polarity on the structural and electrical properties of BP were investigated.

4.2 Experimental Methods and Conditions

BP films were deposited on 4H-SiC and 6H-SiC substrates with on-axis and off-axis orientations: Si-face 4H-SiC(0001) tilted 4° toward [1$\bar{1}$00], Si-face 4H-SiC(0001) tilted 4° toward [1$\bar{2}$10], C-face 4H-SiC(0001) tilted 4° toward [1$\bar{1}$00], Si-face on-axis 6H-SiC(0001), and Si-face 6H-SiC(0001) tilted 3.5° toward [1$\bar{2}$10]. Ultra-high purity phosphine (99.999% PH_3) and diborane (1% B_2H_6 in H_2) were the reactant gases and ultra-high purity hydrogen (99.99999%) purified through a palladium membrane purifier was the carrier gas. More details of the CVD system and deposition process used are given in Chapter 2.1.

Substrates were subjected to *in situ* hydrogen etching at 1650°C for about 15 min prior to BP deposition, to produce atomically flat terraces on the substrate surface.[73] BP films were grown

in the temperature range of 1000 to 1200°C and at gas flow rates in the range of 40 to 200 sccm of PH_3, 20 to 80 sccm of B_2H_6 (1% in H_2), and 3000-8000 sccm of H_2. BP films were grown at three temperatures (1000°C, 1100°C, and 1200°C) at constant reactant flow ratios to study the effect of temperature on growth rate, morphology, and crystalline orientation. The effect of reactant flow rates on the growth rate, surface roughness and overall crystal quality was evaluated by changing the PH_3/B_2H_6 flow rate ratios at each temperature (1000°C, 1100°C and 1200°C). All depositions were performed at 700 torr.

4.3 Results and Discussion

4.3.1 Growth and Morphology of BP Films

During the initial BP depositions, the deposition temperature, flow rates of PH_3 and B2H6, their ratios, and substrate type strongly influenced the morphology, crystal orientation, and film quality. BP films were deposited on both Si-face and C-face SiC(0001) substrates at identical deposition conditions, and their crystalline quality was compared to study the effect of substrate polarity. There was no significant difference in crystalline orientation of BP(111) plane on Si-face and C-face 4H-SiC, but films deposited on C-face substrate had deeper etch pits and rougher surfaces compared to the Si-face substrates. This was perhaps due to the fast etching of C-face during *in situ* hydrogen etching, resulting in deeper etch pits compared to the Si-face. X-ray topography analysis showed large strain in the BP film deposited on C-face 4H-SiC substrate compared to the Si-face 4H-SiC and 6H-SiC substrates. Therefore, growth on Si-face 4H-and 6H-SiC(0001) substrates became the focus of this study.

BP films deposited on 4H-SiC substrates were highly oriented and had better crystalline quality compared to 6H-SiC substrates, due in part to the lower quality of 6H-SiC compared to 4H-SiC. Therefore, a majority of films were deposited on 4H-SiC(0001) tilted 4° toward $[1\bar{1}00]$ and 4° toward $[1\bar{2}10]$, and the properties of BP were compared. Morphologies of BP films grown at temperatures 1000°C, 1100°C, and 1200°C on a Si-face 4H-SiC(0001) tilted 4° toward $[1\bar{1}00]$ and $[1\bar{2}10]$ are shown in Figure 4.5. Films deposited at 1000°C typically had small grains with no geometrical features or specific crystalline orientation. At 1100°C, grain size was larger and crystallites appeared to have triangular features oriented in a specific direction. At 1200°C,

crystallites had regular three-fold symmetric triangular features, and individual small grains merged to form a larger grain with preferred crystalline orientation.

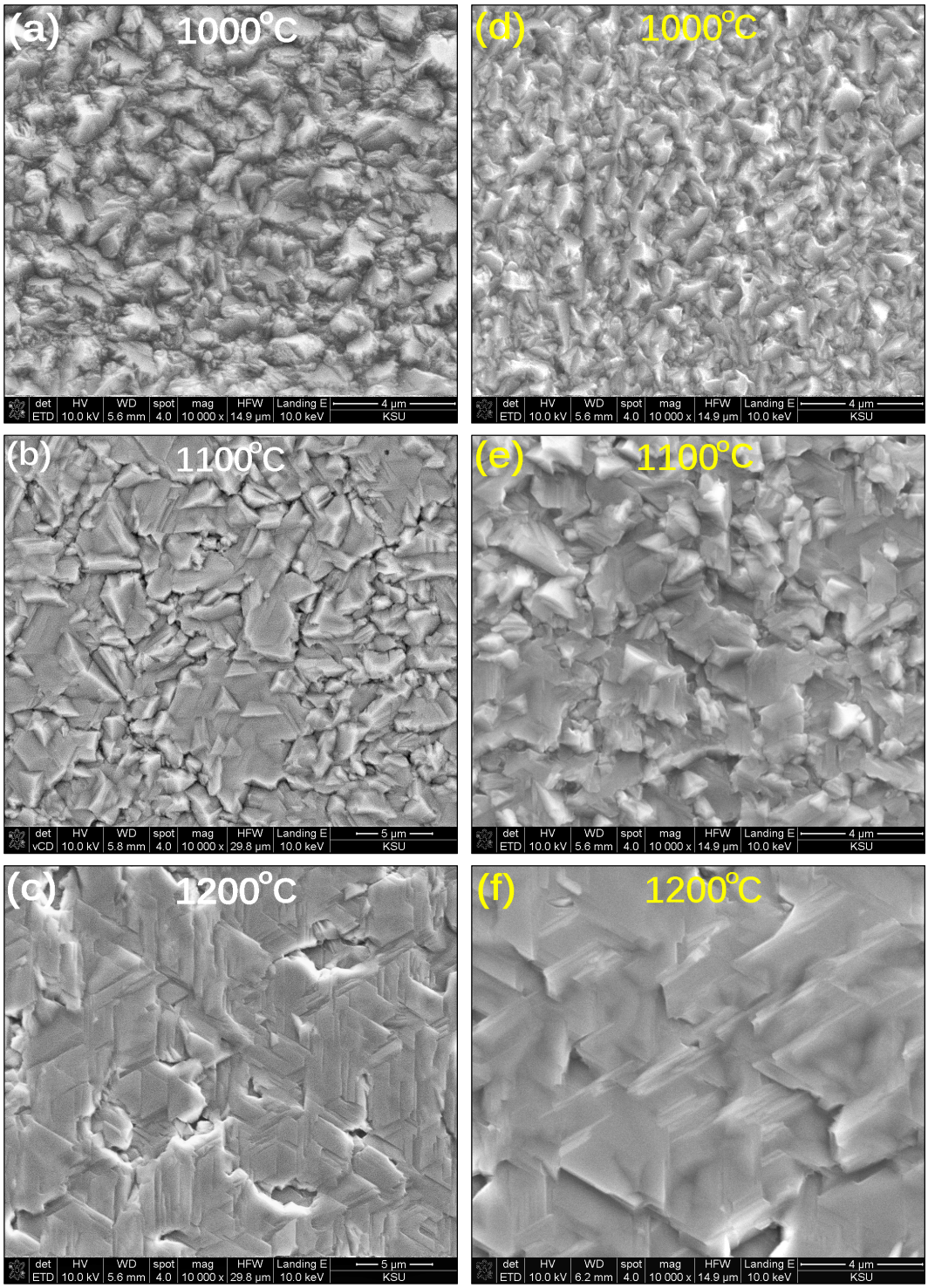

Figure 4.5 SEM micrographs of BP films deposited on Si-face of 4H-SiC(0001) tilted 4° toward (a, b and c) $[1\bar{1}00]$ and (d, e, and f) $[1\bar{2}10]$ at different temperatures.

At higher temperatures (1200°C), individual adatoms were more mobile and aggregate to form a larger gain size and were incorporated preferably at step edges instead of terraces on the substrate surface, resulting in controlled nucleation. Hence, epitaxial film growth resulted due to the advancement of steps along the terraces, which is typical of a step-flow growth mode. A similar trend in crystalline orientation and grain size was observed for BP films grown on other 4H-SiC and 6H-SiC substrates under similar reaction conditions, with only difference in grain size between substrates. In general, growth rate at 1200°C was approximately 5-6 µm/hr.

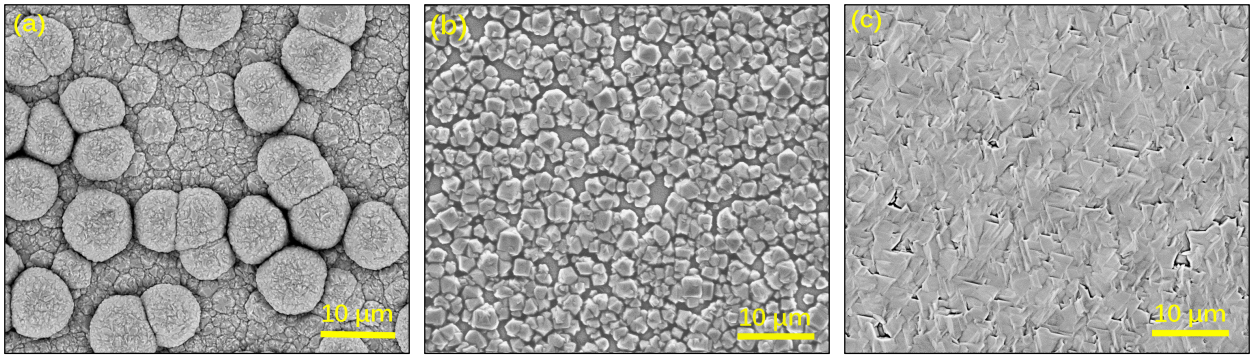

Figure 4.6 (a) Polycrystalline BP film with spheres on the surface grown at high reactant flow rates. (b) Polycrystalline film grown at lower flow rates (c) Smoother and crystalline film grown at optimum flow rates.

As already explained, BP decomposes to $B_{12}P_2$ at higher temperatures; excess phosphine was used to maintain a high phosphorus vapor pressure in order to prevent the decomposition. Consequently, the deposition rate was limited by the diborane flow rate. Initial depositions were performed at 1150°C with gas flow rates of 3500 sccm H_2, 80 sccm PH_3 and 80 sccm B_2H_6 (1% in H_2). These films had rough surfaces with a large number of spheres (or ballas) on the surface formed due to high supersaturation and rapid deposition of reactant materials on the surface (Figure 4.6a). When PH_3 and B_2H_6 (1% in H_2) flow rates were reduced below 30 sccm and 20-30 sccm, respectively, to control the deposition rate, thin, non-uniform and polycrystalline BP films were achieved (Figure 4.6b). Reactant flow rates were subsequently tuned to control the growth rate and to obtain smooth, single crystalline films as shown in Figure 4.6c. The optimum flow rates at temperatures of 1000°C and 1100°C were determined to be 4000 sccm H_2, 40 sccm PH_3 and 20-40 sccm B_2H_6 (1% in H_2).

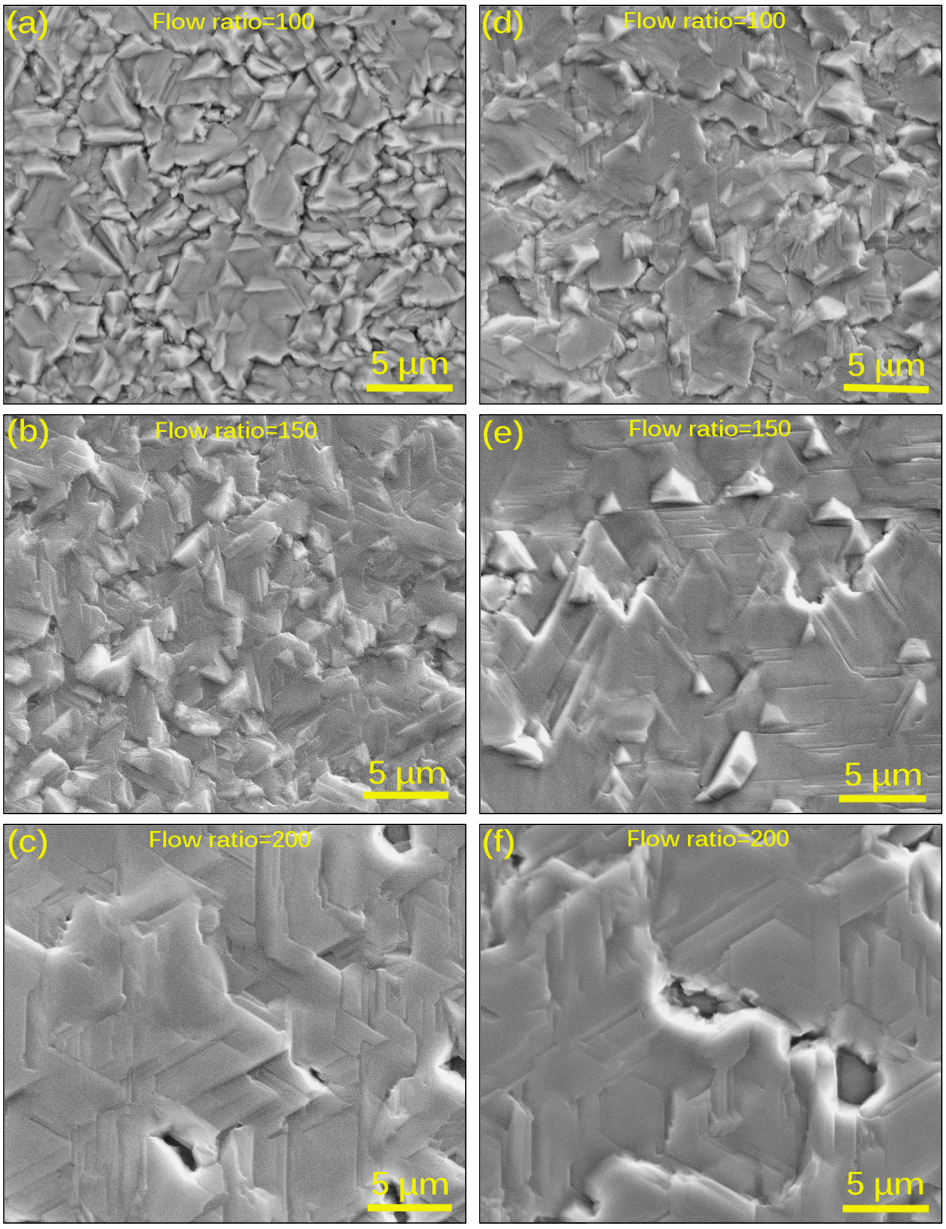

Figure 4.7 Morphology of BP films grown on 4H-SiC(0001) tilted 4º toward (a, b and c) $[1\bar{1}00]$ and (d, e and f) $[1\bar{2}10]$ at 1200ºC and different PH_3/B_2H_6 flow ratios.

Temperatures above 1150ºC required high phosphine flow rates in order to maintain enough phosphorus vapor pressure as it increases exponentially with temperature. Flow rates optimized at 1200ºC were 4000 sccm H_2, 80 sccm PH_3 and 40-80 sccm B_2H_6 (1% in H_2). Figure 4.7 shows SEM micrographs of films deposited on 4H-SiC(0001) tilted 4º toward $[1\bar{1}00]$ and $[1\bar{2}10]$ at 1200ºC and three PH_3/B_2H_6 flow ratios. At a given temperature, for example 1200ºC, when diborane flow rate was decreased, i.e. increased PH_3/B_2H_6 ratio, the crystallites became more

textured and the surfaces were smoother compared to the films deposited at lower PH_3/B_2H_6 ratio. There was no significant change in the crystalline orientation of the films, but the surface roughness decreased with decreasing diborane flow rate, possibly due to a reduced deposition rate.

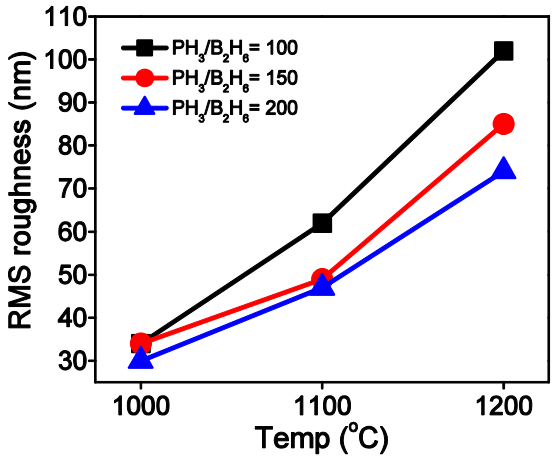

Figure 4.8 RMS roughness values of BP films grown on 4H-SiC(0001) 4° miscut toward $[1\bar{2}10]$ measured by AFM

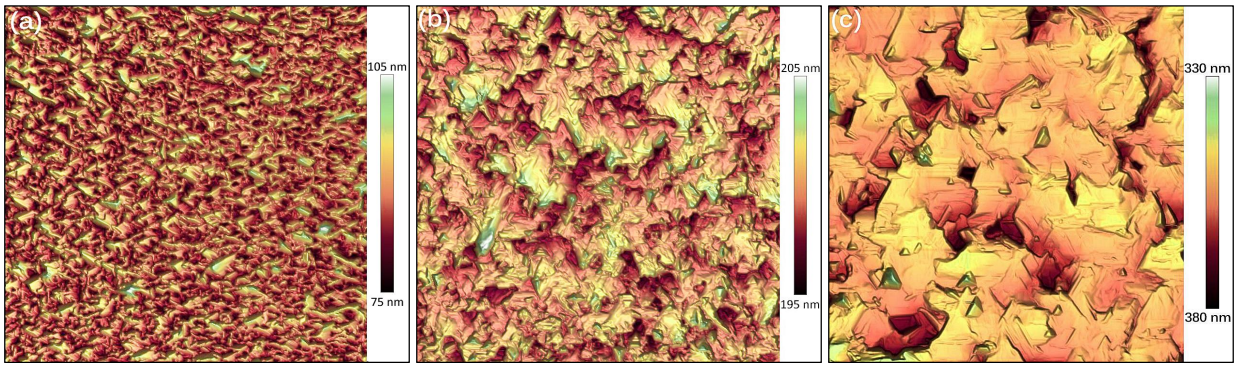

Figure 4.9 AFM images of BP films grown at PH_3/B_2H_6=200 and at temperatures of (a) 1000°C (b) 1100°C, and (c) 1200°C.

A plot of RMS roughness of BP films measured by AFM is shown in Figure 4.8. The surface roughness decreased with increasing the PH_3/B_2H_6 ratio at a fixed temperature, and the magnitude of decrease was highest at 1200°C. At a given PH_3/B_2H_6 ratio (for example PH_3/B_2H_6 =100), surface roughness increased with temperature, perhaps due to increase in reaction rate resulting in thicker films. Figure 4.9 shows the AFM images taken over a range of 30x30 μm^2 of BP films grown on 4H-SiC(0001) tilted 4° toward $[1\bar{1}00]$ at three different temperatures. The grain size increased and better crystalline orientation was obtained at increased temperature at

fixed reactant flow rates, validating the SEM findings. A similar trend of a slight increase in grain size and improved crystalline orientation with increased PH_3/B_2H_6 ratio at a constant temperature was observed.

4.3.2 Crystalline Orientation of BP

A representative θ/2θ scan XRD pattern recorded on BP film deposited on a 4H-SiC(0001) substrate at 1000°C and PH_3/B_2H_6 =200 is shown in Figure 4.10. As stated earlier, BP prefers to align as (111) orientation when deposited on the (0001) face of 4H-SiC, resulting in a major peak in XRD pattern along with peaks from the substrate. However, in addition to the preferred BP(111) peak, unwanted peaks associated with other BP orientations such as BP(200), BP(220) and BP(311) were also detected for a majority of films in the XRD pattern. But the intensity of these unwanted BP peaks were very small compared to the major BP(111) and substrate 4H-SiC(0004) peaks.

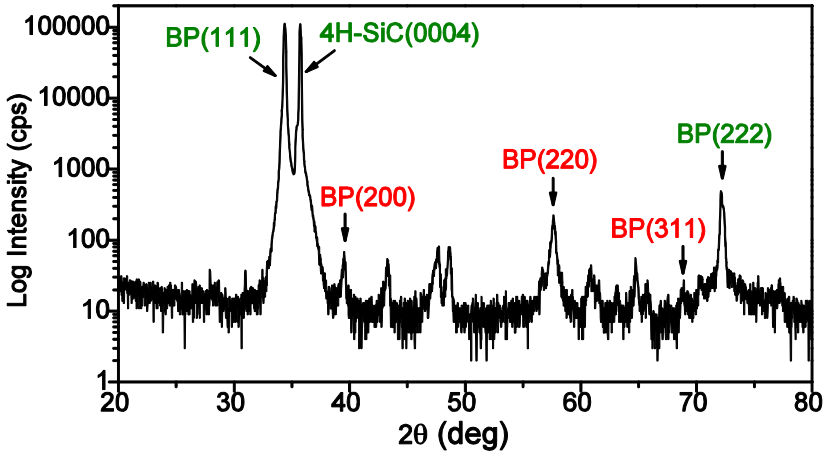

Figure 4.10 θ/2θ scan XRD pattern of BP film deposited at 1000°C and PH_3/B_2H_6 =100 on a 4H-SiC(0001) substrate tilted 4° toward $[1\bar{1}00]$.

It is worth noting that, in addition to the peaks from BP, unwanted BP orientations and 4H-SiC substrate, some small intensity peaks were also present in the XRD pattern. To determine the origin of these peaks, XRD pattern was recorded for a blank 4H-SiC(0001) substrate. After comparing the patterns obtained from a blank substrate with substrate having BP film, most of the small intensity peaks were originating from the 4H-SiC substrate. The crystal quality of BP was assessed by comparing the peak widths of BP(111) and relative intensity ratios of preferred BP(111) with unwanted BP orientations such as BP(111)/(200) and BP(111)/(220). For majority

of BP films, the BP(311) peak was absent, so the assessment of intensity ratio of BP(111)/(311) was ignored. For an ideal single crystalline BP film, the ratios of BP(111)/(200) and BP(111)/(220) should approach infinity.

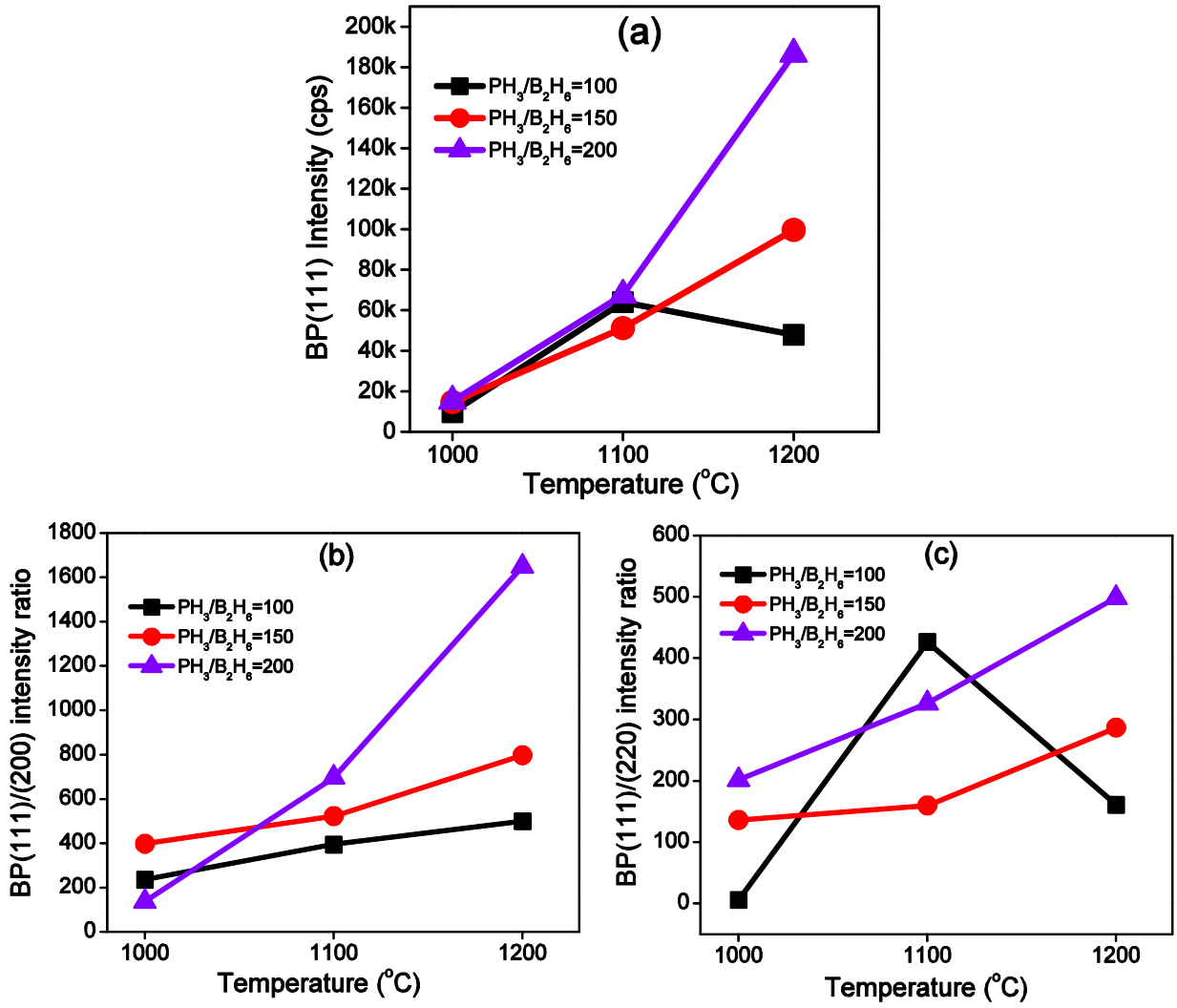

Figure 4.11 (a) BP(111) peak intensity and peak intensity ratios of (b) BP(111)/BP(200), and (c) BP(111)/BP(220) orientations obtained from XRD of BP films grown on 4H-SiC(0001) 4° miscut toward [$1\bar{1}00$].

XRD data of films grown at three temperatures (1000°C, 1100°C, and 1200°C) each with three PH_3/B_2H_6 ratios (100, 150 and 200) were plotted in Figure 4.11. For the majority of films, BP(111) peak intensity increased with temperature at a fixed PH_3/B_2H_6 flow ratio (150 and 200), with the exception for the curve PH_3/B_2H_6=100. The increase in peak intensity was moderate at 1100°C for all three PH_3/B_2H_6 ratio curves, but was steepest at 1200°C for the curve

PH_3/B_2H_6=200. This increase may be partially attributed to deposition of thicker films at higher temperatures due to increased reaction rate. The ratios of BP(111)/BP(200) and BP(111)/BP(220) are shown in Figure 4.11b and c, respectively. Both ratios increased with temperature for a given PH_3/B_2H_6 ratio in most cases; the steepest increase was observed for films grown at 1200°C and PH_3/B_2H_6=200. This confirms that a controlled nucleation and growth, resulting in improved crystalline orientation, was obtained at higher temperature. The highest peak intensity ratios for BP(111)/BP(200) was 1651 and for BP(111)/BP(220) was 499, the highest ever reported in the literature for BP epitaxial films on 4H-SiC substrates.

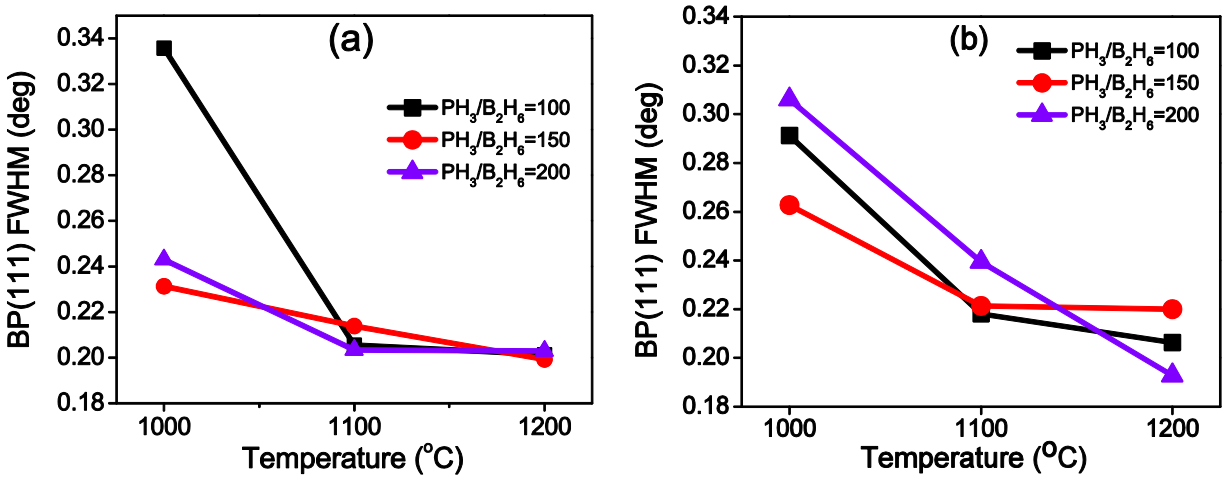

Figure 4.12 FWHM curves of BP(111) deposited on 4H-SiC(0001) 4° miscut toward (a) $[1\bar{1}00]$, and (b) $[1\bar{2}10]$ directions.

The full width at half maximum (FWHM) of BP(111) peak extracted from θ/2θ scans at various reaction conditions are shown in Figure 4.12a and b. For both type of substrates, FWHM sharply decreased as the temperature increased from 1000°C to 1100°C for the curve PH_3/B_2H_6=100, while the decrease was moderate for the other two. The peak width was narrowest at 1200°C for all these three PH_3/B_2H_6 curves. The lowest value of FWHM was 0.19° for film deposited at 1200°C at PH_3/B_2H_6=200 on 4H-SiC(0001) 4° miscut toward $[1\bar{2}10]$ direction. The XRD analysis led to the conclusion that the highest and steepest increase in BP(111) peak intensity, highest relative peak height ratios and narrowest BP(111) peak widths indicate that crystalline quality of the films improved by increasing the deposition temperature and increasing the PH_3/B_2H_6 ratio. This conclusion suggests that higher temperature and reduced diborane flow rate

will enable controlled nucleation at the step edges and improve crystalline orientation of incoming adatoms.

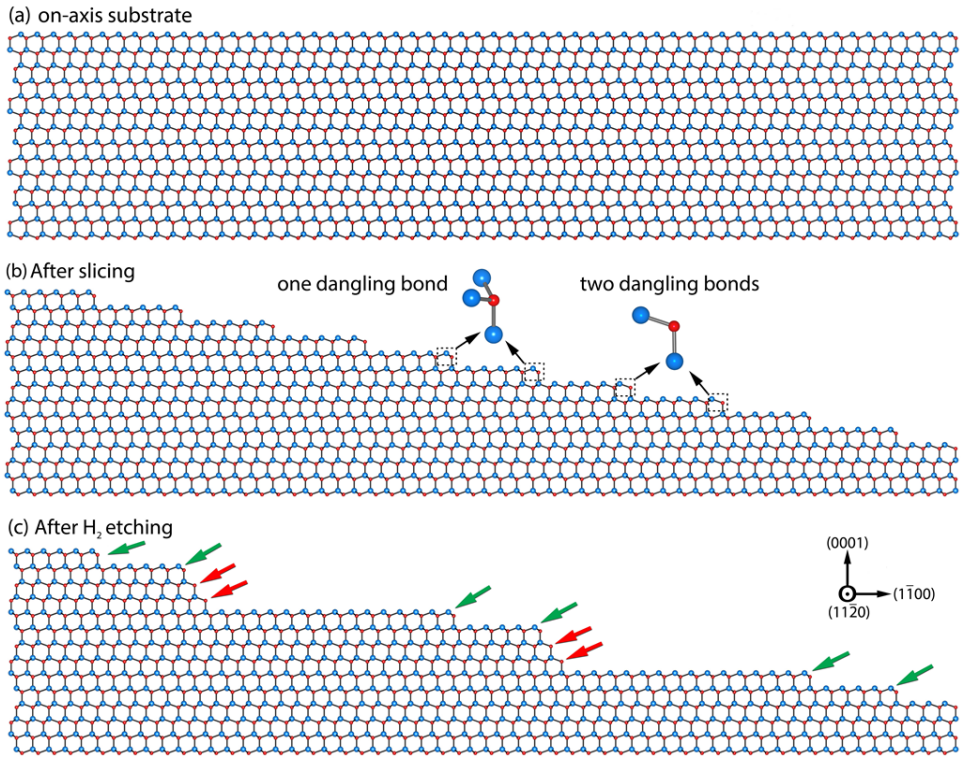

Figure 4.13 Formation of zinc-blende and wurtzitic steps on 4H-SiC surface tilted toward [1$\bar{1}$00] direction

As stated in the objectives of this research work, intentionally misoriented 4H-SiC(0001) and 6H-SiC(0001) substrates were investigated for their ability to eliminate rotational twinning in BP. When a 4H-SiC(0001) wafer is cut slightly misoriented from a low-index (0001) plane in a specific direction such as [1$\bar{1}$00] or [1$\bar{2}$10] direction, its surface breaks up into monoatomic steps with precisely oriented steps as shown in Figure 4.13. These step edges will have atoms with both single dangling bond or double dangling bonds.[72] The length of the terraces depends on the miscut angle and direction. When the surface is etched in H_2, the steps with two dangling bonds react faster compared to the steps with one dangling bond. As the etching process progresses, the atoms with two dangling bonds etch off fast until they meet with the steps having single dangling bonds. After etching, steps and terraces form on the surface (Figure 4.13c). In case of 4H-SiC(0001) tilted 4° toward [1$\bar{1}$00], all the steps will be formed in parallel whereas zigzag steps will be formed when tilted 4° toward [1$\bar{2}$10] direction. The typical pattern of these step and terrace formations

allow either one orientation of BP(111) or two orientations of BP(111), resulting in rotational twinning.

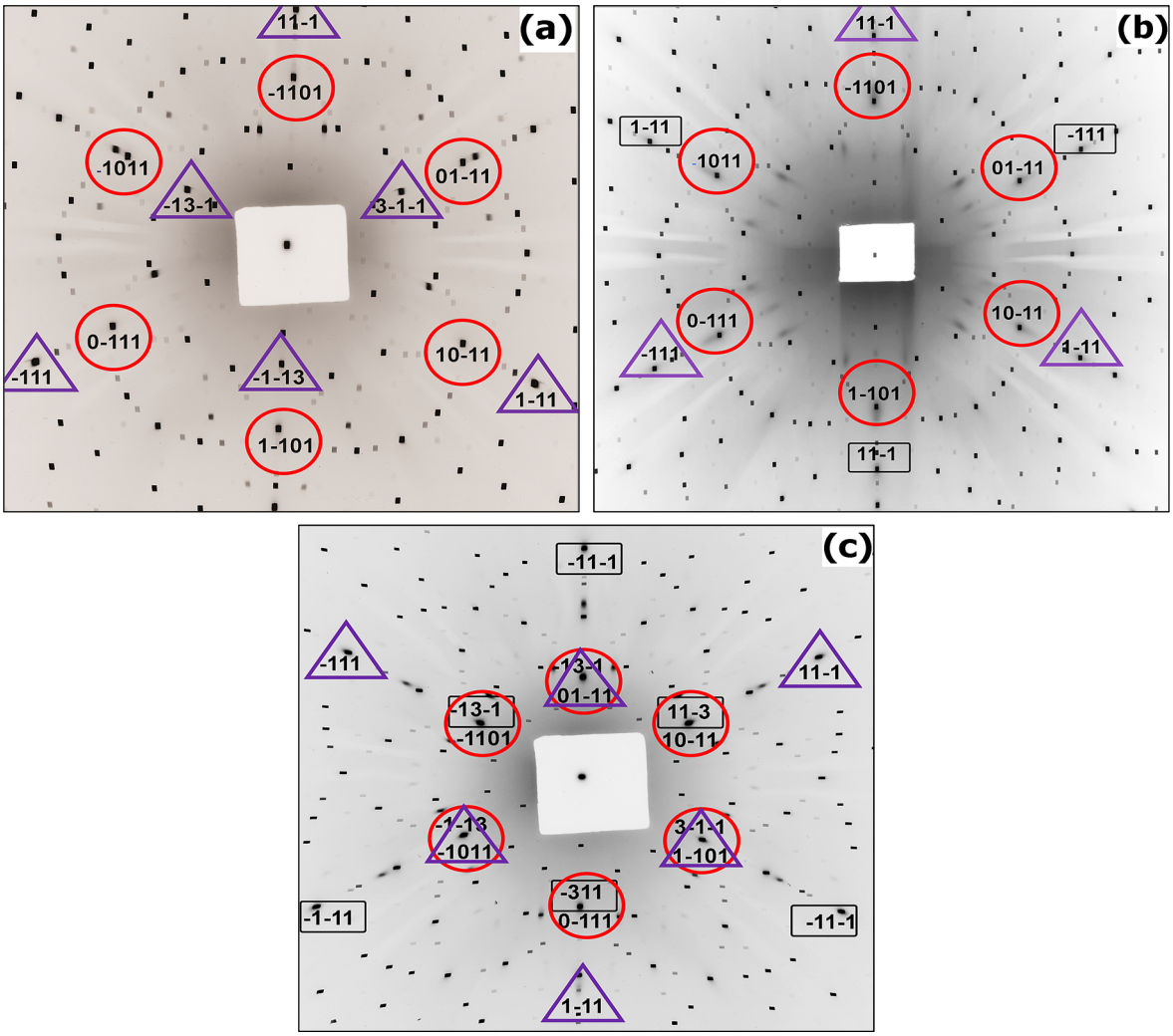

Figure 4.14 Transmission X-ray diffraction patterns of BP films on (a) 4H-SiC 4º miscut toward [$1\bar{1}00$], (b) 4H-SiC 4º miscut toward [$1\bar{2}10$], and (c) on-axis 6H-SiC substrate. Diffraction spots marked in red circles are from the substrate, violet triangles from BP (111) plane and black rectangles from BP (111) twins.

Synchrotron white beam x-ray topographs taken on BP films deposited on 4H-SiC(0001) tilted 4º toward [$1\bar{1}00$], 4H-SiC(0001) tilted 4º toward [$1\bar{2}10$] and on-axis 6H-SiC(0001) are shown in Figure 4.14. Diffraction spots from BP(111) on the 4H-SiC miscut toward [$1\bar{1}00$] had a single orientation with well-defined and free from long range and inhomogeneous strains as shown in Figure 4.14a. During epitaxy, BP crystallites preferentially nucleated at the lower energy

zincblende step and bonded to a terrace and vertical step riser on which only one orientation of BP can nucleate, thereby eliminating rotational twinning. In contrast, diffraction spots revealed two orientations (rotational twins) of BP(111) for BP deposited on 4H-SiC miscut toward [$1\bar{2}10$] and on-axis 6H-SiC substrate, as there was no control on the crystallites nucleation and their orientation. The Laue spots were slightly elongated in the former case (Figure 4.14b), while they were more elongated for on-axis 6H-SiC (Figure 4.14c) compared to the other two substrates, indicating residual strain in the films. The epitaxial relationship between BP film and the SiC(0001) substrates was $(111)_{BP}\langle 11\bar{2}\rangle_{BP} \parallel (0001)_{SiC}\langle 1\bar{1}00\rangle_{SiC}$.

4.3.3 Strain Evaluation of BP Films

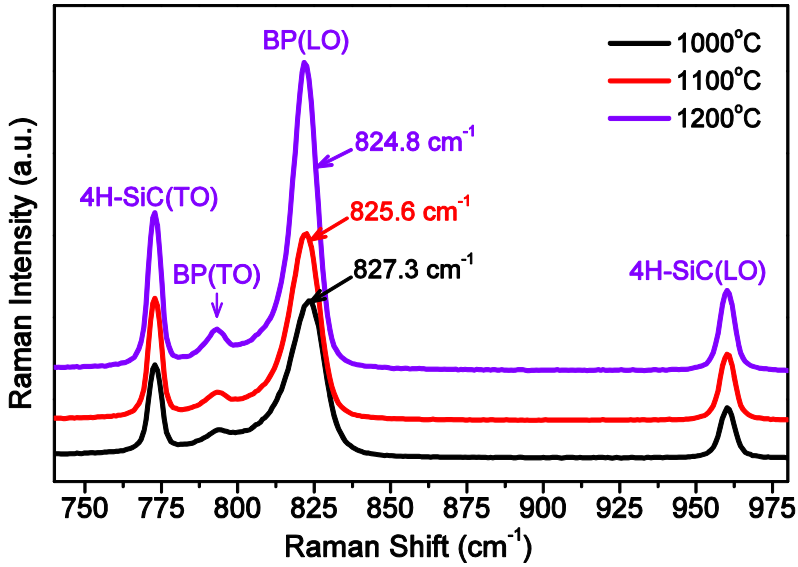

Figure 4.15 Raman spectra obtained from BP films deposited on 4H-SiC(0001) 4° miscut toward [$1\bar{2}10$] directions at PH_3/B_2H_6 =200.

Raman spectra of BP films grown on 4H-SiC substrate tilted 4° toward [$1\bar{2}10$] direction at three temperatures is shown in Figure 4.15. The spectra exhibited two bands: a weak transverse-optical (TO) phonon mode around 794 cm^{-1} and a strong longitudinal-optical (LO) phonon mode around 824-827 cm^{-1}. Peaks at 776 cm^{-1} and 964 cm^{-1} corresponded to TO and LO phonon modes of 4H-SiC(0001) substrate. These phonon peak positions are in agreement with the literature values reported for BP films.[3,12,13] BP peak position shifted to the lower value when the temperature increased from 1000°C to 1200°C. In addition, resolution of the weak TO band that appeared at approximately 794 cm^{-1} improved when the temperature increased. Raman spectra

taken on each sample having an area of 10x10 mm^2 at various locations showed more or less similar values of phonon modes indicating that the films are homogeneous. No additional peaks associated with the presence of icosahedral boron phosphide ($B_{12}P_2$), which typically forms at higher temperatures, were evident.

Table 4.1 FWHM values of BP(LO) peak on 4H-SiC(0001) at various reaction conditions.

Temp (°C)	FWHM (cm^{-1})		
	PH_3/B_2H_6 =100	PH_3/B_2H_6 =150	PH_3/B_2H_6 =200
1000	14.7	13.8	12.3
1100	11.7	11.3	11.3
1200	10.1	9.5	9.5

FWHM values of the BP(LO) peak measured on 4H-SiC(0001) 4° miscut toward [$1\bar{2}10$] are shown in Table 4.1. Narrow peak widths were obtained with increased temperature at a fixed flow ratio (for example PH_3/B_2H_6=100). Similar trend was observed with increased PH_3/B_2H_6 ratio (reduced diborane flow rate) at a given temperature. When the FWHM values at 1000°C, 1100°C, and 1200°C are compared at each PH_3/B_2H_6 ratio (100,150 and 200), the extent of decrease in peak width with temperature is more notable at 1200°C, suggesting that higher temperatures enabled better crystalline quality. The lowest FWHM value obtained was 9.5 cm^{-1} at 1200°C and PH_3/B_2H_6 ratios of 150 and 200.

Confocal Raman imaging of BP films on 4H-SiC(0001) tilted 4° toward [$1\bar{1}00$] was performed to investigate the film quality and residual strain. The image of BP film captured by the CCD camera along with the scanned area (white box) is shown below. The statistical details of the peak values are given in Table 3.2. In the peak shift map (Figure 4.16a), there were some areas of decreased frequency visible indicating small tensile strain as well as few areas having increased frequency indicating compressive strain in the film. These variations of peak shift resulted due to strain in the BP films in the form of dislocations and defects at local points in the scanned area. Strain in BP could be due to lattice mismatch, difference in thermal expansion, defect generation in BP, propagation of defects and dislocation from the starting bare 4H-SiC substrate or combination of these phenomena.

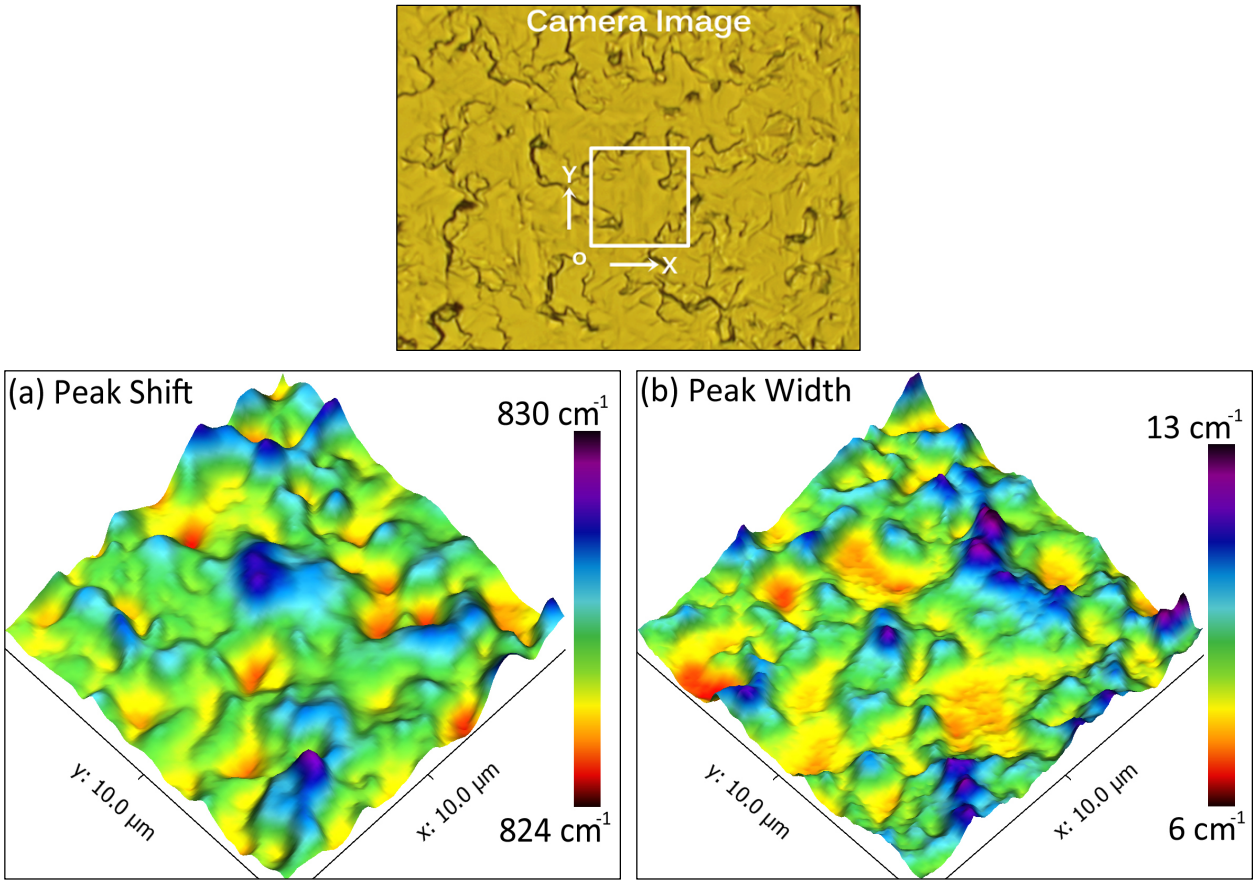

Figure 4.16 Raman images of BP film showing (a) peak shift from center position and (b) FWHM of BP(LO) peak.

It is also important to note that the starting 4H-SiC substrate had few defects on the surface prior to the deposition (see Figure 4.17). Hence, it is very important to have a high quality starting substrate with minimum defects. The peak width map also shows similar variation across the scanned region. The standard deviation (0.98) is almost twice the value measured on an AlN/sapphire substrate.

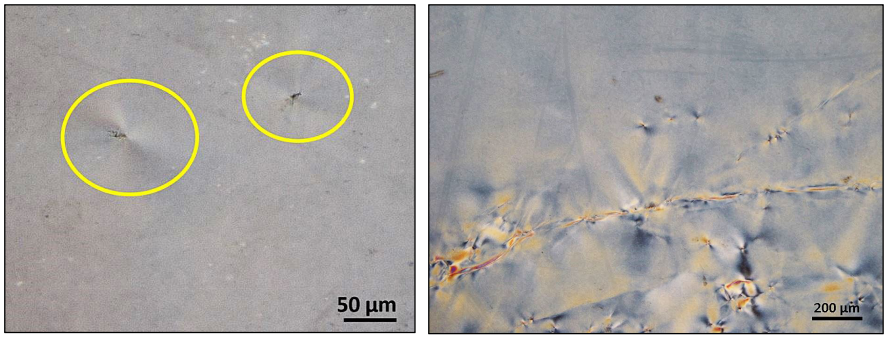

Figure 4.17 Pin holes and defects present on bare 4H-SiC prior to the BP deposition

Out-of-plane strain in the BP films was assessed by measuring the BP(111) ω-2θ rocking curves using HRXRD. The theoretical lattice mismatch and the measured mismatch were calculated as per the procedure given in chapter 2.4.6. The strain values of BP films on various types of SiC substrates are given in Table 4.2. While there was no consistent trend, the strain values measured on 4H-SIC substrates is higher than the AlN/sapphire substrates. The strain values were randomly different for each type of substrates, which could be mostly due to the difference in crystal quality of the substrates. Interestingly, BP films thicker than 15 μm deposited on 4H-SiC and 6H-SiC substrates were cracked occasionally, perhaps due to tensile strain in the films.

Table 4.2 Out-of-plane strain values of BP films on various types of SiC substrates

Substrate	Temp (°C)	PH_3/B_2H_6	ω FWHM (arcsec)	ω-2θ FWHM (arcsec)	Theoretical Mismatch (%)	Measured mismatch (%)	Out-of-plane strain (%)
4H-SiC, 4° off [1$\bar{1}$00]	1000	200	1592	500	4.25	3.92	-7.70
	1100	200	1653	463		4.04	-4.92
	1200	200	1612	863		4.02	-5.30
4H-SiC, 4° off [1$\bar{2}$10]	1000	200	1314	852		4.36	2.54
4H-SiC, P-type, 8° off [1$\bar{1}$00]	1200	100	1350	830		3.38	-20.55
6H-SiC, P-type, 3.5° off [1$\bar{2}$10]	1100	100	2349	926	4.04	3.91	-3.27

4.4 Conclusions

One of the significant result in this study is that 4H-SiC(0001) tilted 4° toward [1$\bar{1}$00] could eliminate the rotational twinning in BP. The epitaxial growth of BP films on 4H-SiC and 6H-SiC(0001) substrates with on-axis and off-axis orientations was investigated. The deposition temperature is one of the most important process parameter which can affect the morphology, crystallites orientation, crystal quality and strain level. Improved crystal quality was achieved at higher temperatures because of incoming atoms have higher mobilities on the surface along with higher activation energies for surface diffusion and bulk diffusion. SEM, AFM, XRD and Raman spectroscopy analysis confirmed these results. Sufficient reactant flow rates and ratios are necessary to grow crystalline films with good surface coverage and smoothness.

Raman spectroscopy revealed tensile strain in the films and because of this reason thicker BP films on these substrates cracked occasionally. It also revealed that starting with a high quality 4H-SiC substrate, strain and defects in the BP films could be minimized. Synchrotron white beam x-ray topography confirmed the presence of rotational twin defects in BP when deposited on on-axis 6H-SiC and 4H-SiC miscut 4° toward $[1\bar{2}10]$, but was absent when grown on 4H-SiC(0001) miscut 4° toward $[1\bar{1}00]$ substrate. The epitaxial relationship confirmed by X-ray topography between BP film and 4H-and 6H-SiC substrates was $(111)_{BP}\langle 11\bar{2}\rangle_{BP} \parallel (0001)_{SiC}\langle 1\bar{1}00\rangle_{SiC}$. Among various types of 4H-SiC and 6H-SiC substrates, the best substrate choice for BP epitaxy was 4H-SiC(0001) miscut 4° toward $[1\bar{1}00]$ because it did not produce rotational twins defects.

Chapter 5 - Growth of BP Films on 3C-SiC Substrates

5.1 Cubic Silicon Carbide (3C-SiC)

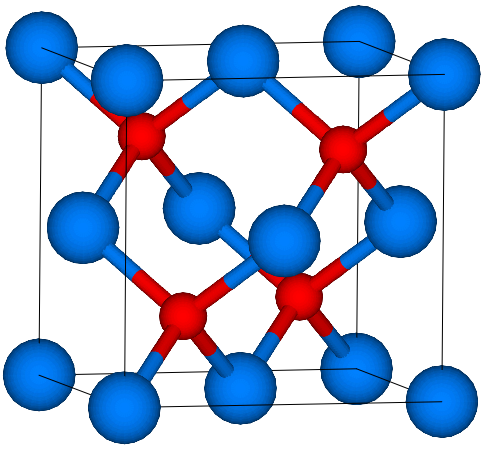

Figure 5.1 Unit cell of zinc blende 3C-SiC

Cubic silicon carbide (3C-SiC), also known as β-SiC, is the most attractive SiC polytype as a substrate for BP epitaxy as both materials have the zincblende structure. Due to the match in crystal symmetry, 3C-SiC has the potential to eliminate in-plane rotational twinning in BP films and variations in stacking sequence at the interface. As discussed earlier, generation of rotational twin defects are common when the substrate material has a higher symmetry than the epilayer crystal. These defects significantly contribute to the modification of electrical properties of BP, such as lifetime of minority carriers and carrier mobility. Other appealing properties of 3C-SiC as a substrate include its isotropic properties, high thermal stability, small lattice constant mismatch (4.1%), and nearly identical coefficients of thermal expansion with BP.[68,69] 3C-SiC has a wide bandgap (2.2 eV) and high electron mobility of ~900 $cm^2/V \cdot s$[74] compared with other SiC polytypes, making it suitable for making heterojunction devices with BP.

Bulk 3C-SiC single crystals with large surface areas would be ideal for growing BP films, but they are not widely available due to the difficulty in growing bulk 3C-SiC crystals. 3C-SiC epitaxial layers deposited on Si substrate is the best current option for obtaining large-area single crystal substrates of this polytype, which are commercially available now a days. These substrates are relatively inexpensive and are available in different orientations. Past studies have shown Si contamination in BP films deposited directly on Si via autodoping and diffusion of Si atoms from

Si substrate into the BP films. Si contamination could possibly be minimized using a 3C-SiC epilayer on Si since the diffusion of Si atoms in SiC is very low at typical deposition temperatures.[75] Furthermore, employing 3C-SiC on 4H-SiC(0001), produced by Jokubavicius et al,[76,77] could minimize Si contamination prevalent with Si substrates significantly. 3C-SiC/4H-SiC substrates have an additional advantage of enabling the deposition of BP at much higher temperatures compared to 3C-SiC/Si due to the enhanced thermal stability of 3C-SiC on 4H-SiC over Si. There are only a few prior reports of BP epitaxy on 3C-SiC in the literature. Li[70] investigated the growth of BP films on a 3C-SiC template, but epitaxy was not achieved; the film was a mixture of amorphous and polycrystalline BP. Li attributed it to the poor quality of initial 3C-SiC epilayer which was thin and non-uniform.

The present study investigates the CVD growth and a detailed characterization of BP films grown on various orientations and types of 3C-SiC substrates. The effects of process variables such as temperature and reactant flow rates on the morphology, crystalline quality, residual strain and defects in the films are reported in detail.

5.2 Experimental Methods and Conditions

BP films were synthesized in a horizontal CVD reactor using ultra-high purity phosphine (99.999%) and diborane (1% in H_2) gases as phosphorus and boron precursors. The carrier gas was ultra-high purity hydrogen. More details of the CVD set-up are given in Chapter 2.1. Three types of substrates were employed for BP deposition: 3C-SiC(100) on Si(100), 3C-SiC(111) on Si(111), and 3C-SiC(111) on 4H-SiC(0001). The 3C-SiC films on Si were polished to minimize their surface roughness before BP epitaxy. The 3C-SiC(100) films had a thickness of ~ 4 μm, total thickness variation of 3 μm and wafer bow of 6 μm over a 4-inch Si(100) wafer, while 3C-SiC(111) films had a thickness of ~ 0.9 μm, total thickness variation of 13 μm and wafer bow of -43 μm over a 4-inch Si(111) wafer. The 3C-SiC(111) templates on 4H-SiC(0001) were not polished and had a thickness of about 50 μm. The hydrogen flow rate was kept constant at 4,000 sccm, and the PH_3 and B_2H_6 (1% in H_2) flow rates were varied between 30-80 sccm and 20-80 sccm, respectively. The deposition temperature was varied between 1000 to 1200 ^oC over a period of 30 min to 3 h. A constant pressure of 700 torr was maintained inside the reactor chamber for all depositions.

5.3 Results and Discussion

5.3.1 Growth and Morphology of BP Films

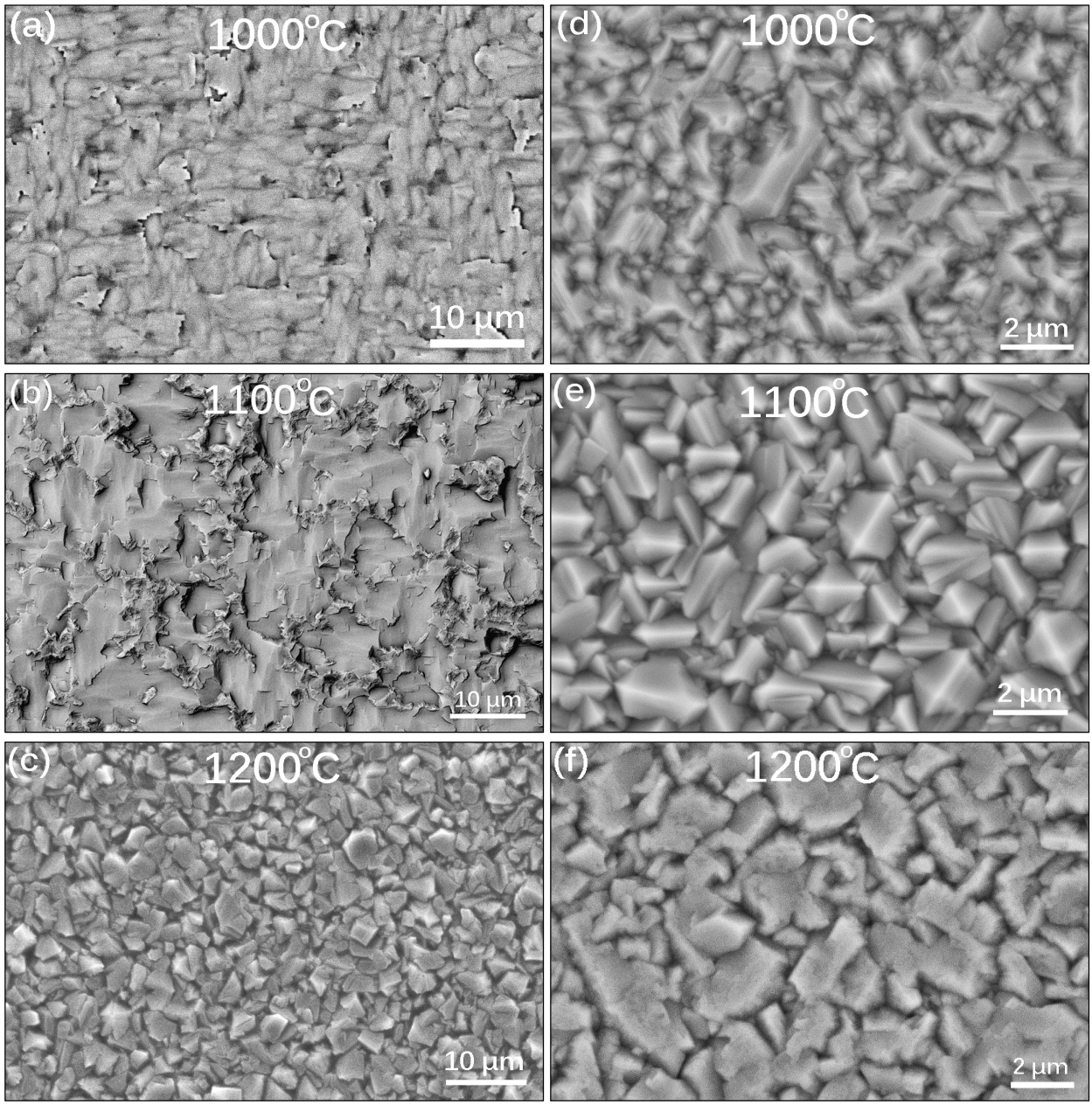

Figure 5.2 SEM pictures of BP films deposited on 3C-SiC(100)/Si (a, b and c) and 3C-SiC(111)/Si (d, e and f) at 1000 °C, 1100 °C, and 1200 °C.

The surface morphology of BP films deposited at various deposition conditions was analyzed by SEM and Nomarski optical microscopy (DIC). SEM micrographs of BP films grown

at 1000 ºC, 1100 ºC, and 1200 ºC on 3C-SiC(100)/Si and 3C-SiC(111)/Si substrates are shown in Figure 5.2. The BP films grown at 1000 ºC and 1100 ºC were typically dark red and had highly faceted crystallites with four-fold symmetry representing the BP(200) orientation on 3C-SiC(100)/Si and three-fold symmetry representing the BP(111) orientation on 3C-SiC(111)/Si substrates. When the deposition temperature was increased to 1200 ºC on both 3C-SiC/Si substrates, the films turned dark gray and were composed of a combination of regular and irregular faceted grains, indicating that the films were partially polycrystalline. This decrease in crystalline order of BP at 1200 ºC was quite contrary to our previous results, where the crystalline order was best at 1200 ºC when deposited on 4H-SiC and AlN/sapphire substrates.[1,3]

In comparison, BP films had better crystalline orientation and overall quality on 3C-SiC(100), partly due to better crystalline quality of bare 3C-SiC(100) compared to 3C-SiC(111). BP epitaxy on a limited number of 3C-SiC/4H-SiC substrates was also explored. An SEM micrograph of BP film deposited on 3C-SiC(111)/4H-SiC(0001) at 1200 ºC is shown in Figure 5.3. The BP(111) crystallites were highly faceted and had larger grain size on this substrate compared to 3C-SiC(111)/Si. Furthermore, the morphology of the film, with few pits on the surface, resembled to that of BP grown on 4H-SiC(0001) substrates in this work.

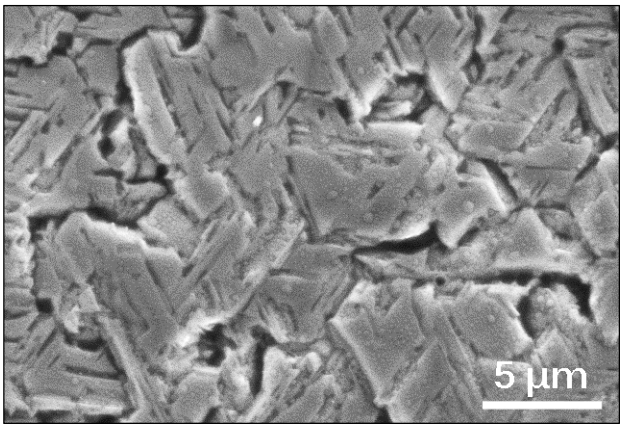

Figure 5.3 BP film grown on 3C-SiC(111)/4H-SiC(0001) at 1200ºC

As discussed earlier, there exists some preexisting strain in the 3C-SiC layer deposited on a Si substrate due to large lattice and thermal expansion mismatches between 3C-SiC and Si. Consequently, BP films grown below 1200 ºC cracked occasionally when deposited on the already strained 3C-SiC/Si substrates. Film cracking was more pronounced when the deposition was increased to 1200 ºC. One probable cause for the degradation of crystalline order of BP on 3C-

SiC/Si substrates could be the increased strain in 3C-SiC at higher deposition temperatures. As a result, the epitaxial orientation of incoming BP atoms with respect to the substrate was disrupted, resulting in polycrystalline films. Another reason for the degradation of crystalline order on 3C-SiC/Si could be due to the diffusion of Si atoms from Si substrate into the BP film through the pinholes (shown in Figure 5.8) in 3C-SiC, and subsequently disturbing the crystal growth and orientation. This can only be proved by comparing the Si impurities in BP films grown on 3C-SiC/Si and 3C-SiC/4H-SiC substrates via SIMS analysis. The above two arguments are consistent with the results obtained on 3C-SiC(111)/4H-SiC(0001), where film cracking and degradation of crystalline order was not observed even at high deposition temperature (1200 ^{o}C). This is perhaps due to the deposition of BP on a relatively less strained 3C-SiC layer grown homoepitaxially on a 4H-SiC(0001) substrate, where the lattice and thermal expansion mismatches are similar for both 3C-SiC and 4H-SiC.

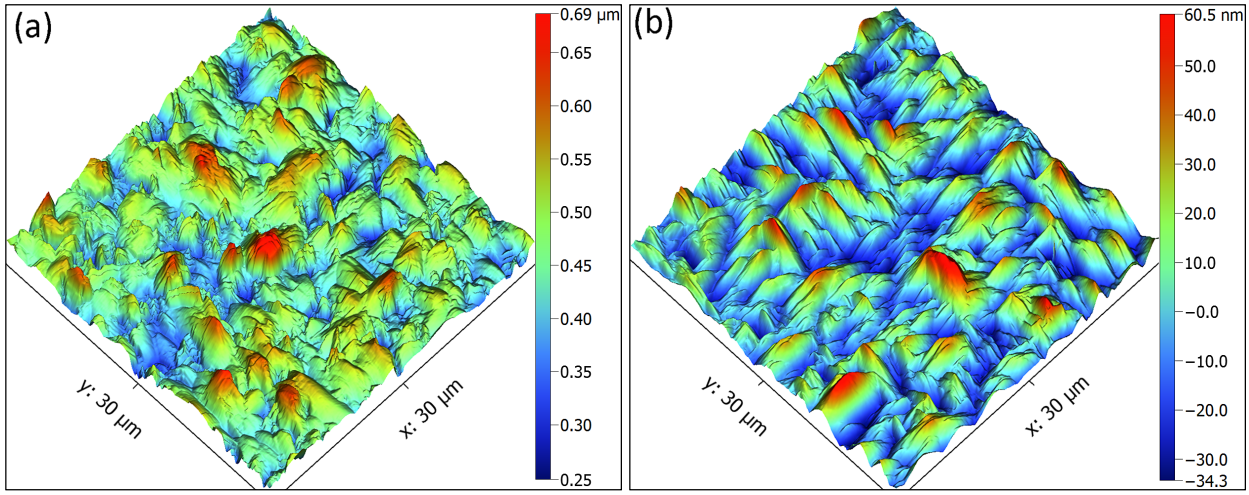

Figure 5.4 AFM images of BP films deposited on 3C-SiC(100)/Si at 1000^{o}C with PH_3/B_2H_6 flow ratios of (a) 100 and (b) 150

The thickness of the BP films was measured by examining the cleaved samples in cross section by SEM. The growth rate was approximately 4-5 µm/hr. Surface roughness of a few BP films on 3C-SiC(100)/Si was measured by atomic force microscopy and are shown in Figure 5.4. The RMS roughness value for a film with a thickness of 3 µm, grown at 1000 ^{o}C with PH_3 and B_2H_6 (1% in H_2) flow rates of 40 sccm each, was 55 nm. When the B_2H_6 (1% in H_2) flow rate reduced from 40 sccm to 26.7 sccm, roughness of the film with a similar thickness decreased to 15 nm, due to the decreased deposition rate. In addition, orientation of BP(200) crystallites was

improved when the flow rate ratio was increased. RMS roughness of BP film on 3C-SiC(100) (15 nm) was the lowest of all substrates tested, including 4H-SiC (36 nm) and AlN/sapphire (27 nm), at identical deposition conditions.

5.3.2 Crystalline Orientation of BP

Evidence of rotational twinning in BP films and the epitaxial relationship between BP and 3C-SiC/Si substrates were analyzed using SWBXT. Figure 5.5a and b display the 4-fold and 3-fold diffraction patterns obtained from BP films grown on 3C-SiC(100)/Si and 3C-SiC(111)/Si substrates, respectively. Diffraction spots from the zincblende structural layers of BP and 3C-SiC overlap completely and partially with diamond structure of Si, confirming that BP layers were epitaxially grown on both substrates. The epitaxial relationship between BP and 3C-SiC was $(100)\ \langle 011\rangle_{BP} \parallel (100)\ \langle 011\rangle_{3C\text{-}SiC}$ and $(111)\ \langle 11\bar{2}\rangle_{BP} \parallel (111)\ \langle 11\bar{2}\rangle_{3C\text{-}SiC}$. Also, absence of diffraction spots from the twin orientations of BP(100) and BP(111) on 3C-SiC(100) and 3C-SiC(111) substrates, respectively, confirmed that rotational twinning was eliminated. This was due to crystal symmetry matching between BP and 3C-SiC at the interface as both have same zinc-blende crystal structure.

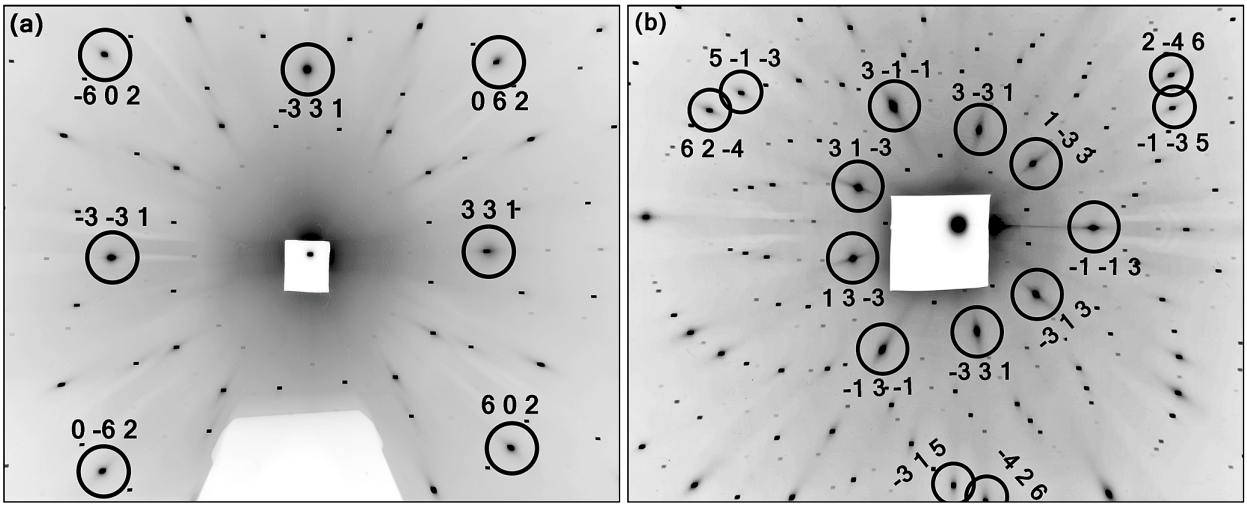

Figure 5.5 Indexed transmission X-ray topographs recorded on (a) 3C-SiC(100)/Si and (b) 3C-SiC(111)/Si. Spots indicated by circles represent overlapped diffraction spots from BP, 3C-SiC and Si.

The Laue diffraction patterns recorded for BP on both 3C-SiC substrates were compared to simulated patterns to evaluate strain in the films. Diffraction spots from BP were highly

elongated, confirming high residual strain in BP compared to well-defined spots from the relatively low strain 3C-SiC and high quality Si substrate. BP films deposited on 3C-SiC(111)/Si were more strained than on 3C-SiC(100)/Si, as the diffraction spots were more highly elongated.

The crystalline orientation of BP films on Si-base substrates was evaluated using X-ray diffraction θ/2θ scans by comparing the peak intensities of preferred BP orientations to other unwanted BP orientations. The relative peak intensity ratios of BP films grown on 3C-SiC(100)/Si and 3C-SiC(100)/Si substrates at three temperatures are shown in Figure 5.6 indicated by black and red lines, respectively. For BP on 3C-SiC(100) layers, intensity ratios of (200)/(111) and (200)/(220) were highest at 1000 ºC, but those ratios decreased sharply with temperature up to 1200 ºC. BP(111) was the preferred orientation on 3C-SiC(111)/Si substrate, and so the intensity ratios of (111)/(200) and (111)/(220) were determined. Intensity ratios on the 3C-SiC(111) substrate initially increased in the temperature range of 1000 to 1100 ºC, but they gradually decreased to the lowest ratio values at 1200 ºC, indicating multiple BP orientations. These results were consistent with SEM findings that films deposited at 1200 ºC were polycrystalline. Based on the surface morphology and XRD intensity ratios, optimum growth temperatures on 3C-SiC(100)/Si, 3C-SiC(111)/Si and 3C-SiC(111)/4H-SiC(0001) substrates were determined to be 1000 ºC, 1100 ºC and 1200 ºC, respectively.

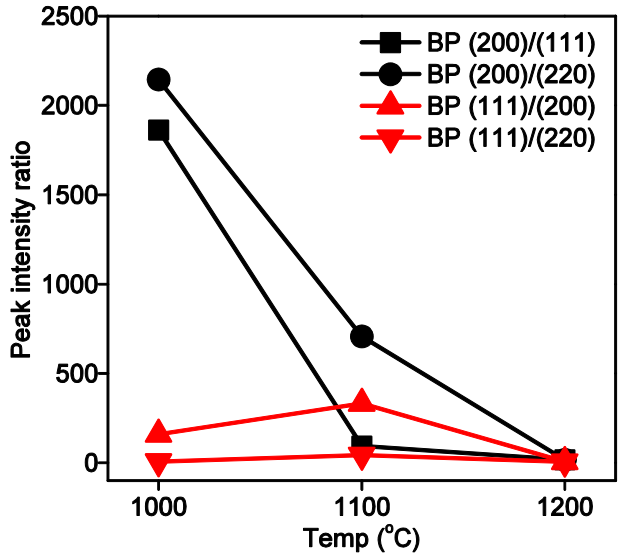

Figure 5.6 θ/2θ XRD relative peak intensity ratios of BP deposited at various temperatures on 3C-SiC(100)/Si (black) and 3C-SiC(111)/Si (red) substrates.

5.3.3 Strain Evaluation of BP Films

3C-SiC epilayers were expected to have significant residual strain due to large lattice and thermal expansion mismatches between 3C-SiC and Si.[68,69] Because the 3C-SiC films on Si were already strained, the BP films were also expected to be strained. Confocal Raman imaging was employed to examine the residual strain and overall quality of the BP films. Raman spectra measured from BP films grown on various 3C-SiC epilayers generally gave two characteristic phonon modes: TO mode at ~798 cm^{-1} and LO mode at ~828 cm^{-1}. The measured peak positions of both phonon modes were in good agreement with the previously published data.[1–4,52,66] However, the Raman peak positions varied with the substrate used for BP epitaxy due to residual compressive or tensile strain generated in the films.

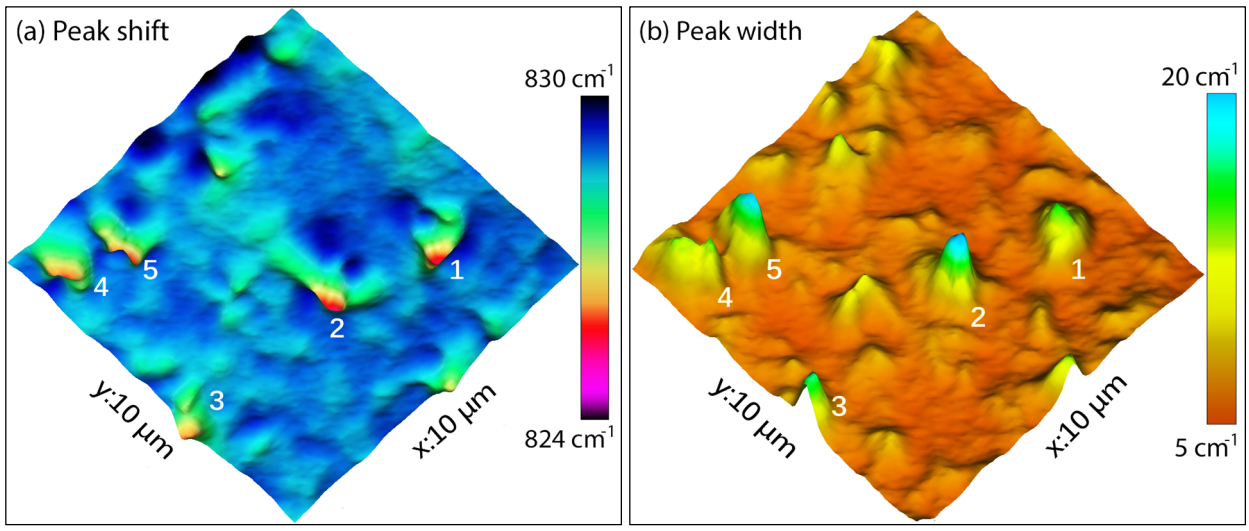

Figure 5.7 Raman images of BP/3C-SiC(100)/Si taken over an area of 10 µm x 10 µm with 532 nm excitation. (a) Map of BP(LO) mode peak shift from center position; (b) Map of BP(LO) mode peak width (FWHM).

Raman spectra were collected at 10,000 points over an area of 10 µm x 10 µm on BP film grown on a 3C-SiC(100)/Si substrate at 1000 ºC. All data points were mapped in a 3D plot with respect to their BP(LO) phonon's peak shift from the center position and peak width (full width at half maximum) as shown in Figure 5.7a and b. The peak shift from the center position is mostly uniform over the scanned area, except at a few places where deep valleys were present (indicated in numbers from 1 to 5). The peak position across these five valleys was about 824.5 cm^{-1} while the average value across the entire scanned area was 828.7 cm^{-1}. This sharp decrease in peak

position in the valleys compared to the surrounding areas or average value indicated local tensile strain in the BP film. Strain in the BP crystal causes structural disorder and can change equilibrium positions of atoms in crystal lattice. Consequently, the phonon frequencies from the film shift to either higher or lower wavenumbers depending on local deformation in the lattice, in this case to the lower side in the valleys. The peak positions at the deepest and highest points were 824.5 cm^{-1} and 830.5 cm^{-1} and the overall standard deviation in peak shift was 0.50 cm^{-1}.

The Raman map of full width at half maximum (FWHM) was also mostly uniform over the scanned area except at some locations where high peaks (numbered from 1 to 5 in Figure 5.7b) were present. The average FWHM value across the scanned area was 6.9 cm^{-1} while it sharply increased to 18.2 cm^{-1} at the peaks. The locations of these peaks were the same as observed for the valleys in peak shift image, suggesting that crystal quality has degraded at locations where tensile strain was present. The FWHM values at the deepest and highest points were 20.5 cm^{-1} and 11.4 cm^{-1} while a high overall standard deviation of 1.65 cm^{-1} was measured due to high values of FWHM at peaks.

An optical image of BP film analyzed for Raman imaging is shown in Figure 5.8a along with the scanned area. A closer look at the surface features of BP film in the scanned region and Raman shift image (Figure 5.7a) indicated that valleys in Raman shift image appeared at locations where huge pits (indicated in numbers) were present on the BP film in Figure 5.8a. Several possible causes of these pits were considered including the natural surface roughness of the BP film, the presence of pinhole/step bunch defects in 3C-SiC epilayer before BP deposition, defects formed in SiC films during BP epitaxy, or a combination of these phenomena. For more insights, the surface of a bare 3C-SiC(100) epilayer was studied by optical microscopy. Several pinholes were clearly observed on the surface, as shown in Figure 5.8b. Furthermore, these pinholes remain even after the BP film was deposited on 3C-SiC(100)/Si substrate as shown in Figure 5.8c and d. A detailed structural characterization of these films would provide more explanation of the defects, but that characterization is beyond the scope of the present work. In summary, the significant shift in Raman peak position around the defects, which indicated strain in the BP film, could be due to a combination of factors.

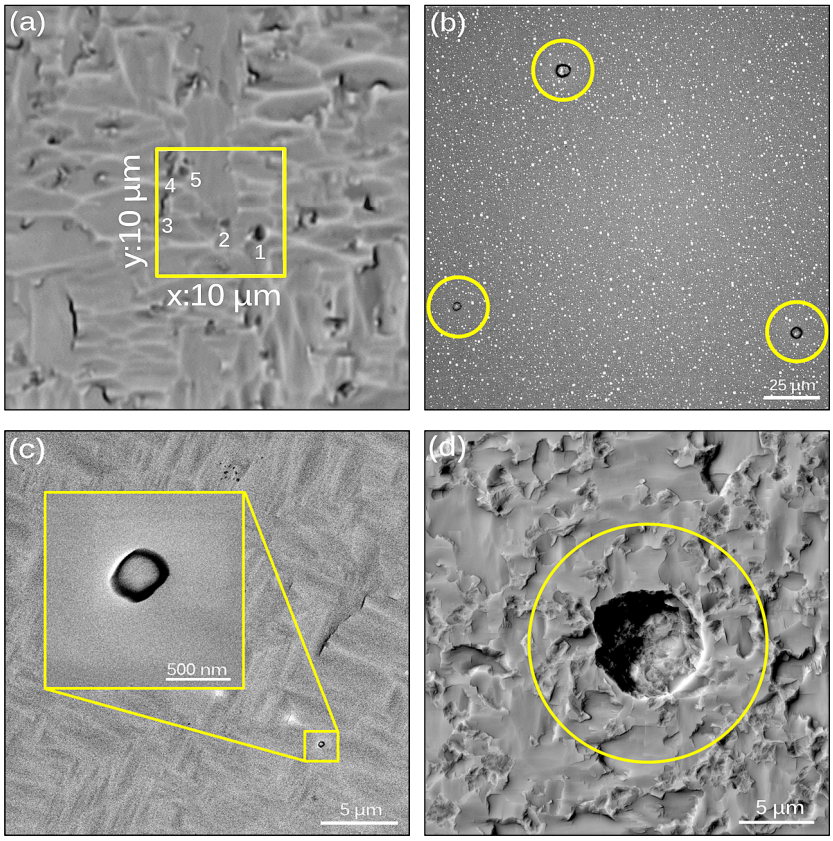

Figure 5.8 (a) Optical image of the BP film and scanned area (shown in box) with Raman imaging. (b) Nomarski image of bare 3C-SiC substrate showing pinholes on surface. (c, d) SEM images of BP film deposited on pinholes on 3C-SiC(100)/Si.

The average LO phonon peak positions of BP grown on 3C-SiC(100)/Si, 3C-SiC(111)/Si, and 3C-SiC(100)/4H-SiC(0001) at 1200 ºC were measured and compared with the peak positions of BP whiskers. The peak positions of BP films on all 3C-SiC layers were consistently lower than that of strain-free BP whiskers as shown in Figure 5.9. The lower shift in peak position indicated tensile strain in the BP films on 3C-SiC layers. This conclusion is consistent with the thermal expansion coefficients of BP and 3C-SiC published in the literature, which support that thermal expansion between BP and SiC produce tensile strain.[68,69,78] Furthermore, the peak positions were very close between 3C-SiC/Si and 3C-SiC/4H-SiC, which indicates that thermal expansion of Si had a minor role to play during BP growth. It can be concluded that the shift was due to a combination of tensile strain from thermal expansion mismatch between BP and 3C-SiC and intrinsic strain in the BP film during growth. Also, BP grown on 3C-SiC(111)/Si had a slightly longer shift (~2 cm^{-1}) compared to other two substrates revealing larger intrinsic strain. Hence, it

is crucial to use high quality 3C-SiC to improve the quality and overall properties of BP. The peak positions also shifted to lower wavenumbers when growth temperatures increased for a given substrate, due to increased tensile strain in the film at higher temperatures. This is consistent with the trend for BP films deposited on 4H-SiC reported in this work. It suggests that the coefficients of thermal expansion of substrates considered in this study are less than that of BP.

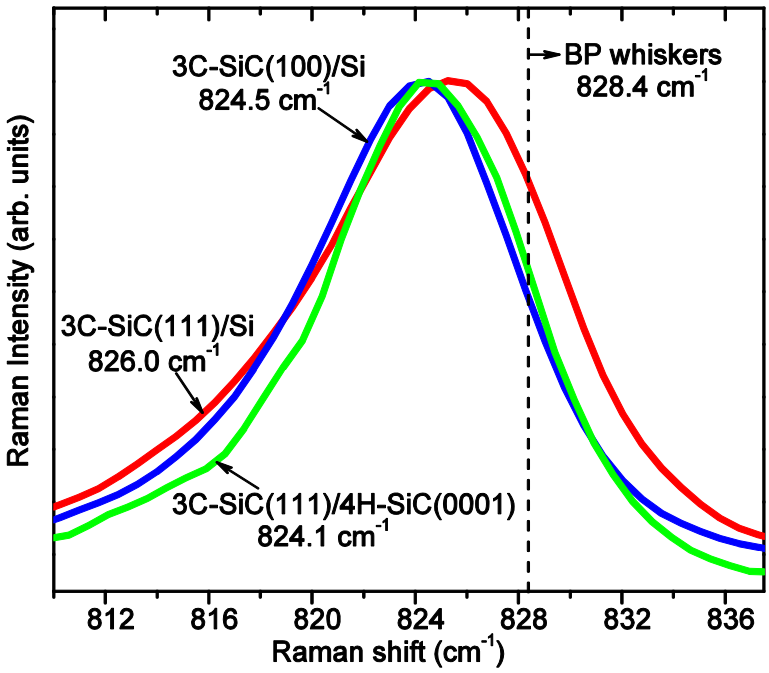

Figure 5.9 Comparison of Raman peak positions of BP deposited on various 3C-SiC layers to strain-free BP whiskers.

HRXRD double-axis rocking curves were measured to estimate the film quality and lattice strain in BP films. The FWHM of ω and ω-2θ rocking curves and lattice strain with respect to BP(100) and BP(111) at various growth conditions are given in Table 5.1. Peak widths of ω and ω-2θ rocking curves decreased when PH_3/B_2H_6 flow ratio increased from 100 to 150 at 1000 ºC. However, at 1100 ºC with similar PH_3/B_2H_6 flow rates, the peak width and out-of-plane strain values increased significantly. As expected, the FWHM and strain values on the 3C-SiC(111)/Si substrate were significantly higher than 3C-SiC(100)/Si substrate at identical temperatures and reactant flow rates since 3C-SiC(111) films are more strained than 3C-SiC(100) films on a Si substrate. In general, the 3C-SiC epilayer has a large lattice constant mismatch and a higher thermal expansion coefficient than the Si substrate.[68,69] Thus, the 3C-SiC films are under tensile strain after cooling from the growth temperature to room temperature.[79–81] Although Raman and

HRXRD results showed tensile strain on 3C-SiC(111)/4H-SiC, BP films usually did not crack due to the very small lattice constant and thermal expansion mismatches between 3C-SiC and 4H-SiC.

Table 5.1 FWHM and strain values of BP films on 3C-SiC/Si substrates

Substrate	Growth temp (°C)	PH_3/B_2H_6 flow ratio	ω FWHM (arcsec)	ω-2θ FWHM (arcsec)	Theoretical mismatch (%)	Measured mismatch (%)	Out-of-plane strain (%)
3C-SiC(100)/Si	1000	100	1228	761	4.09	4.09	-0.22
	1000	150	1140	748		4.11	0.34
	1100	100	2788	949		4.12	0.46
3C-SiC(111)/Si	1000	100	4041	1088		3.71	-9.42

In general, the 3C-SiC epilayer has a large lattice constant mismatch and a higher thermal expansion coefficient than the Si substrate.[68,69] Thus, the 3C-SiC films are under tensile strain after cooling from the growth temperature to room temperature.[79–81] BP films on 3C-SiC(100)/Si and 3C-SiC(111)/Si substrates cracked occasionally as they were deposited on a strained 3C-SiC layer on Si. Cracking was more pronounced at high temperatures (1200°C). Interestingly, BP films on 3C-SiC(111)/4H-SiC up to a thickness of ~6 μm did not crack, even at 1200°C. Although Raman and HRXRD results showed tensile strain on 3C-SiC(111)/4H-SiC, BP films usually did not crack due to the very small lattice constant and thermal expansion mismatches between 3C-SiC and 4H-SiC.

5.4 Conclusions

BP epitaxial films with good crystalline orientation and morphological features were produced on (100) and (111) planes of 3C-SiC epilayers. Rotational twinning in BP was eliminated by depositing it on a crystal symmetry-matched 3C-SiC. Synchrotron white beam X-ray topography showed the epitaxial relationship between BP and 3C-SiC was $(100)\,\langle 011\rangle_{BP} \parallel (100)\,\langle 011\rangle_{3C\text{-}SiC}$ and $(111)\,\langle 11\bar{2}\rangle_{BP} \parallel (111)\,\langle 11\bar{2}\rangle_{3C\text{-}SiC}$.

Raman imaging revealed uniform peak shift and peak widths, except at defects on the film surface. Raman peak positions of BP on all types of 3C-SiC layers shifted to the lower side, indicating tensile strain in the films. The XRD pattern showed BP(100) and BP(111) to be major orientations on 3C-SiC(100) and 3C-SiC(111). HRXRD rocking curves indicated more strain in

BP deposited on 3C-SiC(111)/Si than 3C-SiC(100)/Si. Due to preexisting strain in the 3C-SiC epilayer, BP films on 3C-SiC(100)/Si and 3C-SiC(111)/Si substrates cracked at high deposition temperatures but stayed intact on 3C-SiC(111)/4H-SiC. These results suggest that either high-quality bulk 3C-SiC or 3C-SiC epilayers on 4H-SiC are the substrates for BP epitaxy, as they will produce better quality films than on silicon-based substrates.

Chapter 6 - Growth on BP on ZrB_2 Substrates

6.1 Zirconium Diboride (ZrB_2)

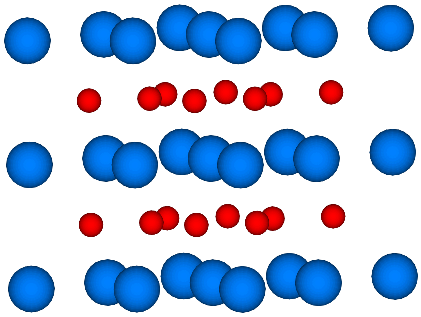

Figure 6.1 Hexagonal structure of ZrB_2

Zirconium diboride (ZrB_2) is an attractive substrate for BP epitaxy due to its high thermal stability, small lattice constant mismatch (1.26%), and high electrical conductivity. It is a highly covalent refractory material with a hexagonal crystal structure (MgB_2-type structure). Its crystal structure is formed by alternating layers of boron atoms in a honeycombed, graphite-like sheets, stacked between hexagonal close packed zirconium layers. Its high melting point (3246^{o}C) and common element (i.e. boron) with BP suggests ZrB_2 will be stable under deposition conditions and hence noncontaminating. It has high electrical conductivity due to its metallic bonding and electron transfer from metal to boron sheet. This may enable vertical devices, as it eliminates the substrate as significant source of electrical resistance. It is available in the form of epitaxial layers on Si, SiC etc.[82–84] and as bulk crystals.[85] Along with these exceptional properties, the in-plane lattice parameter of ZrB_2(0001), a = 3.169 °A, has only a small lattice mismatch of 1.26% with that of BP(111). Previously, Kinoshita et al demonstrated that GaN can be deposited epitaxially on ZrB_2(0001).[86,87] All these properties make it a potentially suitable substrate for growing BP films. Here, ZrB_2 buffer layers on 4H-SiC and few bulk ZrB_2 substrates were tested for the first time as substrates for BP epitaxy.

6.2 Experimental Methods and Conditions

The ZrB_2 (0001) films on 4H-SiC(0001) employed in this study were prepared by high temperature direct current magnetron sputtering as developed by Tengdelius et al.[82–84] Briefly this

consisted of sputtering from a ZrB_2 target onto a 4H-SiC(0001) substrate heated to 900 °C. The bulk ZrB_2 (0001) substrates were diced and polished from a bulk crystal that was grown by a float zone technique by Otani et al.[85]

The BP CVD reactor setup and sample preparation procedure was similar to the procedure used for other substrates mentioned in previous chapters. Most BP films were grown on ZrB_2(0001) buffer layers (~2 μm) deposited on 4H-SiC(0001) substrates; a few were deposited on bulk ZrB_2 (0001). Substrates were heated at 1200°C under H_2 flow for 15 min to clean the surface prior to BP deposition. After *in-situ* H_2 etching, reactant gases, PH_3 and B_2H_6, were introduced into the carrier gas stream to deposit the BP. The growth temperature was varied between 1000-1200°C, and gas flow rates were maintained at 4000 sccm of H_2, 40-80 sccm of PH_3 and 20-40 sccm of B_2H_6 (1% in H_2). Films were typically deposited for about 30 min.

6.3 Results and Discussion

6.3.1 Growth and Morphology of BP Films

The growth temperature had a strong effect on the morphology and crystalline orientation of BP. On both types of substrates, at 1000°C, the films had polycrystalline features such as irregular shaped facets (Figure 6.2). These films resembled the polycrystalline BP films on AlN, 4H-SiC, and 3C-SiC substrates. When the temperature was increased to 1200°C, the deposited films were still polycrystalline. In addition, some icosahedrons formed, scattered across the film, indicating formation of icosahedral boron phosphide ($B_{12}P_2$), despite maintaining a high phosphorus vapor pressure. This is contrary to the results of BP deposited on AlN and 4H-SiC substrates; on these substrates highly ordered films were obtained at 1200°C. XRD and Raman spectroscopy analysis of these films indicated a peak at about 475 cm^{-1}, confirming the formation of $B_{12}P_2$ on both type of substrates (see Figure 6.3 and Figure 6.6a and b). The formation of $B_{12}P_2$ is perhaps due to the segregation of boron atoms on ZrB_2 at higher temperatures and insufficient mobility on the surface of adatoms resulting in the formation of $B_{12}P_2$. Due to both these factors, the deposited films were mostly non-uniform over the substrates with smoother film at some places and rougher deposits at other places.

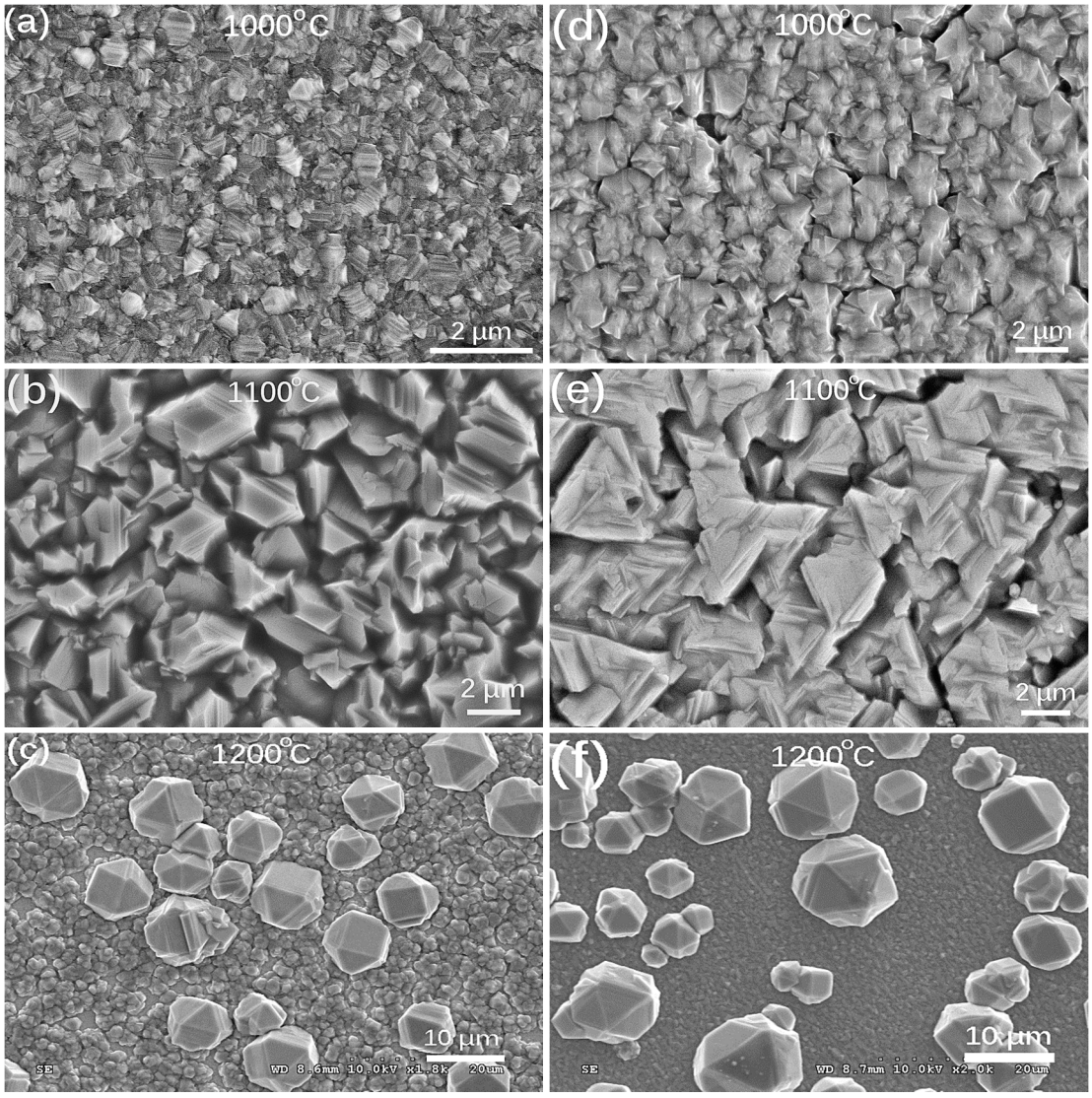

Figure 6.2 Morphology of BP films on ZrB_2/4H-SiC (a, b, c) and bulk ZrB_2 (d, e, f) at various temperatures.

The films deposited at 1100ºC had larger grain size compared to 1000ºC and much better crystalline orientation with triangular BP(111) facets. Interestingly, there was no formation of $B_{12}P_2$ on both substrates at these deposition conditions. Both XRD and Raman results confirmed this observation. SEM indicated the best temperature to deposit a crystalline BP on ZrB_2 was 1100ºC.

6.3.2 Crystalline Orientation of BP

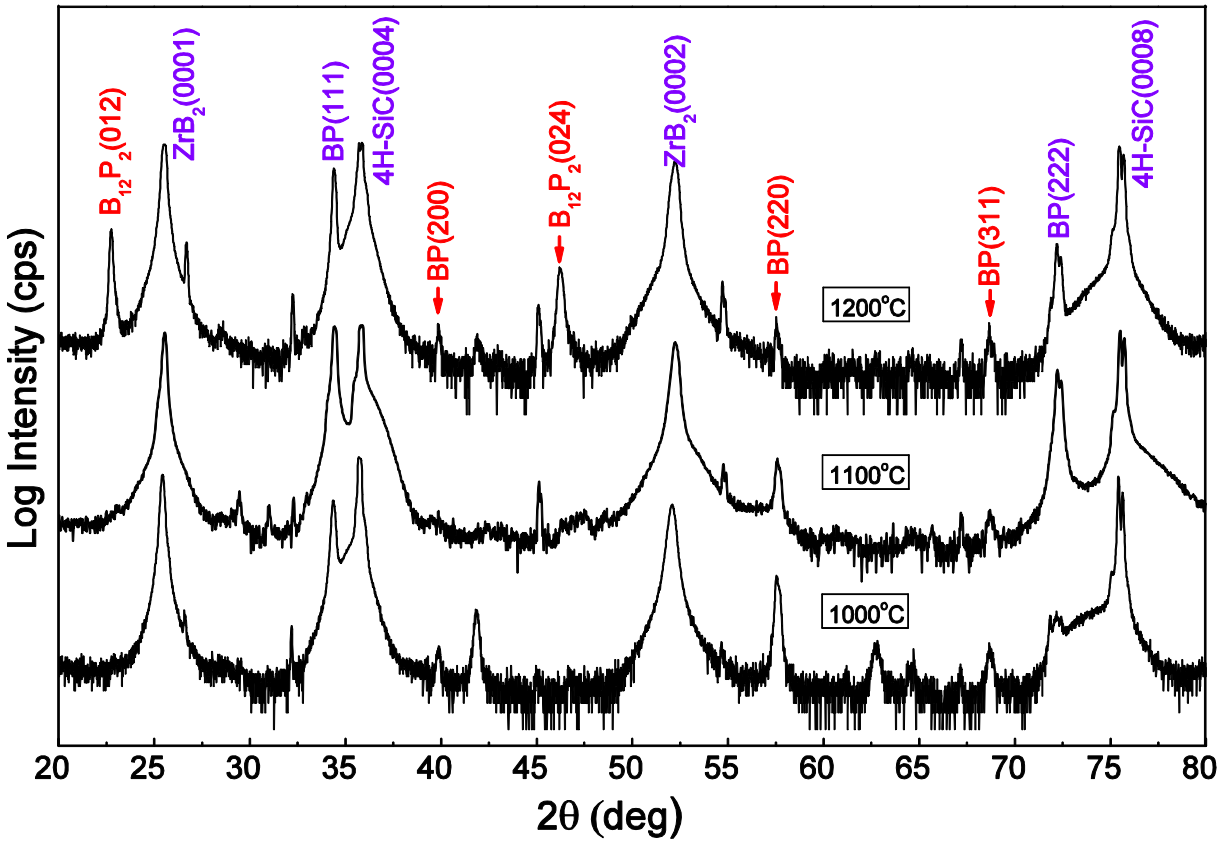

Figure 6.3 Comparison of XRD pattern for BP films on ZrB_2/4H-SiC at different temperatures

The θ/2θ XRD patterns recorded for BP films grown at different temperatures on ZrB_2/4H-SiC substrates are shown in Figure 6.3. Comparing the diffraction pattern at 1000°C and 1100°C showed no significant difference between the two, although SEM micrographs indicated polycrystalline and crystalline films at 1000°C and 1100°C, respectively. Multiple $B_{12}P_2$ peaks were identified (indicated in red) for films deposited at 1200°C, confirming the formation of $B_{12}P_2$.

The details of FWHM of BP(111) peak and relative intensity ratios of BP(111)/BP(200) and BP(111)/BP(220) measured on ZrB_2/4H-SiC substrate are given in Figure 6.4a and b. The FWHM of BP(111) peak has slightly increased from 0.20° to 0.21° when the temperature was increased from 1000°C to 1100°C. However, the FWHM decreased to the lowest value when the temperature was increased further to 1200°C. The intensity ratios followed a similar trend (see Figure 6.4b) with change in temperature. Both plots indicate the evolution of polycrystalline

growth of BP and the degradation of BP's crystalline order at 1000°C and 1200°C. Although the FWHM increased slightly at 1100°C, the SEM and peak intensity ratios indicate the optimum temperature to grow a crystalline BP film on ZrB_2/4H-SiC substrate was 1100°C.

Due to the limited availability of bulk ZrB_2 substrates, only one BP film was deposited on bulk ZrB_2(0001) at 1100°C. The BP(111) peak width was measured to be 0.19° and the peak intensity ratio of BP(111)/(200) and BP(111)/(220) was 909 and 600, respectively. In comparison, the FWHM of BP(111) peak was measured to be 0.21° and the intensity ratios of BP(111)/(200) and BP(111)/(220) were 4881 and 329, respectively for BP deposited on ZrB_2/4H-SiC substrate at 1100°C. Due to the limited number of ZrB_2 substrates, a detailed analysis of BP growth and its properties on both types of ZrB_2 substrates was not made in this study.

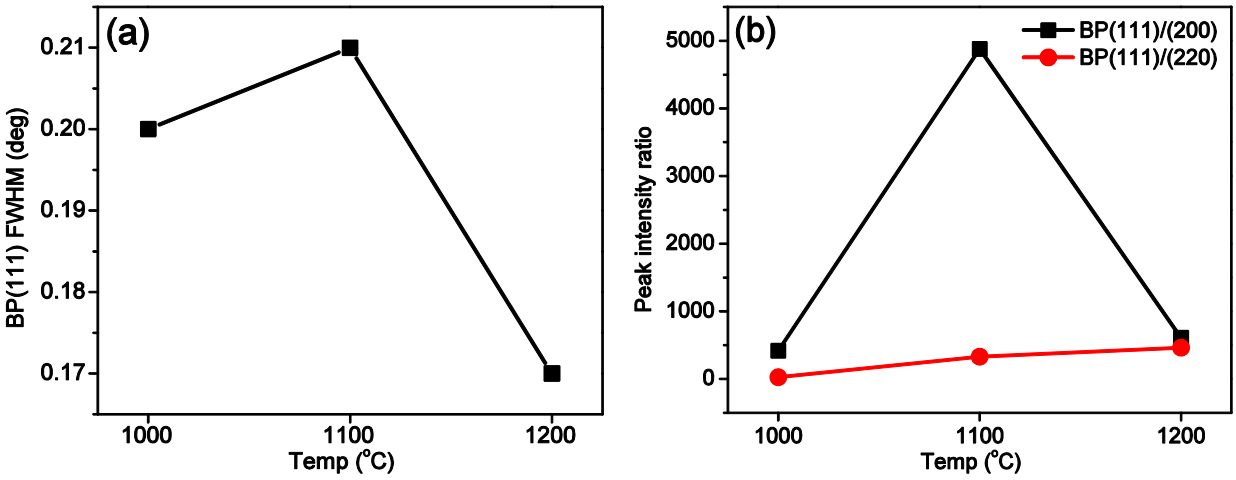

Figure 6.4 (a) BP(111) peak width and (b) relative intensity ratios of BP peaks measured from XRD θ/2θ scans on ZrB_2/4H-SiC substrate.

6.3.3 Strain Evaluation of BP Films

The cross sectional TEM images of the BP interface with bulk ZrB_2 and ZrB_2/4H-SiC substrates are shown in Figure 6.5 for films grown at 1100°C. Close analysis of the interface between BP and ZrB_2 indicate that a nice epitaxial growth was achieved on both types of substrates. But, there were many twin boundaries and stacking faults at the interface indicated by white and yellow arrows. The interface was smoother for the BP film on ZrB_2/4H-SiC substrate, but there were more number of twin boundaries on the {111} planes of BP and dislocations compared to bulk ZrB_2. A deep pit can be viewed at the BP/ZrB_2 interface in Figure 6.5b,

indicating that the ZrB_2 film was not uniformly deposited on bare 4H-SiC, prior to the BP deposition. As explained in the previous chapters, twin orientations of BP(111) were formed on hexagonal ZrB_2 substrates due to the difference in symmetry between 3-fold BP(111) and 6-fold ZrB_2(0001).

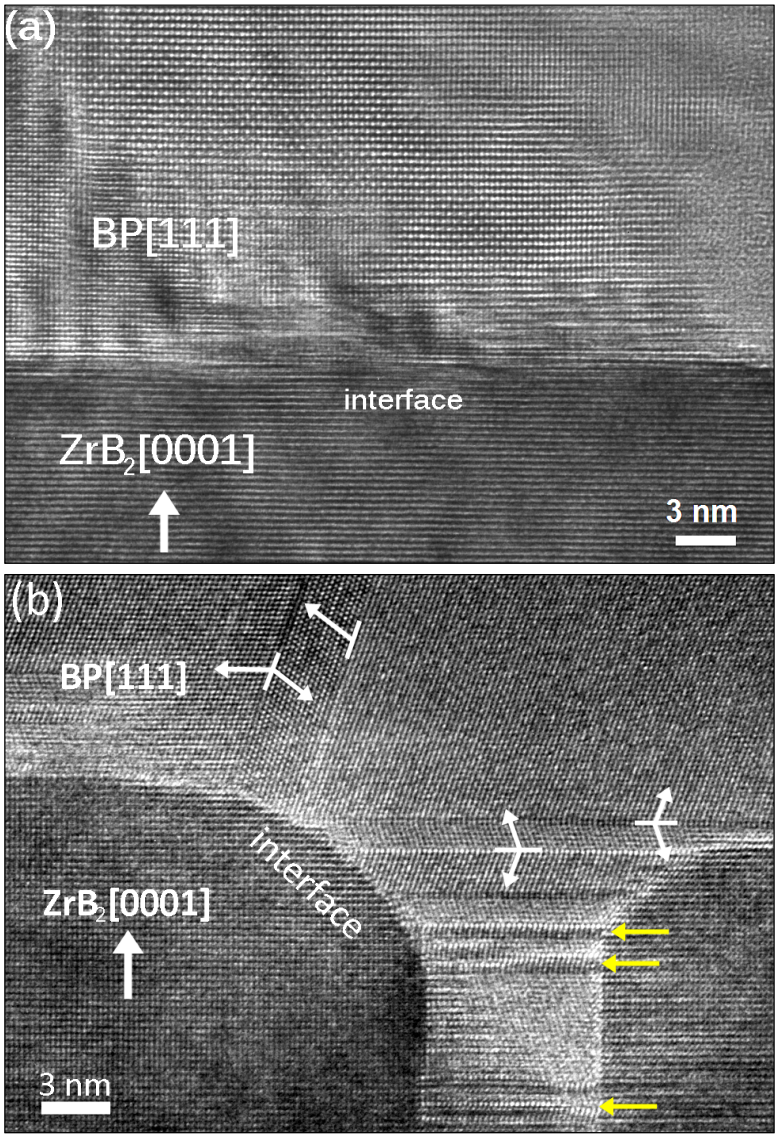

Figure 6.5 TEM images showing the interface between BP and (a) bulk ZrB_2 and (b) ZrB_2(0001)/4H-SiC

Raman spectroscopy measurements of BP on ZrB_2/4H-SiC and bulk ZrB_2 substrates are shown in Figure 6.6(a) and (b), respectively. The films deposited at all temperatures showed BP peaks that are consistent with the reported values in the literature. However, noticeable difference

in the peak positions between ZrB_2/4H-SiC and bulk ZrB_2 substrates was observed, which is discussed in the next paragraph. However, in addition to the BP peaks, the peak at ~475 cm^{-1} indicates $B_{12}P_2$ was also deposited at 1200°C. This peak at ~475 cm^{-1} is typically the most intense Raman peak for $B_{12}P_2$.

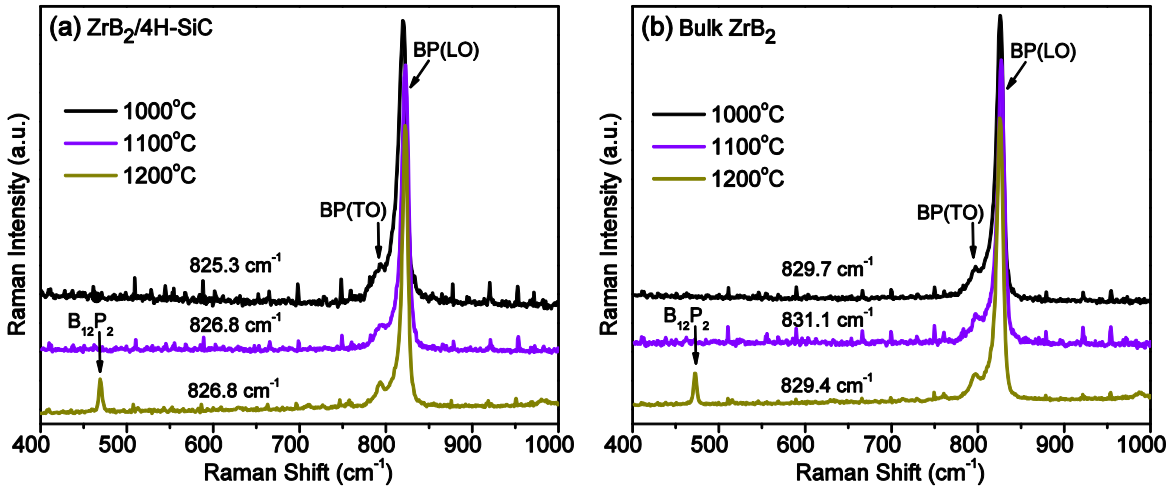

Figure 6.6 Raman spectra depicting the peak positions of BP(LO) mode on (a) ZrB_2/4H-SiC and (b) bulk ZrB_2 at different temperatures

The FWHM of BP(LO) Raman peak and peak position measured on both substrates at three deposition temperatures are tabulated in Table 6.1. The FWHM consistently decreased with temperature, in agreement with the results reported for BP on AlN/sapphire, 4H-SiC and 3C-SiC/Si substrates.[1,3,5]

Table 6.1 Comparison of FWHM and peak shift between Bulk ZrB_2 and ZrB_2/4H-SiC

Temp(°C)	FWHM (cm^{-1})		Shift (cm^{-1})	
	ZrB_2/4H-SiC	Bulk ZrB_2	ZrB_2/4H-SiC	Bulk ZrB_2
1000	11.9	10.1	825.3	829.7
1100	9.7	9.4	826.8	831.1
1200	7.7	8.4	826.8	829.4

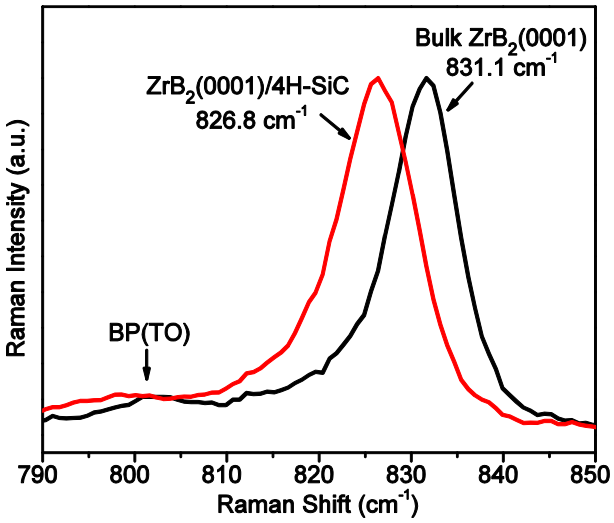

Figure 6.7 Raman peak position measured on Bulk ZrB_2 and ZrB_2/4H-SiC substrates

A considerable difference in the peak positions between ZrB_2/4H-SiC and bulk ZrB_2 substrates was also observed as shown in Table 6.1 and Figure 6.7. Typically, BP(LO) peak was shifted to the lower side on ZrB_2/4H-SiC whereas it shifted to the higher side on bulk ZrB_2, indicating red shift. This trend is primarily due to the differences in thermal expansion between ZrB_2/4H-SiC and bulk ZrB_2 substrates. As reported earlier, BP films experience tensile strain on 4H-SIC, resulting in the blue shift. Although ZrB_2 layer has slightly higher coefficient of thermal expansion than BP, the thermal expansion is dominated by the 4H-SiC. Hence the peak position was shifted to the lower side, consistent with earlier findings. Likewise, the BP films on bulk ZrB_2 experience compressive strain due to the larger coefficient of thermal expansion of ZrB_2 (roughly 6×10^{-6} to 7×10^{-6} K^{-1} from 300 K to 1000 K)[88] compared to BP (roughly 3×10^{-6} to 5.4×10^{-6} K^{-1} from 300 K to 1000 K),[69] resulting in higher peak shift.

6.4 Conclusions

BP epitaxy on bulk ZrB_2 and ZrB_2/4H-SiC was explored on a limited number of substrates for the first time in literature. Temperature is the most important parameter for growing good quality BP films on ZrB_2 substrates. Lower deposition temperature (1000°C) resulted in polycrystalline BP due to the poor movement of the adatoms on the ZrB_2 surface, while higher temperature (1200°C) resulted in the formation of unwanted $B_{12}P_2$ due to increased segregation of boron atoms in ZrB_2 during the BP deposition. The optimum temperature for growing crystalline

BP films without $B_{12}P_2$ formation was 1100°C on both bulk ZrB_2 and ZrB_2/4H-SiC substrates. XRD and Raman analysis of these films corroborated these findings.

The morphology, crystalline orientation, peak width and relative intensity ratios of BP deposited on a limited number of bulk ZrB_2 and ZrB_2/4H-SiC substrates indicated mixed results. Since the number of samples for comparison is less, it is unfair and difficult to compare the quality of BP films on these substrate types. Moreover, the ZrB_2 substrates are not well developed as AlN, 4H-SiC and 3C-SiC substrates. Nevertheless, the initial results of BP on ZrB_2 substrates are encouraging and prove that ZrB_2 is a viable substrate for BP epitaxy.

Chapter 7 - Conclusions and Future Work

7.1 Conclusions

Boron phosphide (BP) is an indirect wide-bandgap (2.0 eV) refractory semiconductor with many outstanding properties such as high thermal neutron capture cross-section of the ^{10}B isotope, high thermal conductivity, high charge carrier mobility, high thermal stability and chemical stability. These properties make BP suitable for various applications such as electronic devices, thermoelectric devices and solid-state neutron detectors, which is the focus of this research. This dissertation investigated the heteroepitaxial growth of BP films on different types of AlN, 4H-SiC, 3C-SiC and ZrB_2 substrates and influence of process parameters on the structural and electrical properties of the undoped BP films. The important conclusions drawn from BP epitaxy on each type of substrate employed in this work are given below.

AlN Substrates

High quality BP epitaxial films were grown on various AlN substrates for the first time in literature. The films were crack-free and adhered well to the AlN substrates. The crystalline quality of the BP films grown at different deposition conditions were analyzed using various characterization techniques. The crystalline orientation, texture and grain size of BP increased consistently with temperature and PH_3/B_2H_6 flow ratio. XRD indicated that the preferred BP(111) orientation improved with temperatures and PH_3/B_2H_6 flow rate ratios based on the narrow BP(111) peak widths and highest relative peak intensity ratios of BP(111)/(200) and BP(111)/BP(220) at 1200^{o}C and a PH_3/B_2H_6 flow rate ratio of 200. The Raman spectroscopy analysis of the films confirmed the improved crystalline quality at higher growth temperatures and PH_3/B_2H_6 flow ratios, validating the SEM and XRD results. The FWHM values of BP Raman peak (6.1 cm^{-1}) and XRD ω rocking curve (352 arcsec) measured on AlN/sapphire substrate are lowest values in the literature for BP epitaxial films.

Raman spectroscopy indicated tensile strain in BP when deposited on bulk AlN and compressive strain on AlN/sapphire substrates based on the BP peak position. HRXRD and Raman spectroscopy results revealed that the deposited BP films were mostly relaxed although small

residual strain could be still present. Confocal Raman imaging showed uniform peak shift and FWHM values across the scanned area, except at the pits on the surface. The BP films had better crystalline quality when grown on AlN/sapphire compared to 4H-SiC and 3C-SiC(100)/Si substrates. Twinned BP films, confirmed by synchrotron white beam X-ray topography, were evident on an on-axis AlN/sapphire substrate due to mismatch of crystal symmetry between 3-fold BP(111) and 6-fold AlN(0001) planes. The produced films were *n*-type with a highest electron mobility of 37.8 $cm^2/V \cdot s$ and a lowest carrier concentration of 3.15×10^{18} cm^{-3}.

Overall, the BP films on AlN/sapphire substrates had better quality compared to the other substrates (4H-SiC, 3C-SiC, ZrB_2) studied in this work, even though twinned BP were produced. The results obtained so far in this work indicate that AlN substrate is viable for producing BP epitaxial films and these substrates have promising potential for further improvement of BP properties.

4H-SiC Substrates

BP epitaxy on 4H-SiC and 6H-SiC(0001) substrates having on-axis and off-axis orientations was investigated. Twin-free BP films were obtained on an off-axis 4H-SiC(0001) substrate tilted 4º toward $[1\bar{1}00]$, but rotational twin defects were identified on on-axis 6H-SiC and 4H-SiC miscut 4º toward $[1\bar{2}10]$. The deposition temperature is one of the important process parameter that affected the crystal quality and residual strain in BP. Sufficient reactant flow rates and ratios are necessary to grow smooth crystalline films with good surface coverage on the substrate. Similar to the results obtained on AlN/sapphire, improved crystal quality was achieved at higher temperatures and reactant flow rate ratios as confirmed by SEM, AFM, XRD and Raman spectroscopy analysis. The films were tensile strained and cracked occasionally when thicker BP films above 20 μm were deposited. The film quality could be improved by employing a high quality 4H-SiC substrate.

Overall, the best substrate choice for BP epitaxy was 4H-SiC(0001) miscut 4º toward $[1\bar{1}00]$ among various types of 4H-SiC and 6H-SiC substrates, because it did not produce rotational twins defects.

3C-SiC Substrates

BP epitaxial films with good crystalline orientation and morphological features were produced on (100) and (111) planes of 3C-SiC epilayers on Si and 4H-SiC substrates. BP rotational twins were absent by depositing on a crystal symmetry-matched 3C-SiC. Due to the preexisting pinhole defects on the starting 3C-SiC substrate, films deposited on the pinholes had increased tensile strain and degraded quality. HRXRD rocking curves indicated more strain in BP deposited on 3C-SiC(111)/Si than 3C-SiC(100)/Si. The films cracked at high temperature due to preexisting strain in the 3C-SiC epilayer on Si, but stayed intact on 3C-SiC(111)/4H-SiC.

As twin-free BP films could be produced on 3C-SiC, high-quality bulk 3C-SiC or 3C-SiC epilayers on 4H-SiC substrates could further improve the crystal quality of BP.

ZrB_2 Substrates

BP epitaxy was explored on a limited number of bulk ZrB_2 and ZrB_2/4H-SiC substrates for the first time in literature. The BP films grown at 1100^{o}C were crystalline while at 1000^{o}C and 1200^{o}C, the films were polycrystalline on both bulk ZrB_2 and ZrB_2/4H-SiC substrates. Furthermore, $B_{12}P_2$ was formed at 1200^{o}C due to increased segregation of boron atoms in ZrB_2 during the deposition. The morphology, crystalline orientation, peak width and relative intensity ratios of BP at three different temperatures on both types of substrates showed mixed results due to limited number of BP samples for comparison.

Overall, the initial results of BP on ZrB_2 substrates are encouraging and the obtained results indicate that ZrB_2 could be a promising substrate for BP epitaxy.

7.2 Future Work

In the future, the following studies could be studied to understand the properties of BP and investigate its neutron detection performance.

- Structural characterization and investigation of defect densities in BP in relation to the growth conditions and substrates employed.
- Study and quantify the unintentional impurities in BP films via secondary ion mass spectroscopy (SIMS).
- Impact of impurities and defects on the electrical characterization of BP films deposited at optimum growth conditions.
- Grow high quality BP films to demonstrate the fabrication of BP heterojunction *p-n* junction diodes.
- Study the electrical performance of BP diodes such as threshold voltage, reverse-bias leakage current, minority carrier lifetime etc.
- Test neutron/alpha testing and evaluate detection performance such as sensitivity, efficiency and lifetime of BP diodes.

References

1. Padavala B, Frye CD, Wang X, et al. Epitaxy of Boron Phosphide on Aluminum Nitride(0001)/Sapphire Substrate. *Cryst. Growth Des.* 2016;16(2):981-987. doi:10.1021/acs.cgd.5b01525.

2. Padavala B, Frye C, Edgar JH, et al. Heteroepitaxial Growth of Boron Phosphide on 3C-SiC/Si(100) and AlN/Sapphire(0001) Substrates. In: *Materials Science and Technology (MS&T)*.; 2014:1583-1590.

3. Padavala B, Frye CD, Ding Z, et al. Preparation, properties, and characterization of boron phosphide films on 4H- and 6H-silicon carbide. *Solid State Sci.* 2015;47:55-60. doi:10.1016/j.solidstatesciences.2015.03.002.

4. Padavala B, Frye C, Edgar JH, et al. Crystal Growth and Characterization of Cubic Boron Phosphide on Silicon Carbide. In: *Materials Science and Technology (MS&T)*.; 2014:1575-1582.

5. Padavala B, Frye CD, Xuejing W, Raghothamachar B, Edgar JH. CVD growth and properties of boron phosphide on 3C-SiC. *J. Cryst. Growth* 2016. doi:10.1016/j.jcrysgro.2016.05.031.

6. P. Popper & T. A. Ingles. Boron Phosphide, A III–V Compound of Zinc-Blende Structure. *Nature* 1957;179:1075.

7. Wentzcovitch RM, Chang KJ, Cohen ML. Electronic and structural properties of BN and BP. *Phys. Rev. B Condens. Matter Mater. Phys.* 1986;34(2):1071-1079.

8. Bouhafs B, Aourag H, Ferhat M, Certier M. Competition between the ionic and covalent character in the series of boron compounds BP, BAs, and BSb. *J. Phys. Condens. Matter* 1999;11(30):5781-5796. doi:10.1088/0953-8984/11/30/309.

9. Archer RJ, Koyama RY, Loebner EE, Lucas RC. Optical absorption, electroluminescence, and the band gap of BP. *Phys. Rev. Lett.* 1964;12(19):11-13.

10. Wang CC, Cardona M, Fischer AG. Preparation, optical properties, and band structure of boron phosphide. *RCA Rev.* 1964;25:159-67.

11. Chu TL, Jackson JM, Hyslop AE, Chu SC. Crystals and epitaxial layers of boron phosphide. *J. Appl. Phys.* 1971;42(1):420-4. doi:10.1063/1.1659614.

12. PERET JL. Preparation and properties of boron phophides. *J. Am. Ceram. Soc.* 1964;47(1):44-46.

13. Takenaka T, Takigawa M, Shohno K. Hardness of boron monophosphide. *Jpn. J. Appl. Phys.* 1976;15(11):2235-2236.

14. Kumashiro Y. Refractory semiconductor of boron phosphide. *J. Mater. Res.* 1990;5(12):2933-

2947. doi:10.1557/JMR.1990.2933.

15. Shohno K, Takigawa M, Nakada T. Epitaxial growth of BP compounds on Si substrates using the B2H6-PH3-H2 system. *J. Cryst. Growth* 1974;24-25:193-196. doi:10.1016/0022-0248(74)90303-0.

16. Stone B, Hill D. Semiconducting properties of cubic boron phosphide. *Phys. Rev. Lett.* 1960;4(6):282-284. Available at: http://link.aps.org/doi/10.1103/PhysRevLett.4.282. Accessed September 6, 2012.

17. Kumashiro Y, Mitsuhashi T, Okaya S, et al. Thermal conductivity of a boron phosphide single-crystal wafer up to high temperature. *J. Appl. Phys.* 1989;65(5):2147-2148.

18. Ejembi JI, Nwigboji IH, Franklin L, Malozovsky Y, Zhao GL, Bagayoko D. Ab-initio calculations of electronic, transport, and structural properties of boron phosphide. *J. Appl. Phys.* 2014;116(10):103711. doi:10.1063/1.4894692.

19. Werheit H. Boron-rich solids: a chance for high-efficiency high-temperature thermoelectric energy conversion. *Mater. Sci. Eng. B Solid-State Mater. Adv. Technol.* 1995;B29(1-3):228-232.

20. Golikova OA. Boron and boron-based semiconductors. *Phys. Status Solidi A Appl. Res.* 1979;51(1):11-40.

21. Nishimura S, Hirai M, Nagayoshi H, Terashima K. Strong Visible Light Emission from Zinc-Blende InGaN/GaN pn Junction on Silicon Substrate. *ECS Trans.* 2013;53(2):87-91.

22. Waddell E. Novel uses of boron phosphide films. *Mater. Res. Soc. Symp. Proc.* 1999;555:91-96.

23. Bernard A. Gruber. PROCESS FOR THE PRODUCTION OF BORON PHOSPHIDE. 1968. Available at: http://www.google.com/patents/US3395986.

24. Ruehrwein RA, Williams F V. CRYSTALLIZATION OF BORON PHOSPHIDE. 1960. Available at: http://www.google.com/patents/US2966424.

25. Lu P, Edgar JH, Pomeroy J, Kuball M, Meyer HM, Aselage T. Growth of rhombohedral B12P2 thin films on 6H-SiC(0001) by chemical vapor deposition. *Mater. Res. Soc. Symp. Proc.* 2004;799:121-25.

26. Kumashiro Y, Yoshizawa H, Shirai K. Preparation of rhombohedral boron phosphide wafer by CVD process. *JJAP Ser.* 1994;10:166-7.

27. Kumashiro Y, Yokoyama T, Nakamura J, Takahashi J. Semiconducting properties of Boron phosphide thin films by MBD process. *JJAP Ser. 10* 1994:168-169.

28. Chu TL, Hyslop AE. Crystal Growth and Properties of Boron Monoarsenide. *J. Appl. Phys.* 1972;43(2):276. doi:10.1063/1.1661106.

29. Nagarajan R, Xu Z, Edgar JH, et al. Crystal growth of B12As2 on SiC substrate by CVD method. *J. Cryst. Growth* 2005;273(3-4):431-438. doi:10.1016/j.jcrysgro.2004.07.068.

30. Mishima O, Era K, Tanaka J, Yamaoka S. Ultraviolet light-emitting diode of a cubic boron nitride pn junction made at high pressure. *Appl. Phys. Lett.* 1988;53(11):962-4.

31. Nishinaga T, Ogawa H, Watanabe H, Arizumi T. Vapor growth of boron monophosphide using open and closed tube processes. *J. Cryst. Growth* 1972;13-14:346-9.

32. Chu TL, Jackson JM, Smeltzer RK. Growth of boron monophosphide crystals by chemical transport. *J. Cryst. Growth* 1972;15(4):254-8.

33. Chu TL, Jackson JM, Smeltzer RK. Crystal growth of boron monophosphide from metal phosphide solutions. *J. Electrochem. Soc.* 1973;120(6):802-6.

34. Kato N, Kammura W, Iwami M, Kawabe K. Crystal growth of boron monophosphide from copper-fluxed melt. *Jpn. J. Appl. Phys.* 1977;16(9):1623-7.

35. Baranov B V., Prochukhan VD, Goryunova NA. Preparation of large boron phosphide crystals from a solution in a melt with cuprous phosphide. *Izv. Akad. Nauk SSSR, Neorg. Mater.* 1967;3(9):1691-2.

36. Ananthanarayanan KP, Mohanty C, Gielisse PJ. Synthesis of single crystal boron phosphide. *J. Cryst. Growth* 1973;20(1):63-7.

37. Kobayashi T, Susa K, Taniguchi S. Syntheses of boron phosphide under high pressures. *Mater. Res. Bull.* 1974;9(5):625-31.

38. Niemyski T, Mierzejewska-Appenheimer S, Majewski J. High-pressure crystallization of boron phosphide from liquid phosphorus. *J. Phys. Chem. Solids, Suppl.* 1967;1:585-7.

39. Takigawa M, Hirayama M, Shohno K. Hetero-epitaxial growth of boron monophosphide on silicon substrate using a diborane-phosphine-hydrogen system. *Jpn. J. Appl. Phys.* 1974;13(3):411-16.

40. Nishinaga T, Mizutani T. Effect of growth parameters on the epitaxial growth of BP [boron monophosphide] on silicon substrate. *Jpn. J. Appl. Phys.* 1975;14(6):753-60.

41. Takenaka T, Takigawa M, Shohno K. Boron monophosphide and some of its electrical properties. *Jpn. J. Appl. Phys.* 1975;14(4):579-580.

42. Shohno K, Takigawa M, Nakada T. Epitaxial growth of boron phosphide compounds on silicon substrates using the diborane-phosphine-hydrogen system. *J. Cryst. Growth* 1974;24-25:193-6.

43. Iwami M, Tohda T, Kammura W, Kawabe K. Crystal growth of boron monophosphide and its properties. *Technol. Reports Osaka Univ.* 1976;26(1276-1307):201-9.

44. Yugo S, Kimura T. Thermoelectric power of boron phosphide at high temperatures. *Phys. Status Solidi A Appl. Res.* 1980;59(1):363-70.

45. Kumashiro Y, Okada, Y.; Gonda S. Crystal growth of thick wafers of boron phosphide. *J. Cryst. Growth* 1984;70(1-2):507-14.

46. Kumashiro Y, Okada Y, Misawa S. Electrical properties of well-characterized boron phosphide wafers up to high-temperatures. *Ext. Abstr. Conf. Solid State Devices Mater.* 1985;17:257-60.

47. Kumashiro Y, Matsumoto M, Yoshizawa H. Heteroepitaxial growth of boron phosphide single crystal on sapphire single crystal. *JJAP Ser. (1994), Proc. 11th Int. Symp. Boron, Borides Relat. Compd.* 1994;10:160-163.

48. Kumashiro Y, Yokoyama T, Sato A, Ando Y. Thermoelectric properties of boron and boron phosphide CVD wafers. *J. Solid State Chem.* 1997;133(1):314-321.

49. Takeuchi T, Nishimura S, Sakuma T, Matsumoto S, Terashima K. Epitaxial growth and characterization of BP on Si(100) substrate for use in c-GaN study. *Mater. Res. Soc. Symp. Proc.* 2006;Date 2005(891):127-131.

50. Kumashiro Y, Nakamura K, Enomoto T, Tanaka M. Preparation and thermoelectric properties of BP films on SOI and sapphire substrates. *J. Mater. Sci. Mater. Electron.* 2011;22(8):966-973. doi:10.1007/s10854-010-0245-1.

51. Schroten E, Goossens A, Schoonman J. Photo- and electroreflectance of cubic boron phosphide. *J. Appl. Phys.* 1998;83(3):1660. doi:10.1063/1.366881.

52. Kumashiro Y, Okada Y, Okumura H. Isotope effects on boron phosphide single-crystal wafers. *J. Cryst. Growth* 1993;132(3-4):611-613. doi:10.1016/0022-0248(93)90090-J.

53. Ohsawa J, Nishinaga T, Uchiyama S. Si contamination in epitaxial boron monophoshide. *Jpn. J. Appl. Phys.* 1978;17(9):1579-1586.

54. Takenaka T, Takigawa M, Shohno K. Diffusion layers formed in Si substrates during the epitaxial growth of BP and application to devices. *J. Electrochem. Soc.* 1978;125(4):633. doi:10.1149/1.2131514.

55. Kim CJ, Shono K. Deviation from stoichiometry of boron monophosphide. *J. Electrochem. Soc.* 1984;131(1):120-2.

56. Udagawa T, Odawara M, Shimaoka G. High-resolution TEM characterization of MOVPE-grown (111)-BP layer on hexagonal 6H (0001)-SiC. *Appl. Surf. Sci.* 2005;244(1-4):285-288. doi:10.1016/j.apsusc.2004.10.129.

57. Li G, Abbott JKC, Brasfield JD, et al. Structure characterization and strain relief analysis in CVD growth of boron phosphide on silicon carbide. *Appl. Surf. Sci.* 2015;327:7-12. doi:10.1016/j.apsusc.2014.11.037.

58. Ganesan S, Maradudin a. ., Oitmaa J. A lattice theory of morphic effects in crystals of the diamond structure. *Ann. Phys. (N. Y).* 1970;56:556-594. doi:10.1016/0003-4916(70)90029-1.

59. Shohno K, Ohtake H, Bloem J. Crystal growth of boron monophosphide using a B2H6-PH3-H2 system. *J. Cryst. Growth* 1978;45:187-191.

60. Nishimura S, Hanamoto H, Terashima K, Matsumoto S. Growth of GaN on Si(100) substrate using BP as a buffer layer-selective epitaxial growth. *Mater. Sci. Eng. B Solid-State Mater. Adv. Technol.* 2002;93:135-138.

61. Odawara M, Udagawa T, Shimaoka G. Organometallic chemical vapor deposition growth of heterostructure of wide band gap and transparent boron phosphide on silicon. *Jpn. J. Appl. Phys.* 2005;44(1B):681-683. doi:10.1143/JJAP.44.681.

62. Udagawa T, Shimaoka G. Heteroepitaxial growth of boronphosphide III-V semiconductor on silicon by organometallic chemical vapor deposition. 2003;4(2):80-83.

63. Suzuki A, Takigawa M, Shohno K. Free boron monophosphide wafers. *Jpn. J. Appl. Phys.* 1977;16(6):1053-1054.

64. Neave JH, Dobson PJ, Joyce B a., Zhang J. Reflection high-energy electron diffraction oscillations from vicinal surfaces—a new approach to surface diffusion measurements. *Appl. Phys. Lett.* 1985;47(2):100. doi:10.1063/1.96281.

65. Williams F V., Ruehrwein RA. The preparation and properties of boron phosphides and arsenides. 1959;744:1330-1332.

66. Schmitt JO, Edgar LJH, Liu L, Nagarajan R, Szyszko T, Podsiadlo S. Close-spaced crystal growth and characterization of BP crystals. *Phys. Status Solidi C Conf. Crit. Rev.* 2005;2(3):1077-1080.

67. Sanjurjo J, Lopez-Cruz E. Dependence on volume of the phonon frequencies and their effective charges of several III-V semiconductors. *Phys. Rev. B* 1983;28:4579–4584.

68. Reeber RR, Wang K. Lattice Parameters and Thermal Expansion of Important Semiconductors and Their Substrates. *MRS Proc.* 2000;622(JANUARY):T6.35.1-6. doi:10.1557/PROC-622-T6.35.1.

69. Slack GA, Bartram SF. Thermal expansion of some diamondlike crystals. *J. Appl. Phys.* 1975;46(1):89. doi:10.1063/1.321373.

70. Li G. Growth and properties of boron phosphide films on silicon carbide. 2013. Available at: .

71. Odawara M, Udagawa T, Shimaoka G. Morphological investigation of double positioning growth of (1 1 1)-boron phosphide (BP) on the (0 0 0 1)-GaN. *Appl. Surf. Sci.* 2005;244:289-292. doi:10.1016/j.apsusc.2004.10.147.

72. Zhang Y, Chen H, Dudley M, et al. Growth mechanisms and defect structures of B12As2 epilayers grown on 4H-SiC substrates. *J. Cryst. Growth* 2012;352(1):3-8.

73. Ramachandran V, Brady MF, Smith AR, Feenstra RM, Greve DM. Preparation of atomically flat surfaces on silicon carbide using hydrogen etching. *J. Electron. Mater.* 1998;27(4):308-312.

74. Nelson WE, Halden FA, Rosengreen A. Growth and Properties of β-SiC Single Crystals. *J. Appl. Phys.* 1966;37(1):333. doi:10.1063/1.1707837.

75. Casady JB, Johnson RW. Status of silicon carbide (SiC) as a wide-bandgap semiconductor for high-temperature applications: A review. *Solid. State. Electron.* 1996;39(10):1409-1422.

76. Jokubavicius V, Yazdi GR, Liljedahl R, Ivanov IG, Yakimova R, Syväjärvi M. Lateral Enlargement Growth Mechanism of 3C-SiC on Off-Oriented 4H-SiC Substrates. *Cryst. Growth Des.* 2014;14(12):6514-6520. doi:10.1021/cg501424e.

77. Jokubavicius V, Yazdi GR, Liljedahl R, et al. Single Domain 3C-SiC Growth on Off-Oriented 4H-SiC Substrates. *Cryst. Growth Des.* 2015;15(6):2940-2947. doi:10.1021/acs.cgd.5b00368.

78. Takashi M, Jun O, Tatau N, Susumu U. Thermal Expansion Coefficient of Boron Monophosphide. *Japan Soc. Appl. Phys.* 1976;15(7):1305-1308.

79. Anzalone R, Camarda M, Locke C, et al. Stress evaluation on hetero-epitaxial 3C-SiC film on (100) Si substrates. *Mater. Sci. Forum vols* 2012;717-720:521-524.

80. Volinsky AA, Kravchenko G, Waters P, et al. Residual Stress in CVD-grown 3C-SiC Films on Si Substrates. *Mater. Res. Soc. Symp. Proc.* 2008;1069:D03-05.

81. Mukaida H, Okumura H, Lee JH, et al. Raman scattering of SiC: Estimation of the internal stress in 3C-SiC on Si. *J. Appl. Phys.* 1987;62(1):254-257.

82. Tengdelius L, Birch J, Lu J, et al. Magnetron sputtering of epitaxial ZrB2 thin films on 4H-SiC(0001) and Si(111). *Phys. Status Solidi Appl. Mater. Sci.* 2014;211(3):636-640. doi:10.1002/pssa.201330308.

83. Tengdelius L, Samuelsson M, Jensen J, et al. Direct current magnetron sputtered ZrB2 thin films on 4H-SiC(0001) and Si(100). *Thin Solid Films* 2014;550:285-290. doi:10.1016/j.tsf.2013.11.040.

84. Tengdelius L, Greczynski G, Chubarov M, et al. Stoichiometric, epitaxial ZrB2 thin films with low oxygen-content deposited by magnetron sputtering from a compound target: Effects of deposition temperature and sputtering power. *J. Cryst. Growth* 2015;430:55-62. doi:10.1016/j.jcrysgro.2015.08.012.

85. Otani S, Korsukova M., Mitsuhashia T. Preparation of HfB2 and ZrB2 single crystals by the floating-zone method. *J. Cryst. Growth* 1998;186(4):582-586.

86. Kinoshita H, Otani S, Kamiyama S, et al. ZrB2 substrate for nitride semiconductors. *Japanese J. Appl. Physics, Part 1 Regul. Pap. Short Notes Rev. Pap.* 2003;42(4 B):2260-2264. doi:10.1143/jjap.42.2260.

87. Kinoshita H, Otani S, Kamiyama S, et al. Zirconium diboride (0001) as an electrically conductive lattice-matched substrate for gallium nitride. *Japanese J. Appl. Physics, Part 2 Lett.* 2001;40(12 A):10-13. doi:10.1143/jjap.40.l1280.

88. Okamoto NL, Kusakari M, Tanaka K, Inui H, Otani S. Anisotropic elastic constants and thermal expansivities in monocrystal CrB2, TiB2, and ZrB2. *Acta Mater.* 2010;58:76-84.